THE HONG KONG POLYTECHNIC UNIVERSITY

DEPARTMENT OF LAND SURVEYING AND

GEO-INFORMATICS

Improvement and Estimation of Classification Accuracy for Remotely Sensed Images

HAIXIA MAO

A thesis submitted in partial fulfillment of the requirements

for the Degree of Doctor of Philosophy

April 2009

Certificate of Originality

I hereby declare that this thesis is my own work and that, to the best of my knowledge and belief, it reproduces no material previously published or written nor material which has been accepted for the award of any other degree or diploma, except where due acknowledgement has been made in the text.

_____(Signed)

Haixia MAO (Name of Student)

Abstract

A land use inventory provides the means from which data can be extracted to enable such as land management and the decision making necessary to promote sustainable environmental development, where image classification is one of the most important procedures. The overall aim of the study in this thesis is to improve the reliability of the land use inventory, by specific focus on the development of methods, to improve and estimate the classification accuracy of remotely sensed images. The following research objectives are thus identified:

- to unmix the mixed pixels for hyper/multi-spectral remotely sensed images;
- to propose a new multiple classifier system;
- to propose a spatial sample strategy.

Firstly, a solution of unmixing mixed pixel, including endmember extraction, abundance generation and sub-pixel mapping, for hyper-spectral images is proposed. One of the main contributions of this research is the proof for AMEE assumption and the proposal of the Improved AMEE to enhance the performance of endmember extraction. Pre-judgment before applying the Least Squares is carried out to calculate the abundances. To further improve the performance of pixel unmixing, Reliability-based Sub-pixel Mapping is proposed to locate each endmembers in a mixed pixel.

Secondly, pixel unmixing for multi-spectral remotely sensed image based on

single band is addressed. The Mountain Clustering is introduced to extract endmembers. The Grey Correlation method is still used to generate the abundance of each endmember. And the Improved Cellular Automata is proposed for sub-pixel mapping. As pixel unmixing is implemented in each single band, the Multiband Synthesis is proposed to integrate the result from partial overall.

Thirdly, to improve the accuracy of land use classification, an Eigen-values based Multiple Classifier System is proposed in this study. A posterior probabilities matrix of each component classifier is obtained and the eigen-values are calculated based on the matrix. In Eigen-values based Multiple Classifier System, the eigen-values are used to weight the classifiers. With the proper correspondence between eigen-values and classifiers, the proposed method has proved to be effective for image classification land use inventory.

Fourthly, a sampling strategy based on error-distribution is proposed to assess the accuracy of the image classification results. The error surface is generated, based on image classification errors, where those errors are regarded as noise in the research field of signal processing. Firstly, after a approximate classification, a prior partition of the original spatial data, based on the different error levels, is found. Secondly, based on the assumption that the errors follow the normal distribution, different Gaussian filters are used to remove them in each region. Error-free spatial data can then be obtained. Finally, the difference between the original spatial data and the error-free data is used to build an error surface. Hence, the extreme points on the error surface are considered as the

representative points of the sample and the least sample size is determined.

In summary, mixed pixels are one of the main obstacles for image classification; the classification method itself has direct impact on the classification accuracy; the accuracy assessment system will influence on the evaluation of the classification result. If all the above problems can be solved effectively, a great success can be obtained in image classification. Consequently, this research focuses on above objectives and contributes to the quality of the land use inventory in the following two areas: (a) it improves image classification accuracy by solving the mixed pixel problem and thereby provides an improved multiple classifier system; (b) it contributes to the improvement of the reliability of the accuracy assessment result, by the means of a new spatial sample strategy.

Publications

Shi, W., Liu, K.F. and Mao H.X. et. al, 2010, Methods for Improving Image Classification Accuracy, *International Journal of Applied Earth Observation and Geoinformation*. (submitted)

Tian Y., Shi W.Z., and Mao H.X., 2009 et. al, A Two-Dimensional Empirical Mode Decomposition Method -- with Application for Fusing Panchromatic and Multi-spectral Satellite Images, *International Journal of Remote Sensing*. 30(10), pp:2637-2652.

Mao H.X. and W.Z. Shi, 2008, A preliminary study on spatial sampling of topographic map, chapter in *Quality Aspects in Spatial Data Mining*, (Stain A. et. al eds), pp: 59-72.

Mao H.X. and W.Z. Shi, 2008, New Methodology of Representing the Positional Error of Non-point Features in GIS, 21st ISPRS Congress, 3rd-11th Jul, Beijing, China.

Mao H.X. and W.Z. Shi, 2008, Uncertainty and Its Propagation in Land Investigation, in Proceedings of the 8th International Symposium on Spatial Accuracy Assessment in Natural Resources and Environmental Sciences, 25th-27th Jun, Shanghai China. pp: 134-137.

Mao, H.X., W.Z., Shi and Y., Tian, 2007, A preliminary study on spatial sampling of topographic map, the 5th International Symposium of Spatial Data Quality, 13th-15th, Jun, 2007, Enschede, Netherlands.

Shi, W.Z., H.X., Mao, Y., Tian and K. Bruce, 2006, A review and analysis of the methods for building extraction from airborne LIDAR images, Journal of Geospatial Engineering, Vol. 8, No. 1-2, pp: 75-85.

Acknowledgements

I would like to thank my supervisor Prof. Wenzhong Shi for his contributions to my research. Prof. Shi has provided discussions and comments throughout the research. Without his kind assistance, I could not complete this thesis within the normal period of a PhD study in The Hong Kong Polytechnic University.

I also sincerely thank Prof. Yan Tian for his invaluable assistance, sharp advice and inspiration. Prof. Tian is an insightful mathematician and image processing expert, his valuable suggestion do me a great favor to complete part of the study.

Special thanks are given to Dr. Kimfung Liu and Mr. Huang Zhang for their supports and share with the research. I would also like to thank all the PhD candidates in my office for their encouragement during three years of research.

I sincerely appreciate my family for their support during three years of research. Especially, I would like to thank my husband, Mr. Xiaopeng Fan. His selfish support and encouragement make me have the confidence to conquer the difficulties during PhD study.

I gratefully acknowledge the financial and administrative support from the Departmental Research Committee and the Research Office of The Hong Kong Polytechnic University. The work described in this thesis was substantially supported by grants from the Research Grants of the Hong Kong Polytechnic University (Project No. RGMG).

Table of Contents

List of Figures

List of Tables

1 Introduction

1.1 Background

Land is recognized as one of the physical foundations of human history and has an influence on the sustainable development of life: human and otherwise. Land cover is a fundamental variable of the natural features on the earth. In association with climate change, land cover change is regarded as an important variable of global change affecting the ecological and environmental systems (Foody, 2002). A land use inventory has been devised to define and master the function of each kind of land cover (Comber, 2008). As a consequence an investigation and subsequent management of land resources is significant and necessary work.

1.1.1 Land Use Inventory

A land use inventory has been widely implemented in many countries, as an important means for land resource management and decision making in the increasingly important area of sustainable environmental development. For example, USGS and NASA have collaborated on a research project: Land Cover Trends, which focuses on understanding the rates, trends, causes and consequences of contemporary US land use and land cover change. In the UK, the government and universities have compiled a land inventory. In China, there was the first land use inventory extended from 1984 to 1996, and now, based on the current requirement trends, the Central Government has arranged for a second national land use inventory beginning in 2007 and to carry on for the

foreseeable future.

The main tasks of a land use inventory include: investigating categories, area, distribution and adscription of the land cover, building perfect land investigation, statistics and registration system, realizing information and network management, and finally implementing some form of social service for all people. The operational procedures of land use inventory are roughly illustrated in Figure 1.1.

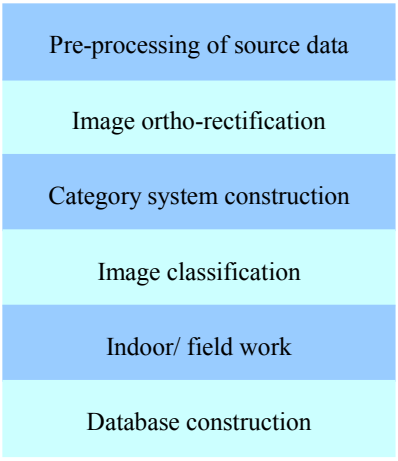

Figure 1.1 Operational procedure of the land use inventory

Among all procedures, image classification is one of the most important and typical applications of remote sensing as regards a land use inventory (Tang et al., 2005; Berberoglu et al., 2007; Zhang et al., 2008). Moreover, image classification is one of the main uncertainty sources in land use inventory. In other words, if the accuracy of image classification is very low, poor land cover categories will provide for land use inventory. Consequently, classification accuracy has great impact on land use inventory. To this point, we will study

some important aspects of the image classification to contribute to land use inventory.

1.1.2 Several Main Issues Related to Image Classification

There are other issues related to image classification, such as training sample size and selection, in this study, we focus on:

1.1.2.1 Image quality

The presence of mixed pixels, an inevitable feature of remotely sensed image, directly influences the accuracy of image classification. Owing to the intersection of ground objects, the boundaries of different features are difficult to distinguish, the low spatial resolution of remotely sensed images result in the presence of mixed pixels. This issue poses a problem which is revealed as one of the largest obstacles when classification methods are explored. Generally, such mixed pixels are classified to the class that is most possible, however, it is noted that mistakes will occur when mixed pixels are categorized to any typical land cover while they actually not belong to any of the existing land covers.

In general, almost all the classification methods produce relatively better results in the internal feature regions. While in the boundary regions where lack of certainty, it has a direct and negative influence on the final classification result. One method to improve the accuracy of image classification is thus to unmix the mixed pixels. If the presence of mixed pixel can be removed or unmixed, the accuracy of classification should be greatly improved.

1.1.2.2 Image classification methods

Classification methods are directly responsible for indicating to which land cover on an image should be assigned and to which category that land cover belongs. If the classified results have insufficient accuracy, the land cover assignment accuracy will be incorrect.

There are many classification methods for image classification, some get good result in some case, while bad in other case. Therefore, almost non method can be regarded as a generic classification solution for all kinds of remotely sensed images. Generally, the degree and characteristics of uncertainty differ greatly with the use of different classification method. Consequently, an exploration into the performance of classification method is significant in the interests of classification uncertainty.

1.1.2.3 Quality evaluation of classified images

The objectives of quality evaluation of classified images include describing classification error based on an error matrix and the spatial pattern of classification errors, comparing different classification schemes etc. (Stehman, 2000). In this study, as limited time, we focus the accuracy assessment of image classification only on the latter.

To the description of classification error, it is necessary to configure the error matrix and decide the measurements. Generally, there are descriptive statistic and analytic statistic from the error matrix. Overall accuracy, producer's accuracy (omission error) and user's accuracy (commission error) as well as

Kappa statistic belong to descriptive statistic. In addition, the discrete multivariate techniques are used as the analytical techniques (Congalton et. al, 1983). Rosenfield (1981) proposed variance analysis for accuracy assessment. All in all, assessing error will accumulate and propagate through spatial layers (Skidmore and Turner, 1989) and the measurements for accuracy evaluation are important index to depict the quality of image classification.

To obtain spatial pattern of classification errors, it is verified by sample strategy in fact. It is impossible to survey every pixel, so sample is definitely necessary for this procedure. A sample strategy is the means to choose proper number of sample individuals from the population. Sample individuals should be selected as the representative of the population to reflect the real situation. On the other hand, sample size should be large enough so that the analytical result has the statistical characteristics, while be reduced to as much as possible from the cost point of view. Consequently, the sample strategy should be well designed based on the consideration of sample individuals and sample size.

1.1.3 Summary

Image quality is identified as one of the major sources of uncertainty in land use inventory where the problem of mixed pixels occurs. Unmixing solutions to improve the quality of remotely sensed images can generate a better image. We consider the results of this stage form a better image base for the next stage of image classification in land use inventory, comparing with the image before the unmixing processing. We think the further critical issue to be tackled is a higher precise classification method for land use inventory. After the images are

classified based on the proposed classification method, we can obtain the accurate land cover categories. What we need finally is to assess the quality of the classification results, where sample strategy is identified as a very important issue.

As an elaborate but not exhaustive solution to the problem of classification uncertainty, three research issues are defined in the study presented in this thesis: 1) mixed pixel unmixing, 2) new classification method and 3) new spatial sample strategy. All these issues are aimed at finding solutions to further reduce the uncertainty in image classification procedure.

1.2 Objectives of this Study

The classification of the remotely sensed images has played an important role in the procurement of an accurate land use inventory. The presence of mixed pixel, classification methods and sample strategies are all the key factors to be considered in the determination of image classification accuracy. A study of these research topics, when combined, has effect on the reliability of land use inventory. As indicated above, the aim of this research is to improve and estimate the accuracy of the classification of remotely sensed images. The objectives are as follows:

(a) to unmix the mixed pixels in classification for hyper -spectral remotely sensed image,

(b) to unmix the mixed pixels in classification for multi-spectral remotely sensed image based on single band,

(c) to improve the accuracy of image classification by proposing a new

multiple classifier system,

(d) to estimate the accuracy of image classification by proposing spatial sampling strategy.

1.3 Structure of the Thesis

This thesis is composed of seven chapters. To clarify the structure of the thesis, a framework is drawn in Figure 1.2:

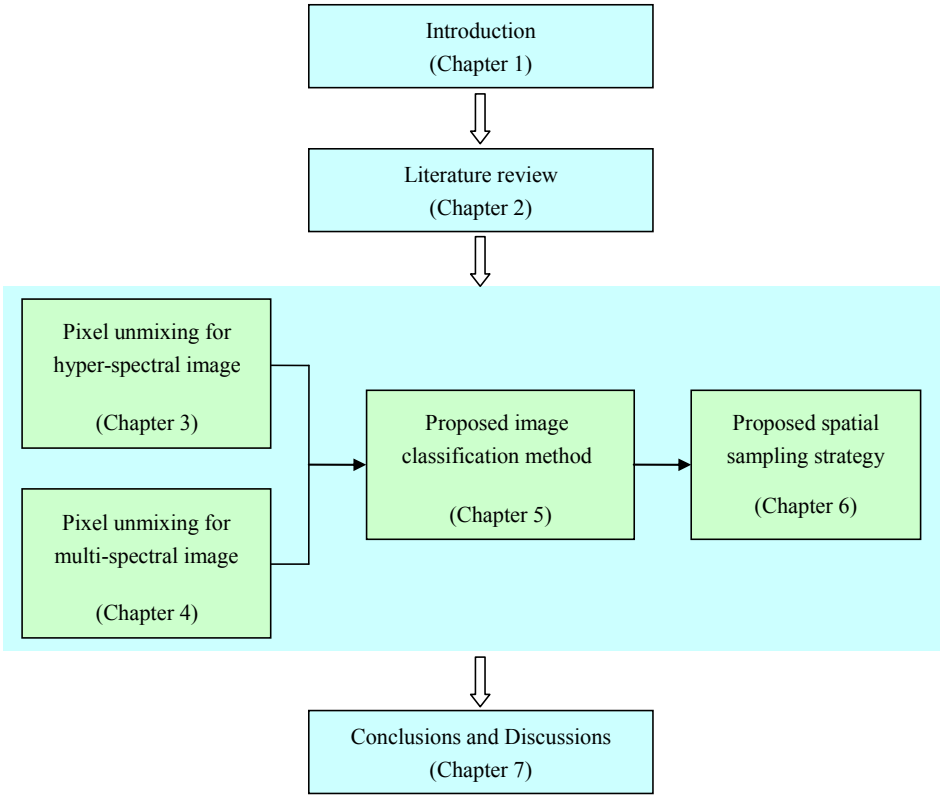

Figure 1.2 Structure of the thesis

Following this introduction, in Chapter 2, the current technologies of the related three research topics are reviewed. It reviewed the development of the solutions for the mixed pixel unmixing, the image classification and the spatial sampling strategies for the accuracy assessment of classified images.

In Chapter 3, as the classical problem in image classification, mixed pixel is unmixed in the hyper-spectral remotely sensed image. Firstly, the algorithm named Improved AMEE is proposed to improve the performance of endmember extraction. Secondly, abundance of each endmember within the corresponding mixed pixel is generated by the Least Squares method with pre-judgment. Finally, we propose the Reliability-based Sub-pixel Mapping to locate all the endmembers within a mixed pixel.

In Chapter 4, due to the less spectral information, the principle of mixed pixel unmixing for multi-spectral images is different from the proposed methods in Chapter 3. Here, we make use of the spatial information to finish the task of mixed pixel unmixing. Firstly, Mountain Clustering Endmember Extraction, based on the famous mountain clustering algorithm, is introduced to improve the performance of pure endmember extraction. Secondly, the Grey Correlation Method is still used to generate the abundance of each endmember within a mixed pixel. Thirdly, we propose another algorithm named Improved Cellular Automata-based Sub-pixel Mapping to locate each endmember within the mixed pixel. Finally, multiband synthesis technology is proposed to integrate all unmixing results from each single band.

In Chapter 5, a new method of Multiple Classifier System (MCS) is proposed as the classification method by given a meaningful weight to each of the classifiers. This method is implemented by configuring the posterior probabilities matrix of component classifiers and calculating the eigen-values based on the matrix. We can get a better Multiple Classifier System after assigning appropriate weight to

each single classifier based on corresponding eigen-value, in order that the accuracy of image classification is improved.

In Chapter 6, selection of spatial sample points is explored on an error surface. To capture the error surface, error of image classification is thought as noise in the signal processing. By means of several filters with different scale, error surface is obtained as the difference between the original data and error-free data. Then, the extreme points on the error surface are seen as the representative points of the sample individuals. The sample size of the extreme points on the error surface is thought as the least amount.

The thesis ends with conclusions and recommendations in Chapter 7.

2 An Review and Analysis of Related Research

2.1 Pixel Unmixing for Remotely Sensed Images

2.1.1 Research Background

The value of the pixels on a remotely sensed image indicates the spectral reflection of the corresponding land covers on the ground. If the land cover categories are very close or interlaced, moreover these objects are mapped into one pixel, the spectral reflection will turn to the common spectral reflection of these objects. In other word, the limitation of spatial resolution of remotely sensed images and heterogeneous mixture of the pixels commonly lead to the fuzzy boundary between different feature classes. Those pixels on the fuzzy boundary include more than one constituent material, and are called as mixed pixel.

In hyper-spectral images or multi-spectral ones, they include both pure pixels that represent only one kind of ground objects, and mixed pixels locating the boundaries of various ground objects. Obviously, it is not reasonable to classify those mixed pixels as classify those pure pixels into any type of ground objects, due to their radiation different from that of any typical pixels. Therefore, how to classify mixed pixels has a great impact on the classification accuracy of remotely sensed images.

To solve this problem, the technology of pixel unmixing can enhance the image quality before classification, which can identify the constituent materials,

calculate their corresponding proportions and locate them properly within the space of a mixed pixel. Here, the constituent materials within the mixed pixel are called as endmembers. Each endmember refers to one component of a mixed pixel, which has the pure spectral reflection from one type of the constituent materials. The corresponding proportions of constituent materials are called as abundance, which can be computed based on a mixing model.

The strategies and steps of the pixel unmixing for hyper-spectral and multi-spectral remotely sensed images are basically similar, both of which are based on the spectral or spatial information. However, it is fairly easier to unmix a hyper-spectral image because of its high spectral resolution, which makes the radiant values of pixels to be an almost continuous spectral curve. While for a multi-spectral image, its spectral resolution is too low to describe the fine reflectance of ground objects. Therefore, the unmixing method for multi-spectral images should be different from that for hyper-spectral ones, which should make good use of higher spatial information.

Currently, the unmixing of mixed pixel becomes a growing research topic with a wide range of applications. Besides image classification, pixel unmixing has been applied to sub-pixel object quantification (Chang and Heinz, 2000), mineral identification (Neville et al., 1999), area estimation (Gebbinck, 1998) etc.

2.1.2 Pixel Unmixing Models

In general, before pixel unmixing, it is necessary to explore the spectrum

imaging mechanism, simulate the spectrum mixing process, and then decide different unmixing methods based on corresponding spectrum mixing models. In the past years, many models of spectrum mixing have been proposed. The existing works can be classified into two categories, including linear mixing models and non-linear mixing models (Keshava, 2003).

In a linear mixing model, the spectral reflectance of a mixed pixel is a linear combination of the spectral reflectance of all the component endmembers with their corresponding abundances (Figure 2.1(a)). This model is simple, easy to be used, and clear with physical meanings. The abundances of endmembers can be calculated by the least squares method. In a non-linear mixing model, there are multiple reflections of radiation among the randomly distributed, heterogeneous mixture of materials. This model is normally described by a high order polynomial, in which the non-linear utility is presented by the cross product items among endmembers (Figure 2.1(b)). However, it is much difficult to build-up and compute non-linear model, and it can not easily represented by simple mathematical solutions.

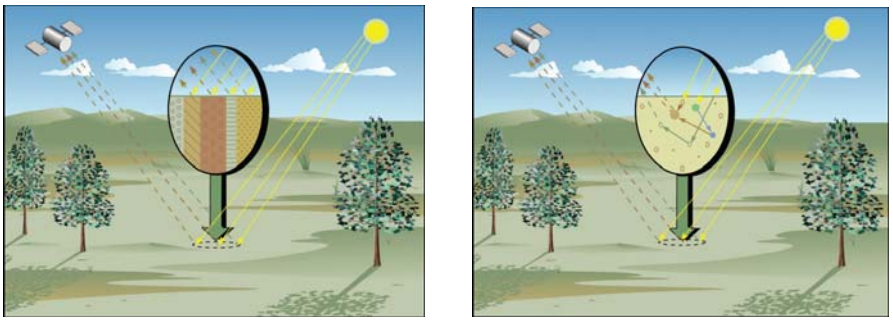

(a) Linear mixing model (b) Non-linear mixing model

Figure 2.1 Pixel Mixing Model (from Keshava, 2003)

Generally, linear mixing model can be regarded as the special example when the multiple reflections are neglected, and are capable of explaining the real situation and help researchers to seek efficient ways to perform unmixing. Therefore, the linear model is a more commonly used model comparing the non-linear model. On the basis of literature review, we summarize the advantages and disadvantages of linear and non-linear unmixing method.

2.1.2.1 Linear Unmixing Methods

The spectrum of a mixed pixel is a linear combination of the spectrums of all the component endmembers. The proportion of all the component endmembers can be determined by linear mixing model. The abundances can be solved by a group of linear equations under the constraints that the sum of all the proportions is 1 and each proportion is positive. Let the total error be minimized and we can calculate the abundance of each endmember by the least squares method. Obviously, greater error occurs if the endmembers are not accurately identified.

The weighted averaging method (Marsh et al. 1980) is a simplified version of the linear mixing modeling approach. It models a mixed pixel as a linear mixture of only two components, thus resulting in a mixture equation. Another model is based on linear regression. March et al. also proposed the linear regression model to unmix pixels consisting of two components by using an equation.

The probabilistic mixing model (Pech et al., 1986) is to estimate the fraction of

a mixed pixel by the linear combination of the fraction vectors of pixels in a training set. One of the advantages of this model is that there is no limitation on the number of classes a pixel can be unmixed into.

The grey system theory is a branch of applied mathematics to study the phenomena with incomplete information and with uncertainty in nature. Grey relation-based unmixing method (Yang and Zhang, 2004) applies grey relationship to unmix mixed pixels. This method considers a pixel classified as an endmember category when the grey value of the pixel within the range of the grey values decided by the endmember. Similarly, the sum of the proportions of all the endmembers are equal to 1 and each proportion is positive.

2.1.2.1 Non-linear Mixing Models

Besides the linear mixing modeling approach, there are also non-linear reflectance models.

The fuzzy theory has also been introduced for modeling the mixture. Wang (1990) proposed the fuzzy classification method, which is an extension of the well-known maximum likelihood classification technique. The proposed method does not merely use the relative order of the class-specific probabilities, it also applies their actual values to determine the proportions of the types that make up the mixed pixel. Another method named the fuzzy c-means approach is based on the fuzzy set theory (Foody and Cox, 1994; Foody, 1994; Atkinson et al., 1997). These algorithms classify the data in the space into c fuzzy groups or classes.

The relaxation model (Arai and Terayama, 1992) takes the compositional information about neighboring pixels into account. This method is based on the observation that the segments of linear features such as roads often consist of mixed pixels with a similar composition. Relaxing an initial estimation of the proportions using the proportions of a neighboring pixel can make a better estimation.

The regularization model (Settle and Drake, 1993; Drake and Settle, 1989) is proposed to modify the linear mixture model in order to accommodate for a favored mixture. To fit both the data and the noise contained in each pixel, the regularization also considers the best estimation of the composition of the entire region rather than each individual pixel. Some interesting works apply the higher order moments to decompose the mixed pixels (Bosdogianni et al., 1994). The proposed model incorporates class distributions instead of reflectance values.

The last model we introduce is the neural networks. Since the neural networks become a powerful classification tool, there are several works introduced into mixed pixels unmixing (Foody, 1994, 1997; Schouten and Gebbinck, 1997a, 1997b). These artificial neural networks (ANN) shows that the output of an ANN trained with pure pixels can be regarded as class membership grades, whose strength can be used to derive class proportions. This result can also be applied to mixed pixels.

2.1.3 The Procedures of Mixed Pixel Unmixing

The procedures of pixel unmixing for hyper-spectral and multi-spectral images are almost same. Firstly, endmembers extraction is done by the means of pure pixels selection, according to a pre-defined number of endmember categories. Secondly, the abundances of endmembers are generated by applying spectrum mixing models to obtain the area proportions of all endmembers in a mixed pixel. Finally, sub-pixel mapping is carried out to fill the component endmembers into the proper locations in the mixed pixel. The logic flow of mixed pixel unmixing is shown in Figure 2.2.

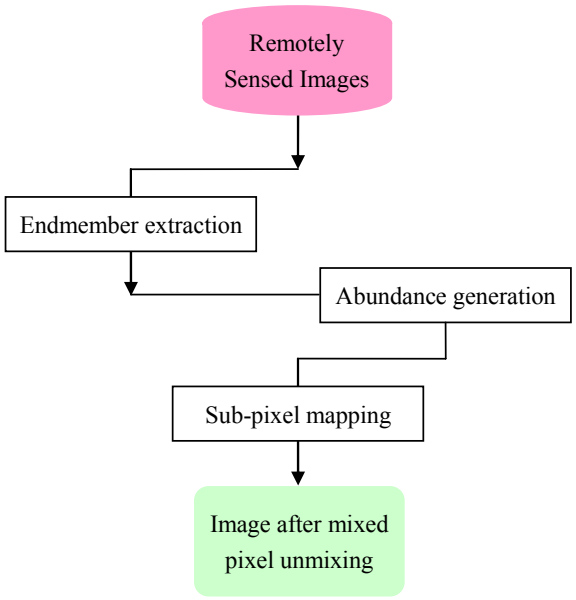

Figure 2.2 The logic flow of mixed pixel unmixing

Sometimes, pixel unmixing for hyper-spectral images includes the procedure of dimension reduction before above three steps. This step is optional and used only by part algorithms, in order to identify and preserve the features of the lower-dimensional space that still allow algorithms to achieve acceptable

performance, but to minimally represent the original data in a lower dimension while including the requisite information for the subsequent unmixing procedure, which is quite different from data compression.

2.1.3.1 Endmember Extraction

The second necessary step is endmember extraction, which yields the first primary output of unmixing mixed pixels. Endmembers can be considered as the pure pixels in an image. Therefore, the objective of endmember extraction is to identify these pure pixels as reliable as possible, and obtain their spectral information. At present, there are three major means to extract the endmembers from the images (Rashed et al., 2001, 2003).

(a) The endmembers are measured from filed work, or selected from the databases. Endmembers identified by this way are called “reference endmember”.

(b) The endmembers are extracted from the original image. Endmembers adjusted and improved by an iterative way are called “image endmembers”.

(c) The endmembers are selected by the integration way of above two.

However, when we extract endmembers from the spectrum databases, it is required to carry out field work and mark the component endmembers or select them from the database in order to match the their spectrums on a image with those in the spectrum database. The weakness of this method is the high cost and time consuming to carry out enough field work. Obviously, this means is

difficult to implement and easily subjected to the external conditions. Therefore, endmembers are normally extracted from the image itself.

At present, there are mainly two means to extract endmembers from the image itself, including interactive styles and automatic styles, such as Pixel Precision Index (PPI) method (Boardman et. al, 1995), N-FINDER method (Winter, 1999), AMEE (Plaza et al., 2002; 2006), IEA method (Neville et al., 1999) and ORASIS (Bowles et al., 1995). Among them, N-FINDER, AMEE and PPI were the most popular ones. The PPI method requires interactive operations. However PPI can not provide the final endmember set, so that it is considered as a direction but not a solution. N-FINDR can obtain the final endmember set, but the precise of this method is greatly dependant on the selection of the initial endmember vector. Because the initial vector is firstly given randomly, and updated iteratively until obtain the final endmember set. Unlike other methods, AMEE makes use not only of the spectral information but also the spatial information. Therefore, the AMEE method was chosen as the starting point for further improvement in this research.

2.1.3.2. Abundance Generation

The results of abundance generation mainly depend on and calculated from the spectral mixing models. On the basis of literatures review, there are generally linear mixing and non-linear mixing model. According to various mixing models, there are corresponding methods to obtain the ratio for each endmember in a mixed pixel, such as linear unmixing method, probabilistic unmixing method, grey relation-based unmixing method, fuzzy unmixing method, and

neural network unmixing method, etc.

2.1.3.3 The Sub-pixel Mapping

Sub-pixel mapping is a further step to unmixing mixed pixels in the original remotely sensed images. After the abundances of all the component endmembers in mixed pixels are obtained, by applying an unmixing method, the original mixed pixels are divided into smaller ones, i.e., sub-pixels. The characteristics of the spatial distribution of sub-pixels are then investigated. Each sub-pixel is assigned a combination of various endmembers, to satisfy the condition that the proportions of various endmembers to sub-pixels are equal to the abundances of these endmembers in the whole image. Finally, the spatial distribution of each endmember in mixed pixels is obtained. The classification accuracy of remotely sensed images can be increased and more details of these images can be displayed.

The sub-pixel mapping is based on the correlation of spatial distribution of land covers, i.e., there are the correlation among the spatial distributions of pixels and in-pixels, under the premise that the scale of spatial variables is greater than that of pixels in remotely sensed images. In detail, it is possible, compared with sub-pixels within long distances, sub-pixels within short distances are much similar and can be categorized into the same type of land cover among mixed pixels and various pixels. This theory has been effective in most of the cases.

Atkinson et al. (1997) proposed the concept of sub-pixel mapping, which describes the process of assigning the concrete classification of endmembers to

the smaller units of a pixel. In other word, sub-pixel mapping can determine the most likely locations of the fractions of each land cover type within the pixel while keeping the same ratios of these endmembers during unmixing mixed pixel. Therefore, sub-pixel mapping is one of the hard classification methods and it extends the soft classification method to a much higher level in the spatial dimension. Some related works has been done in this field. For example, the mapping of sub-pixel can be translated into a linear programming problem by defining a linear equation in linear optimization (Verhoeye and De Wulf, 2002). Another work is to use the output from a soft classification to constrain a Hopfield neural network formulated as an energy minimization tool (Tatem et al., 2000). By utilizing information contained in surrounding pixels, the land cover within each pixel is mapped using a simple spatial clustering function coded into a Hopfield neural network. The BP neural network model obtains the classification results by adjusting the network topology and training initial classification images (Merten et al., 2003a). Another model combines the wavelet coefficients with the neural network to process the classification in different dimensions (Mertern et al., 2004). There are other models, such as the Markov random field-based model (Kasetkasem et al., 2005), and the model based on genetic algorithms (Merten et al., 2003b).

2.2 Multiple Classifier System for Remotely Sensed Images Classification

2.2.1 Image Classification Methods in Land Use Inventory

Land cover classification is one of the most important and typical applications in remote sensing (Zhang et al., 2008; Tang et al., 2005; Andrew et al., 2001). Such classification includes ground surface cover classes, such as forest,

grassland, and water. At present, the category of classification can be classified into supervised or unsupervised classification, and its methods include 1) Statistical Methods, 2) Neural Network Methods, 3) Fuzzy Classification etc. And in each kind of methods, there are a lot of detail offsets, such as Maximum Likelyhood Classification, Minimum Distance Classification, K-mean Clustering method, Markov Random Field method etc. Among them, some methods are good at a certain data situation, and others are good at other certain data situation. In all, no one classification method prevails on all kinds of remotely sensed images.

One of research focus in image classification is to improve accuracy of classification either for high resolution images (such as Ikonos satellite images or aerial photographs), or medium resolution satellite images (such as Landsat satellite images). For high resolution satellite image classification, multilevel context-based system (Bruzzone and Carlin, 2006) and 'background-interior-boundary' approach (Gamba et al., 2007) are applied to improve the image classification. Tseng et al. (2008) proposed a rule-based classifier to automatically determine knowledge rules for remote sensing land cover classification. Other researchers have used texture measures to increase land cover classification accuracy (Shih and Schowengerdt, 1983; Lee and Philpot, 1991; Jakomulska and Stawiecka, 2002; Berberoglu et al., 2007). Multiple classifier system is another type of classification method which is talked about a lot in recent years to improve the classification accuracy (Fumera and Roli, 2005; Xu et al., 1992; Kittler et al., 1998).

2.2.2 Multiple Classifier System

The research on multi-classification system arose during 1990's, especially focusing on scientific communities, such as information fusion, machine learning, neural networks, pattern recognition, and statistics. Josef Kittler and Fabio Roli initiate the International workshop on Multiple Classifier Systems from 2000. The year of 2005 seems the turning point that the application of MCS begin to be specific to a certain application field. In MCS 2009, the application is specific to remote sensing.

Multi-classification System can also be named such as combination of multiple classifiers, classifier fusion, mixture of experts, committees of neural networks, consensus aggregation, composite classifier system or classifier ensembles etc. It is supposed that the components of multi-classification system can attain a different degree of success, but no one is totally perfect. However, the combination of several complementary classifiers will improve the performance of individual classifiers.

Generally, to decide a multi-classification system, there are two main steps, first to select the number and type of individual (primary) classifiers or classifier ensembles; second to decide the fusion algorithms or combination rules. With the combination rules and algorithms, multi-classification system can finally build up.

The concept of Multiple Classifier System (MCS) is based on the assumption that different types of classifiers complement in terms of classification

performance (Fumera and Roli, 2005; Xu et al., 1992; Kittler et al., 1998). Given this assumption it appears reasonable to integrate the often conflicting classification results from individual classifiers of identical images, so that, in the ideal case, strengths of each method can be enhanced and weaknesses eliminated. For example, classifier *A* has advantage on classifying certain classes, so if the pixel belongs to those classes, the classifier *A* can strengthen the classification for this class *A*, otherwise, it can weaken the classification for other classes. Thus, MCS provides a means to integrate the conflicting results from individual classifiers in classifying the same image by the different classifiers. The strengths of individual classifiers can be enhanced while the weaknesses of the individual classifiers can be reduced or even eliminated in the ideal situations. Generally, several rules are used to combine the outputs from each of the classifiers, the purpose of combining multiple classifiers being to generate the best classification output. After Xu et al. (1992) suggested combing the three classifiers, many researchers proposed several different combination rules by using the sum rule or the product rule (Woods et al., 1997; Steele, 2000; Fumera and Roli, 2005).

The objective of combining a set of classifiers, is thus, to achieve a higher accuracy than the accuracy of the best individual in the set. There are generally two types of combinations: classifier selection and classifier fusion. Classifier selection is based on the assumption that the most suitable classifier is chosen to match the needs of a specific class or classes. Classifier fusion assumes that all classifiers are trained to cover all classes and are thereby considered as competitive rather than complementary. Wilkinson (2005) has compared with

different types of classification method such as neural network method and non-neural methods.

According to Ho et al., (1994) a combination of classifiers was, in general, a good strategy to improve pattern recognition systems accuracy. Xu et al. (1992) suggested combining three classifiers and Steele (2000) combined two classifiers using a sum and a product rule which takes the sum or product of posterior probabilities (based on the producer accuracy) for all classifiers. An improved accuracy of 64% from an initial 61%, was achieved. Mesev et al. (2001) noted that standards per pixel classification were as accurate as textural and contextual methods and also as accurate as those acquired by the use of fuzzy datasets, providing the pixels were adequately trained. They suggested using ancillary GIS data as well as ways of improving the accuracy of maximum likelihood classification, in order to improve the accuracy of MCS.

Huenupan et al. (2008) proposed a method for combining multiple classifiers by applying Bayes-based confidence measures. This combination method has lead to an equal error rate (EER) reduction of 37% in speaker verification. Woods et al. (1997) presented a method for combining classifiers, by using an unknown test sample to estimate individual classifier's local accuracy, in small regions. Briem et al. (2002) applied bagging algorithms, boosting algorithms, and consensus-theoretic classifiers to combine multi-source remote sensing and geographic data to improve the accuracy of land cover classification. Fumera and Roli (2005) presented a theoretical and experimental analysis of linear combiners for multiple classifier systems. The analytical result was extended to

the case of correlated error, through a numerical analysis. Melnik et al. (2004) examined a combination method for small groups of classifiers with large numbers of classes.

Different classifiers generate different classification results, from the same satellite images. The classification results contain errors from a variety of sources, such as working approaches, the use of different assumptions or the nature of classes associated with each classifier. Assuming that these classes are spectrally distinct, it is likely that in the heterogeneous urban and semi-urban landscape classification accuracy (Gorokhovich and Voustianiouk, 2006) will be compromised by the coarse resolution of the sensor, owing to a large number of mixed pixels, because , in general, the pixel size is larger than the extent of landscape objects. Such mixed pixels would be allocated to a class whose spectral signature is the average of a pixel's constituent cover type. Sharper boundaries are not seen between cover types, although the linear spectral unmixing approach permits knowledge of the class content of each pixel, the reason being that the class location within each pixel is unknown. Additionally, classification of mixed pixels is computationally intensive as these mixed pixels must be assigned a particular class The available per-pixel classifiers have different methods for computing pixel assignments and some may be more successful than others at setting the spectral class boundaries, in order to accommodate varying mixtures of cover types.

2.3 Sample Strategy for Accuracy Assessment of Image Classification

The objectives of accuracy assessment include describing classification error

based on an error matrix and the spatial pattern of classification errors, comparing different mapping techniques and classification schemes etc (Stehman, 2000).

When describing the classification accuracy of remotely sensed image, it is impossible to survey every pixel, so sample is definitely necessary for this procedure. A sampling design is the procedure for employing sampling strategies to estimate and predict the characteristics of a population (Cochran, 1977), where a sampling strategy is the means to choose samples from the population. If it is designed as completely and appropriately, it can reflect the real situation, otherwise it is either cannot reflect the real situation of population, or it only reflects the bias situation of a population because the sample individuals are not enough representatives.

Sample size is also very important in a sampling design. We can not sample all the individuals from the population, but we have to sample necessary amount of individuals from the population, so that they can portray the real situation of the population. From the cost point of view, we should make the cost maintain the least, which means we need reduce the sample size as much as possible and make the unit cost for each sample units smaller. On the other hand, sample size should be large enough so that the analytical result has the statistical characteristics, while the redundant sample individuals can be removed out so that we can save the cost.

Consequently, we need to decide the sample strategy and sample size when

design a sample scheme to assess the accuracy of image classification. Traditional sample strategies have been researched and used in many other research fields, even a lot has been applied in our research field. However, with the specific characteristics of spatial data, there will be actually a lot of spatial sample methods for spatial data, such as for remotely sensed image.

2.3.1 Traditional Sampling Strategies

Traditional sampling strategies are mainly designed based on the probability (Stehman, 1999). In conventional sampling programmes, sampling strategies such as random sampling, stratified sampling, systematic sampling or hot-spot sampling are commonly used, depending upon sampling objectives and available resources.

Simple random sampling is the simplest probability sampling techniques. In statistics, a simple random sample is a subset of individuals (a sample) chosen from a larger set (a population). Each individual is chosen randomly and entirely by chance, such that each individual has the same probability of being chosen at any stage during the sampling process. Advantages are that it is free of classification error, and it requires minimum advance knowledge of the population other than the frame. Simple random sample may poorly choose in one area while over choose in other area without considering the inherent junction among areas, and result in significant biases.

Systematic sampling is a statistical method involving the selection of elements from a regular sampling frame. Each element in the population has a known and

equal probability of selection. It is explored assuming the given population is logically homogeneous, because the periodicity will threaten randomness. Systematic sample is also facing the situation which may over or under estimate the true accuracy, because the periodicity in errors confuses the sample procedure.

Stratification is the process of grouping members of the population into relatively homogeneous subgroups before sampling. Every element in the population must be assigned to only one stratum. Then random or systematic sampling is applied within each stratum. This often improves the representativeness of the sample by reducing sampling error. It can produce a weighted mean that has less variability than the arithmetic mean of a simple random sample of the population. Stratified random sample seemed be able to resolve the above problem, there still are other problem, because some reference data are difficult to be assessed and collected, or the cost to obtain such data are very expensive.

Clustering sample is also been used to assess the accuracy, which is sensitive to the cluster size, because of the spatial autocorrelation of the features between cluster range. Generally the cluster is in the form of pixel block, linear arrangement, aerial photo etc, where these polygon aggregations consist of several pixels. On the basis of whether think the cluster itself or the pixels within the clusters as the sample units, we can classify the cluster sampling into two categories, namely one-stage cluster sample and two-stage cluster sample. Clustering sample is cost-effective and its spatial control is very high. However,

the unequal probabilities of the selection for SSUs result that the estimation formulas are complicate to assess. So a compromise limitation should be regulated to solve this problem.

To look for the balance between the statistical variability and practical operation, many other sample schemes have been addressed, such as the combination of random and systematic sample etc. However, we can choose adapt sample strategy aiming at a certain data style, because there are some inherent flaw of each sampling strategy.

2.3.2 Spatial Sampling Strategies

In designing a sampling method we need to consider the following issues (a) variance, (b) sample size and (c) the dispersion variance. exisitng sampling techniques cover a relationship between the variance of the population estimate, the sampling size and sampling scheme (Cochran, 1977; Journel and Huijbregts, 1978; Griffith, 1988; Haining, 1990; Ronald, 2006).

Spatial sampling methods are a further development from the classic sampling techniques (Cochran, 1977) where the advance in the latest research on spatial statistics (Dunn and Harrison, 1993) is applied. In a spatial sampling, the location of the sample is related to the spatial distribution of the graphic objects of the population, this is a difference between spatial sampling methods and the classical sampling methods. The spatial distribution of the samples and correlation between the samples are used to estimate variance and sample support related information (Congalton, 1988).

Based on the spatial sample distribution and correlation, a good sample design can efficiently estimate the mean, covariance function, or prediction of values at unsampled sites (Fotheringham et al. 1996; Bellehumeur and Legendre 1997; Zhu and Zhang, 2006). The emphasis of the spatial sample design varied with the objectives of estimating the covariance function or predicting the characteristics of the population. For example, some optimal sample strategies were solely designed for estimating the covariance function (Bogaert and Russo, 1999; Muller and Zimmerman, 1999). Linear transects with exponentially spaced sampling locations is recommended by Pettitt and McBratney (1993) when they design the spatial sample strategy with the restricted maximum likelihood (REML) method. Further, Zhu and Stein (2005) estimated covariance parameters with maximum likelihood (ML) method and searched for optimal designs on a fine grid using an annealing algorithm among all possible designs. Generally in practice, parameter estimation and spatial prediction are analyzed at the same time with the same data set. Caselton et al. (1992), Banjevic and Switzer (2002), Wang et al. (2002), Wiens (2005), Zimmerman (2006), and Zhu and Stein (2006) have considered different aspect of this problem in recent years.

Due to the spatial correlation of the spatial data, it is difficult to explicitly design an optimal design for both estimation and prediction. However, the development of computing technology makes it possible to use a numerical approach to find optimal or near optimal sample designs. To find optimal sample design, a lot of technologies were applied. For example, the maximum entropy was employed by Ko et al. (1995); the simulated annealing algorithm

(SAA) was applied by Van Groenigen and Stein (1998), Lark (2002); furthermore, a two-step algorithm based on SAA was developed by Zhu and Stein (2006), which yields desirable designs for moderately large sample size.

3 Pixel Unmixing for Hyper-spectral Images

In this chapter, we propose our work on pixel unmixing for hyper-spectral image. Firstly, we improve the existing AMEE algorithm to make the component endmembers be extracted more reliably. Secondly, we apply the linear mixing model to generate abundances for the endmembers. We exclude some pure pixels by pre-judgment before applying the least squares method, which is more accurate and reduce the computation cost. Finally, we adopt the reliability-based sub-pixel mapping technology to appropriately locate all the component endmembers within a mixed pixel, by investigating the spectral correlation among pixels.

3.1 The Framework for Hyper-spectral Image Unmixing

Generally, a hyper-spectral image is with higher spectral resolution but lower spatial resolution. So we mainly make use of the spectral information to unmix hyper-spectral image. In this study, we assume that a mixed pixel is a linear combination of various endmembers and can be unmixed by the linear mixing model. Firstly, we introduce the existing AMEE algorithm, but further add with our own mathematical proof. Then we improve AMEE by proposing new solution for selecting better endmembers. Secondly, we carry out the pre-judgment on the pure pixels which is different from the routine computation involved in the least squares method. Finally, we present the concept of reliability on the basis of spectral correlation and locate all the endmembers within the space of mixed pixel. The logic flow of the algorithm is proposed as follows in Figure 3.1:

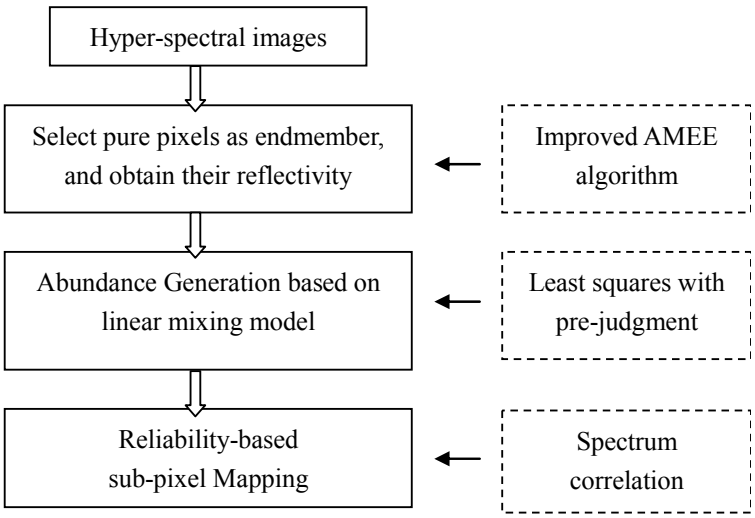

Figure 3.1 The logic flow of unmixing hyper-spectral images

3.2 Endmember Extraction

3.2.1 AMEE Algorithm

3.2.1.2 Existing AMEE Algorithm

Antonio Plaza et. al propose the AMEE (Automatic Morphological Endmember Extraction) algorithm in 2002, in which both the spectral information and the spatial information are considered. The basic assumption in AMEE is that the longer the spectral angle distance between two pixels is, the less similar the two pixels are. This principle is also applicable to the pixel's neighboring region, if the sum of the spectral angle distance between one pixel and other pixels is greater, it is more possible that the pixel is pure. Based on the mathematic morphology, AMEE algorithm extends two basic operations, dilation and erosion, from a binary image to a hyper/multi-spectral image. In a structuring element with some coordinates as its center, the pixel with the maximum sum of the spectral angle distances between itself and other pixels, is considered as the result of dilation, $\vec{d}(x, y)$. On the other hand, the pixel with the minimum sum

is marked as the result of erosion, $\vec{e}(x,y)$. Their definitions can be described as follows:

$$\vec{d}(x,y) = (\vec{f} \oplus K)(x,y) = \arg\_ Max_{(s,t)\in K}\{D(\vec{f}(x+s,y+t),K)\} \quad (3.1)$$

$$\vec{e}(x,y) = (\vec{f} \otimes K)(x,y) = \arg\_ Min_{(s,t)\in K}\{D(\vec{f}(x+s,y+t),K)\} \quad (3.2)$$

In Eq. (3.1) and (3.2), K is a structure element with its center (x,y) and $D(\vec{f}(x,y),K)$ is the sum of the spectral angle distances.

$$D(\vec{f}(x,y),K) = \sum_s \sum_t dist\{\vec{f}(x,y),\vec{f}(s,t)\}, \quad (s,t \in K) \quad (3.3)$$

Where, $dist$ is the spectral angle distance between two pixels.

According to the assumption of AMEE, the pixel as the result of dilation should be a pure pixel, i.e., an endmember. Morphological Eccentricity Index (MEI) is defined to describe the purity of the pixel as follows (Plaza et al., 2002; 2006):

$$MEI' = MEI + dist[\vec{d}(x,y),\vec{e}(x,y)] \quad (3.4)$$

Then we select a new coordinates as the center of a structuring element to compute new results of dilation and erosion and update the corresponding $MEIs$ if necessary. These operations are repeated and some of the candidate pure pixels update their $MEIs$ continually. The accumulate value is getting

greater and greater. To some extent, the greater a *MEI* of a pixel is, the purer the pixel is. If we traverse all the pixels in an image by the above operations, the set of *MEIs* of all the candidate pure pixels can be obtained. Next, we select the endmembers by analyzing all the *MEIs* .

To summarize the AMEE method, we describe the flow chart of AMEE algorithm in Figure 3.2:

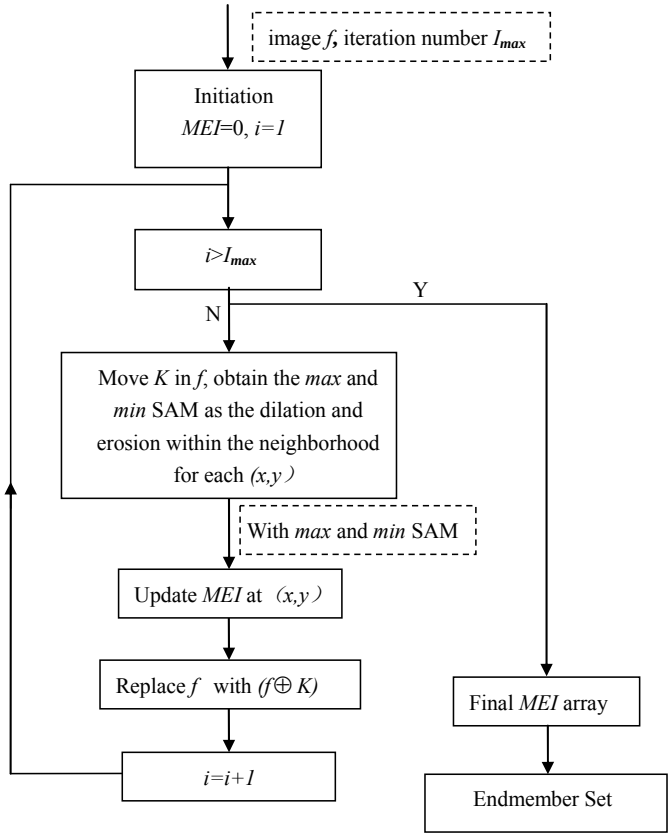

Figure 3.2 The logic flow of the AMEE algorithm

In the definition proposed by Plaza et al., the value of a *MEI* depends on the spectral angel distance between the pixel by dilation and the pixel by erosion. *K* is the size of a structuring element, *i* is the iterative parameter, and I_{max} is the

maximum number of the iterations. After we analyze the *MEIs* of all the pixels, we select the pure pixels as endmembers.

3.2.2 Proof for AMEE Algorithm

Although AMEE is designed with the assumption that the greater the spectral angle distance is, the more possible the pure pixel is an endmember. However there is no any mathematic proof to support this assumption in the early studies. Consequently, in the following, a rigorous proof for the assumption is one of the contributions to the improved AMEE.

It is assumed that one mixed pixel is composed of *m* endmembers, each of which is an *n*-dimension vector.

$$x = \sum_{i=1}^{m} r_i a_i \tag{3.5}$$

Where, $a_i = (a_{i1}, a_{i2}..., a_{in})$, $x = (x_1, x_2, ..., x_n)$ and $x_i = r_1 a_{1i} + r_2 a_{2i} + ... + r_m a_{mi}$. Let $dist(a_i, x)$ be cosine of the spectral angle distance between a_i and x . We now prove the relation between $dist(a_i, x)$ and r_i . In Eq. (3.6), $\langle \cdot, \cdot \rangle$ is the inner product,

$$dist(a_i, x) = \frac{\langle a_i, x \rangle}{|a_i||x|} \tag{3.6}$$

$$= \frac{(a_{i1}, a_{i2}, ..., a_{in}) \cdot (x_1, x_2, ..., x_n)}{\sqrt{a_{i1}^2 + a_{i2}^2 + ... + a_{in}^2}\sqrt{x_1^2 + x_2^2 + ... + x_n^2}}$$

$$= \frac{(r_1 a_{i1} a_{11} + \ldots + r_i a_{i1}{}^2 + \ldots + r_m a_{i1} a_{m1}) + \ldots + (r_1 a_{in} a_{1n} + \ldots + r_i a_{in}{}^2 + \ldots + r_m a_{in} a_{mn})}{\sqrt{a_{i1}{}^2 + a_{i2}{}^2 + \ldots + a_{in}{}^2}\sqrt{(r_1 a_{11} + r_2 a_{21} + \ldots + r_m a_{m1})^2 + \ldots + (r_1 a_{1n} + r_2 a_{2n} + \ldots + r_m a_{mn})^2}}$$

$$= \frac{r_1(a_{i1} a_{11} + \ldots + a_{in} a_{1n}) + \ldots + r_i(a_{i1}{}^2 + \ldots + a_{in}{}^2) + r_m(a_{i1} a_{m1} + \ldots + a_{in} a_{mn})}{\sqrt{a_{i1}{}^2 + a_{i2}{}^2 + \ldots + a_{in}{}^2}\sqrt{(r_1 a_{11} + r_2 a_{21} + \ldots + r_m a_{m1})^2 + \ldots + (r_1 a_{1n} + r_2 a_{2n} + \ldots + r_m a_{mn})^2}}$$

$$= \frac{\sqrt{a_{i1}{}^2 + a_{i2}{}^2 + \ldots + a_{in}{}^2}}{\sqrt{[(r_1 / r_i) a_{11} + (r_2 / r_i) a_{21} + \ldots + (r_m / r_i) a_{m1})]^2 + \ldots + [(r_1 / r_i) a_{1n} + (r_2 / r_i) a_{2n} + \ldots + (r_m / r_i) a_{mn})]^2}}$$

$$+ \frac{\sum_{\substack{j=1 \\ j \neq i}}^{m} r_j (a_{i1} a_{j1} + \ldots + a_{in} a_{jn})}{\sqrt{a_{i1}{}^2 + a_{i2}{}^2 + \ldots + a_{in}{}^2}\sqrt{(r_1 a_{11} + r_2 a_{21} + \ldots + r_m a_{m1})^2 + \ldots + (r_1 a_{1n} + r_2 a_{2n} + \ldots + r_m a_{mn})^2}} \tag{3.7}$$

Next we divide $\sum_{\substack{j=1 \\ j \neq i}}^{m} r_j (a_{i1} a_{j1} + \ldots + a_{in} a_{jn})$ into m items. Each item can be described as the following:

$$\frac{r_j (a_{i1} a_{j1} + \ldots + a_{in} a_{jn})}{\sqrt{a_{i1}{}^2 + a_{i2}{}^2 + \ldots + a_{in}{}^2}\sqrt{(r_1 a_{11} + r_2 a_{21} + \ldots + r_m a_{m1})^2 + \ldots + (r_1 a_{1n} + r_2 a_{2n} + \ldots + r_m a_{mn})^2}} (\mathrm{j} \neq \mathrm{i})$$

$$\leq \frac{r_j (a_{i1} a_{j1} + \ldots + a_{in} a_{jn})}{\sqrt{(r_1 a_{11} a_{i1} + \ldots + r_i a_{i1}{}^2 + \ldots + r_m a_{m1} a_{i1})^2 + \ldots + (r_1 a_{1n} a_{in} + \ldots + r_i a_{in}{}^2 + \ldots + r_m a_{mn} a_{in})^2}} \tag{3.8}$$

$$\leq \frac{r_j (a_{i1} a_{j1} + \ldots + a_{in} a_{jn})}{\sqrt{(r_j a_{j1} a_{i1})^2 + \ldots + (r_j a_{jn} a_{in})^2}} \tag{3.9}$$

$$\leq \frac{(a_{i1} a_{j1} + \ldots + a_{in} a_{jn})}{\sqrt{(a_{j1} a_{i1})^2 + \ldots + (a_{jn} a_{in})^2}} \tag{3.10}$$

In Eq. (3.8) and (3.9) among the deduction above, the results can be reduced or

enlarged by making use of the nonnegative property of the items in the product $r_1 a_{11} a_{i1}$. Consequently, the result in Eq. (3.10) has nothing to do with r. Therefore, r has the impact on the $dist(a_i, x)$ owing to the first item of Eq. (3.7). Therefore, it is clear that the value of the operator is greater when r_i is greater, which also demonstrates that the spectral angle distance between endmembers and mixed pixel is proportional to the ratio of the endmembers. Finally, the assumption in AMEE is held.

3.2.3 The Improved AMEE Algorithm

The final endmember set is mainly dependent on the strategy of selection from the set of *MEIs* of all the candidate pure pixels from AMEE. In other words, selecting candidate endmembers has a great impact on the correctness of the final endmembers. In our study, we consider that an *MEI* from a final endmember should be with the following characteristics: 1) the value of *MEI* should not be too large, otherwise some noise point may also be wrongly identified as endmembers; and 2) the variation between the selected *MEI* and other *MEIs* should not be too greater because the pure endmembers should be similar to the endmembers in the same local neighborhood. Thus reliable pure endmembers can be selected based on the two proposed rules above. Sequent steps will be followed based on the obtained *MEIs* as Figure 3.3.

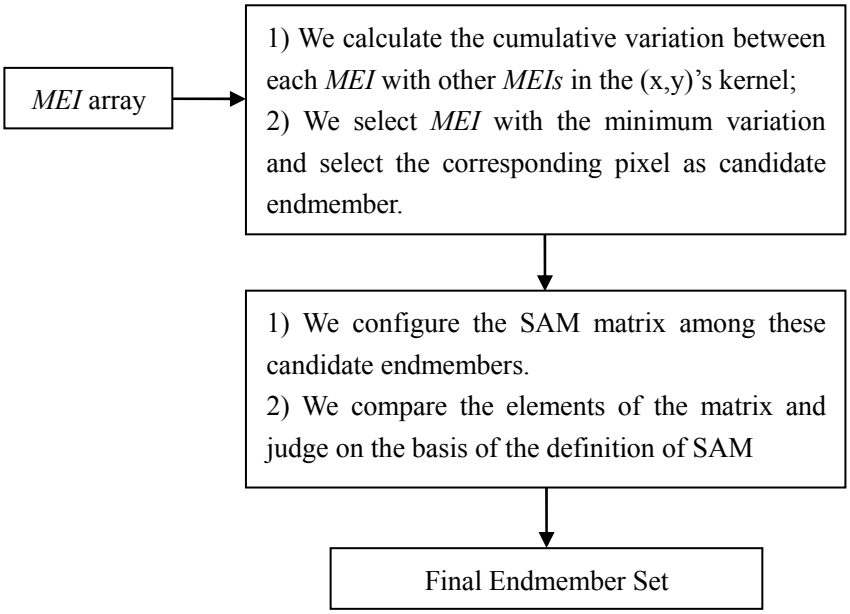

Figure 3.3 The logic flow of the improved AMEE algorithm

After we obtain the *MEIs* of all the pure pixels, the cumulative variation between each *MEI* with other *MEIs* within the same neighborhood should be calculated. The pixel with the minimum cumulative variation is selected as a candidate endmember. It is noted that this process is still not enough because we select redundant candidate endmembers. In order to guarantee the correctness of endmember extraction, we will take measures based on these candidate endmembers. Let N be the number of types of endmembers. The Improved AMEE algorithm is described in detail as the follows.

Step 1. Take the *MEI* of a pixel (x, y) as the center. For each *MEI*, we calculate the cumulative variation between *MEI* of center pixel (x, y) and the *MEIs* of other 8-neighboring pixels. Then we select the pixel with the minimum cumulative variation as one candidate endmember. By following the above operations, we obtain the set of candidate

endmembers.

Step 2. Calculate the spectral angle distance for each endmember candidate and build the symmetric spectral angle matrix D by making use of these spectral angle distances of all the candidate endmembers.

Step 3. Select the maximum element D_i in D. The two candidate endmembers corresponding to D_i are selected as two endmembers, denoted by a_1 and a_2. The spectral angle distances of D_i in D are then reset to 0.

Step 4. Select the next maximum elements D_j in D. The two candidate endmembers corresponding to D_j are considered as quasi endmembers. Then we will evaluate the spectral angle distances between a_1, a_2 and the two quasi endmembers respectively.

Step 5. Let T be the threshold of the spectral angle distance. If the spectral angle distance between two quasi endmembers and the selected endmembers are larger than T, we consider two quasi endmembers as the endmembers that should be selected. Otherwise, the quasi endmembers can not be selected as the endmembers. The spectral angle distances of D_j in D are still requested to rest to 0 if not enough endmember has been extracted. Here T is an experimental value, which depends on total number of kinds of endmembers.

Step 6. Repeat step 4 and 5 to find all endmembers and output the endmember set.

3.2.4 Experiment and Analysis

The expected endmembers will be extracted based on above Steps. To compare the experiment result, we first apply the AMEE algorithm, which selects endmember candidates with maximum *MEI* value within a local area, and selecting from maximum value to minimum value. Figure 3.4 is the result of endmember extraction with AMEE algorithm. Improved AMEE method is applied and the result is showed from Figure 3.5 to Figure 3.6.

Shown in Figure 3.4 and Figure 3.5, five types of endmembers are water, highway, building, grassland, and vegetation. In the final endmember image, water, highway, building, grassland, and vegetation are denoted by green, blue, pink, azury, and red colors respectively.

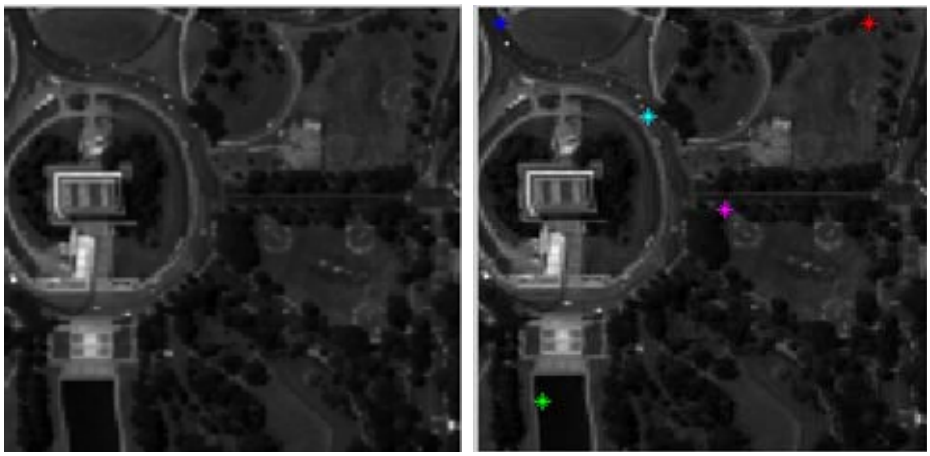

(a) Original image (b) Endmember image

Figure 3.4 Experiment of endmember extraction by AMEE

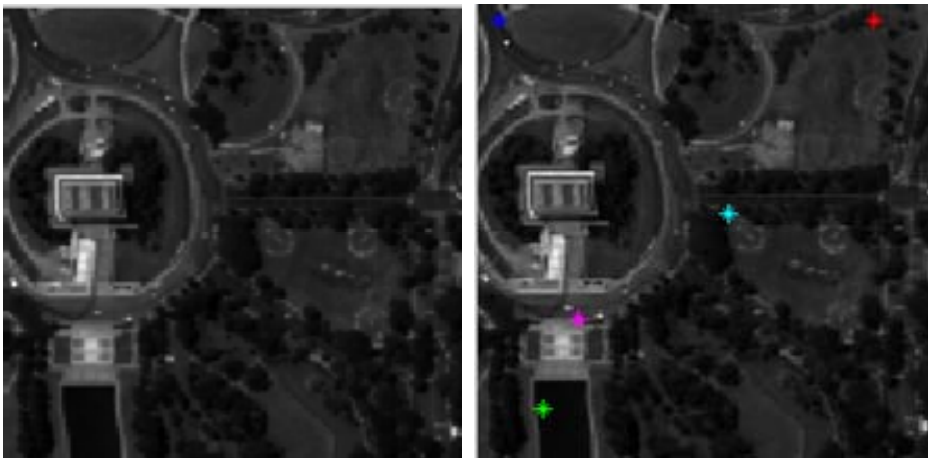

(a) Original image (b) Endmember image

Figure 3.5 1st Experiment of endmember extraction by Improved AMEE

From the above experiments, it can be seen that the endmember representing "building" is incorrectly selected and the endmember representing grassland locates its boundary and is not representative enough. On the contrary, all types of endmembers are identified successfully and satisfied results are obtained by applying the Improved AMEE algorithm, moreover, there is no incorrect endmember can be observed from the result.

To validate the improved AMEE algorithm, more experiments from Data 1 and Data 2 are showed in Figure 3.6 and Figure 3.7 respectively. These data are all hyper-spectral AVRIS image, including 224 continuous spectrum with the wavelength from 400~2500nm. The spatial resolution is 20m. The size of the data in the experiments are all 191*128*128, namely 191 bands, where the wavelength is between 0.40129 nm to 2.4732 nm, and the image size of each band is 128*128. In Data 1, there are land covers of water, shrub, grassland and road etc. In Data 2, there are mostly water, shrub, mud road, concrete road,

grassland and building etc.

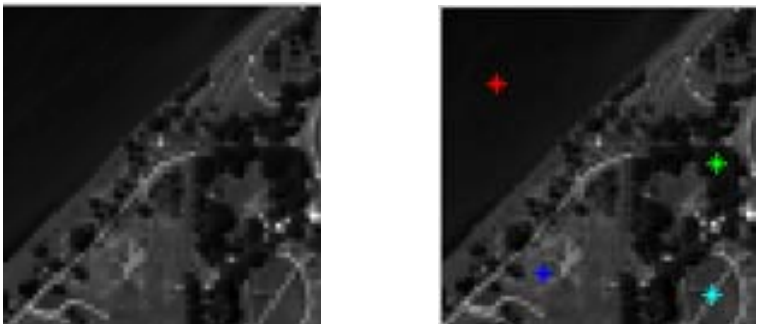

(a)Original image (b)Endmember image

Figure 3.6 2nd Experiment of endmember extraction by Improved AMEE

In Figure 3.6(b), we can find the water, grassland, shrub and road are evidently identified from the image and are depicted in red, blue, green and azury.

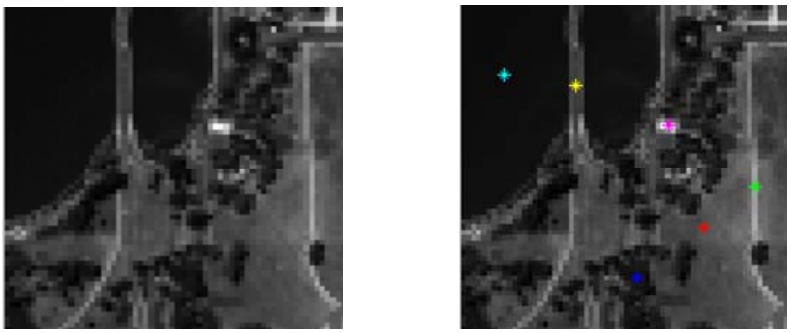

(a)Original image (b)Endmember image

Figure 3.7 3rd Experiment of endmember extraction by Improved AMEE

Similarly, there are much more endmembers we should extract from the image, including water, grassland, shrub, mud road, concrete road and building. In Figure 3.7(b), we see the endmembers are all identified properly and represented in azury, red, blue, yellow, green and pink respectively.

3.3 Abundance Generation

Normally, the next step in the process of unmixing mixed pixels is to determine the proportion of each endmembers within the mixed pixel after the types of all the endmembers within the mixed pixel are identified. The linear mixing model is used to generate the abundance of each endmember.

3.3.1 Linear Mixing Model

The basic assumption in the linear mixing model is that a mixed pixel is a linear combination of several pure ground objects (endmembers) with their corresponding proportions. The spectral reflectance of some pixel at each spectrum is denoted by the linear combination of the reflectance of the component endmembers with their corresponding abundances, i.e., the spectral reflectance of a pixel at the i^{th} band can be denoted by Eq. (3.11)

$$x_i = \sum_{j=1}^{m} r_{ij} a_j + e_i \tag{3.11}$$

Where, x_i is the spectral value of a pixel at the i^{th} band, m is the total number of endmembers, r_{ij} is the reflectance of the j^{th} endmember at the i^{th} band, a_j is the abundance of the j^{th} endmember, and e_i is the error at the i^{th} band. The abundance computation should be under two constraints: the sum-to-one constraint and the positive constraint, i.e., $\sum_{j=1}^{m} a_j = 1$ and $a_j > 0, j \in (1,...,m)$ (Hu et al. 1999) (Heinz and Chang, 2001). Let n be the number of bands. The linear mixing model can be described by the matrix in Eq.

(3.12):

$$X = RA + E \tag{3.12}$$

where, X is the $n \times 1$ received pixel spectrum vector, R is the $n \times m$ reflected radiation of each component endmember in n bands, A is the $m \times 1$ abundance vector, E is the $n \times 1$ additive observation error vector.

Abundance generation in the linear mixing model is the process of solving the abundance vector A when the additive observation error vector E is minimized. Given the spectrum vector X and obtained the matrix R after endmember extraction, therefore, we can generate the abundance matrix A by solving the linear simultaneous equations at each band with the least squares method.

3.3.2 Abundance Generation with Pre-judgment

The least squares method is widely used and the results for abundance generation are also fairly correct. However, we sometimes find mistakes when calculate the percentages of endmembers with the least squares method. The reason is that all the endmembers involved are constrained and compromised with each other to obtain the objective that total error is minimized. In other words, if the pixel is pure enough but we still involve all the endmembers in the least squares method, the results will be not right, i.e., we regard a pure pixel as a mixed pixel. Therefore, we carry out a pre-judgment before we apply the least squares method to generate abundances. This pre-judgment excludes pure pixels

from the image and only mixed pixels are left for the least squares method-based data processing. By this way, we can make abundance generation more reasonable and also reduce the computation cost. During the pre-judgment, we consider both the impact from the pixels themselves by estimating whether a pixel is pure or not, and the impact from its spatial correlated pixels.

We introduce two relation matrixes to estimate whether a pixel is pure or not. We define the relation matrix D^1 as the matrix with each element as the cosine of the spectral angle distance between an objective pixel and every extracted endmember. We refer to the relation matrix D^2 as the matrix with each element as the sum of the cosine of the spectral angle distances between the pixels in the objective pixel's 8-neighboring region and an endmember. From the proof in section 3.2.2, we know that the greater the spectral angle distance between two pixels is, the less similar two pixels are. Here, we expect that an objective pixel is related with one endmember in the way that the spectral angle distance is as smaller as possible, where zero is the best. That is also the reason why we select the cosine as the element in the relation matrixes.

If the element in D^1 between an objective pixel and the k^{th} endmember is greater than the threshold T_1, and the corresponding element in D^2 is also greater than the threshold T_2, we consider the objective pixel is very similar with the k^{th} endmember. Thus the objective pixel is pure and belongs to the k^{th} endmember category. The abundance is obtained directly with 100%. Otherwise, the objective pixel is considered as a mixed pixel and should be involved in the least squares method.

After the pre-judgment, we focus on mixed pixel and first select two component endmembers, which are correspond to the largest two elements in D^2. We apply the least squares method to generate the abundance with an error e. If e is smaller than the threshold T_3, the unmixing is completed. Otherwise, we determine the third component endmember by finding the 3^{rd} largest element in D^2, and include all three endmembers into the linear simultaneous equations. We repeat the process until the error is smaller enough. The logic flow is described as follows in Figure 3.8:

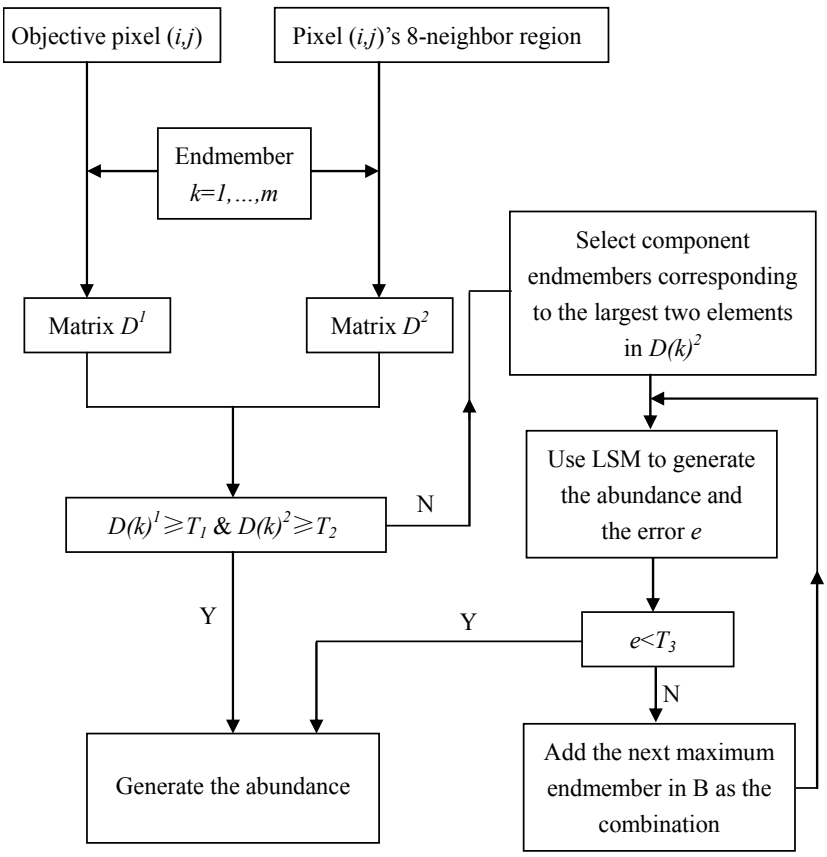

Figure 3.8 The logic flow of abundance generation with pre-judgment

In our study, the least squares method is not only under the sum-to-one

constraint and the positive constraint, but also to consider the spatial correlation among pixels. The pure pixels are excluded from the solving of the least squares method and only mixed pixel are involved. Therefore, pre-judgment before applying the least squares, makes the results of unmixing better and the computation cost reduced. Accurateness of abundance can obviously improve the quality of sub-pixel mapping later.

3.3.3 Experiment and Analysis

3.3.3.1 1st Experiment

Based on the endmember extraction, there are four categories of endmembers, including water, grassland, shrub and road on the image below. We take four pixels on the image as examples to unmix the pixels and generate the abundance as follows.

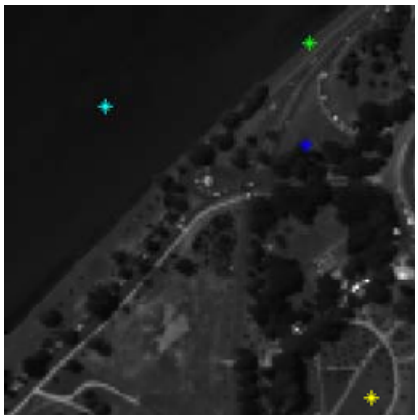

Figure 3.9 1st Experiment of Abundance Generation

In Figure 3.9, there are four pixels locating at (95,12), (32,32), (94,44), (114,122) highlighted with green, azury, blue and yellow. We call them pixel 1, 2, 3 and 4, then we will use linear mixing model to unmix them. Each abundance matrix is

denoted by $A = \begin{bmatrix} ratio\ of\ lake \\ ratio\ of\ grassland \\ ratio\ of\ shrub \\ ratio\ of\ road \end{bmatrix}$.

Before unmixing the mixed pixel with the least squares method, we try to apply pre-judgment to exclude pure pixels. After, we can judge that pixel 2 and 4 is pure, and they belong to water and grassland respectively. Therefore, the abundance of water is 100% in pixel 2; and the abundance of grassland is also 100% in pixel 4.

Then we use least squares method to unmix pixel 1 and 3, we find they are both the combination of two materials. Pixel 1 is mixed by water and grassland, with the abundance matrix $A_1 = \begin{bmatrix} 39.36\% \\ 60.64\% \\ 0.00\% \\ 0.00\% \end{bmatrix}$; Pixel 3 is mixed by grassland and shrub, with the abundance matrix $A_3 = \begin{bmatrix} 0.00\% \\ 85.52\% \\ 14.48\% \\ 0.00\% \end{bmatrix}$.

3.3.3.2 2nd Experiment

Based on the endmember extraction, there are six categories of endmembers, including lake, grassland, shrub, mud road, concrete road and building on the image below. We also take four pixels on the image as examples to unmix the pixels and generate the abundance as follows.

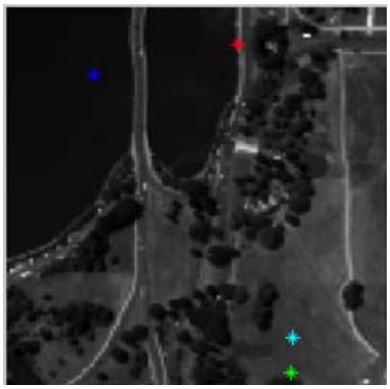

Figure 3.10 2nd Experiment of Abundance Generation

In Figure 3.10，there are four pixels locating at (13,78), (30,23), (112,97), (124,96) highlighted with red, blue, azury and green. We also call them pixel 1, 2, 3 and 4, then we will use linear mixing model to unmix them. Each abundance matrix is denoted by $A = \begin{bmatrix} ratio\ of\ lake \\ ratio\ of\ grassland \\ ratio\ of\ shrub \\ ratio\ of\ mud\ road \\ ratio\ of\ concrete\ road \\ ratio\ of\ building \end{bmatrix}$.

Similarly, we find the pixel 2 and pixel 3 are pure pixels based on pre-judgment, and they belong to water and grassland respectively. Therefore, the abundance of water is 100% in pixel 2; and the abundance of grassland is also 100% in pixel 4.

We find they are both the combination of two materials when we use least squares method to unmix pixel 1 and 4. Pixel 1 is mixed by water and concrete

road, with the abundance matrix $A_1 = \begin{bmatrix} 64.74\% \\ 0.00\% \\ 0.00\% \\ 0.00\% \\ 35.26\% \\ 0.00\% \end{bmatrix}$; Pixel 4 is mixed by grassland and shrub, with the abundance matrix $A_4 = \begin{bmatrix} 0.00\% \\ 49.08\% \\ 50.92\% \\ 0.00\% \\ 0.00\% \\ 0.00\% \end{bmatrix}$.

3.4 Sub-pixel Mapping

3.4.1 The Reliability-based Sub-pixel Mapping

After endmember extraction and abundance generation, the next step is sub-pixel mapping, which is based on the known component endmembers with their corresponding proportions. The assumption of sub-pixel mapping technology is that there is a correlation among the sub-pixels with closer distance. In a hyper-spectral image, there is a spectral correlation among sub-pixels, and this characteristic can be used as the measurement of reliability for sub-pixel mapping.

Firstly, a pixel in an original image can be divided into 4 sub-pixels, or 9 sub-pixels, even smaller ones. However, we divide each pixel into 4 sub-pixels in this study to ensure the accuracy. On the other hand, it may also mean each mixed pixels is composed of 4 sub-pixels. Secondly, we calculate the spectral correlation between a sub-pixel and its 8-neighboring sub-pixels by using the

reliability as the measure of correlation. For example, there is a mixed pixels with two component endmembers, including a_1 and a_2. After the division, the mixed pixel with "gray 2" consists of four sub-pixels with "gray 2" as in Figure 3.11, where one of the sub-pixel is depicted by the combination of a_1 and a_2.

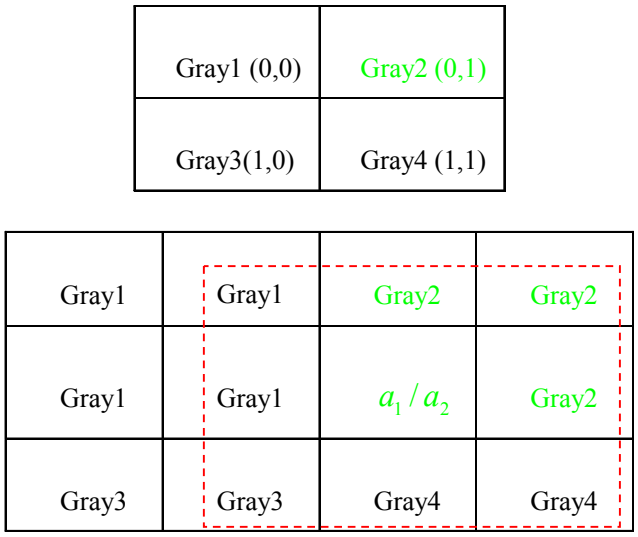

Figure 3.11 Reliability-based Sub-pixel Mapping

Secondly, we generally measure the reliability of each endmember in each sub-pixel in the order of their corresponding abundances. On the basis of above picture, we will provide detail steps of how to calculate the reliability for a sub-pixel as an example.

Step 1. Give the gray value of each sub-pixel by the gray value of the original mixed pixel.

Step 2. Take one of the sub-pixels as the objective sub-pixel and assign it as the component endmember a_1, which has a greater abundance. Then we calculate the mean of the gray values of the sub-pixels around the

objective sub-pixel's 8-neighboring region. Then we reset the gray to the mean value for the other three sub-pixels which belong to the same mixed pixel with the objective sub-pixel.

Step 3. Calculate the reciprocal of the sum of the variances of the grey values between the objective sub-pixel and the sub-pixels in the objective sub-pixel's 8-neighboring region. The reciprocal is marked as the reliability that component endmember a_1 can be filled at the objective sub-pixel. Then we fill a_1 into the other three sub-pixels and calculate the corresponding reliability. By this way, we can obtain the reliability matrix for filling component endmember a_1 into a certain mixed pixel in sub-pixel mapping.

Step 4. Repeat step 2 and step 3 by replacing component endmember as a_2. Then we can obtain the reliability matrix for filling component endmember a_2 into the same mixed pixel in sub-pixel mapping.

Whereafter, we compare the corresponding element in each reliability matrix after we obtain all the reliability matrixes of all the component endmembers. Then we assign the sub-pixel to the endmember with the largest reliability, usually following the order of endmembers' abundance, until the filling proportion is equal to its corresponding abundance. Note that we should mark the location of a mixed pixel after we fill it. This is because we avoid filling the location more than once.

Finally, we complete the procedure of sub-pixel mapping by repeating all the above steps for each mixed pixel.

3.4.2 Experiment and Analysis

We implement the experiments based on Data set 1 and Data set 2, including the comparison among the improved agent-based sub-pixel mapping method, our method and the interpolation method. The objective of this experiment is to prove the unmixing result of our method is good, so the strategy of the experiments can be explained as follows:

First, we obtain the unmixing result from the improved agent-based sub-pixel mapping and our reliability-based sub-pixel map and obtain an interpolation result from an interpolation method. Second, we configure comparable objects, which are the classified images by C-mean classification method on above three unmixing results. Thirdly, we compare the classification results with confusion matrixes, which described by the Kappa statistic and the overall accuracy. Finally, we compare the accuracy performance of the unmixing method with other methods.

The Improved Agent-based Sub-pixel Mapping (IASM) is based on the idea of converging similar endmembers to the center of a circle, defined by a pure endmember (Wu et. al, 2009). Firstly, the endmember with the maximum abundance in mixed pixels is selected as the initial land cover in the pixel p_1. The abundances of other sub-pixels in p_1's 8-neighboring region are then updated. How to update the abundances is one of the most important problems. If the pixel p_2 is one of the pixels in p_1' 8-neighboring region, the p_2's abundance is equal to the average abundances above all the weighted abundances in p_2's 8-neighboring region. The maximum one in the abundances

in p_1's 8-neighboring region is selected as the center of the mixed pixel. The objective is to investigate the arrangement trend of these kinds of endmembers so that the distances between the center of the circle and each sub-pixel in the mixed pixel, can be calculated and all the sub-pixels in the mixed pixel are ranked. From the sub-pixel with the minimum distance, the corresponding endmember is assigned to the sub-pixel until all the sub-pixels with the same endmember are filled. In this way, each endmember repeats the above procedure until all combinations in the mixed pixel find the correct locations. However, the ability of this method for unmixing is weak and if the granularity of the regressed image is smaller than 2*2 pixels, the results are even worse. In Figure 3.12, the simulation results show that IASM is more suitable for the round shape than for the rectangular shape. In addition, we also tested that IASM are not good for irregular shapes. However, most of the objects in natural world are irregular, so IASM has limitations.

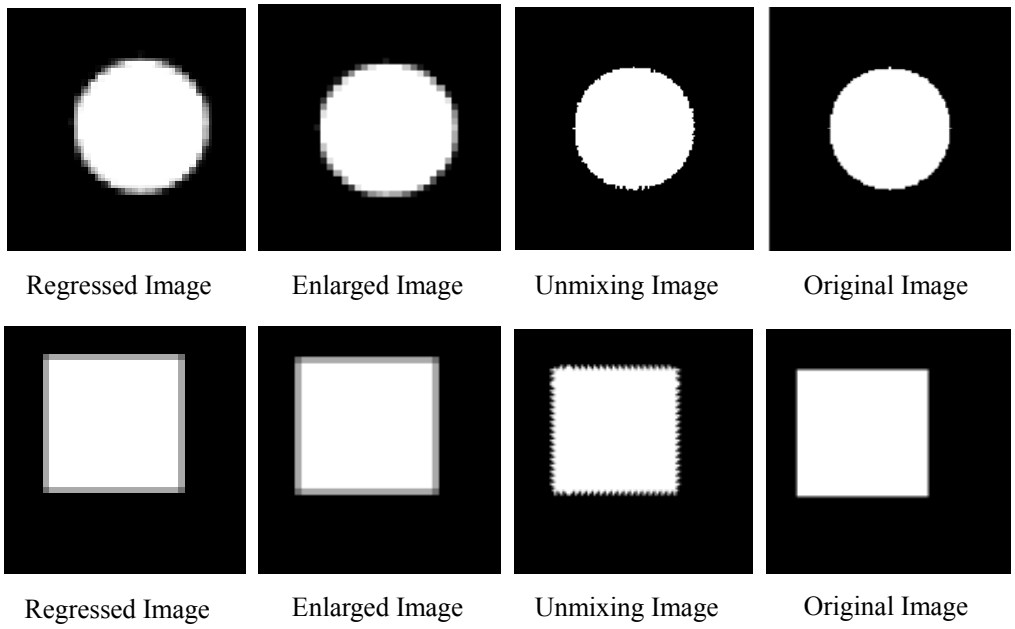

Figure 3.12 Experiments of converging to the center by Improved Agent-based Sub-pixel Mapping

This IASM method will be compared with our proposed method; in addition, we also introduce classical interpolation method as a comparison. As the sub-pixel mapping and interpolation will upgrade the resolution of the image to fourfold, before the experiments, we will degrade the original map and so that we can compare all the classification results from three methods with that of the same original image.

3.4.2.1 1st Experiment based on Data set 1

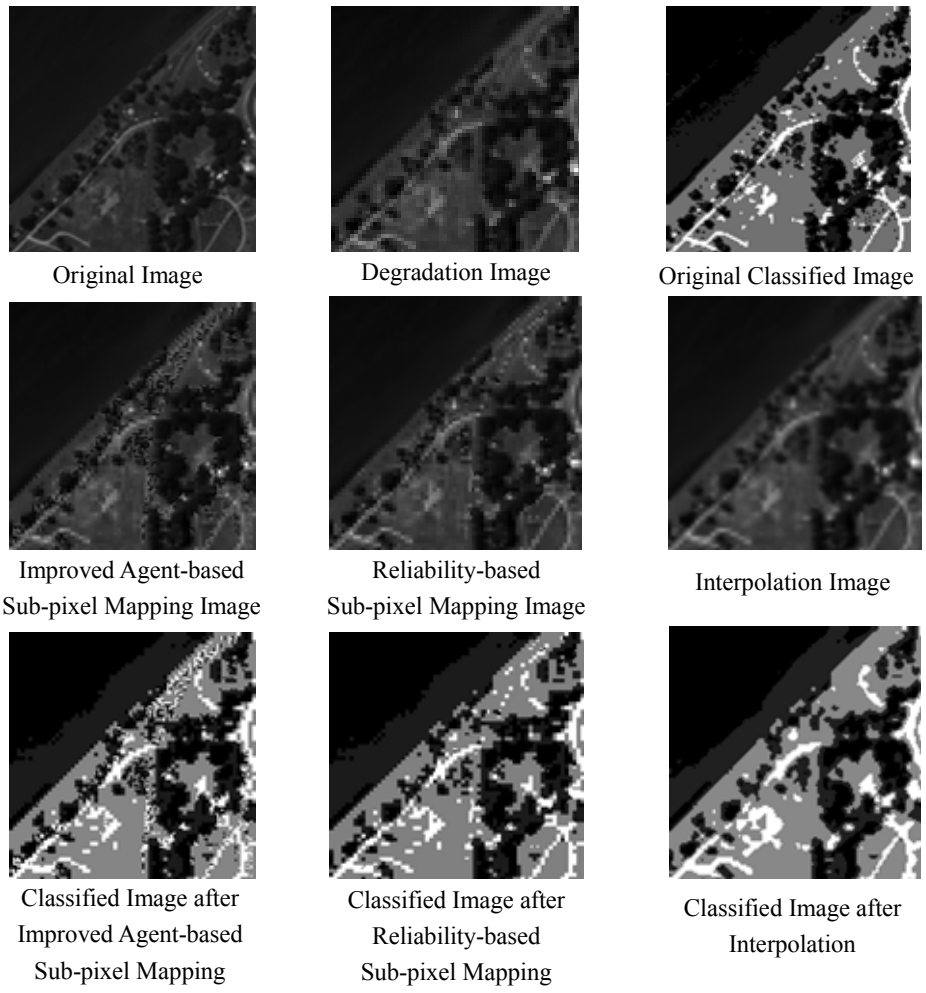

Figure 3.13 Unimproved Sub-pixel Mapping

From Figure 3.13, we can find that there are a lot of breaking points on the improved agent-based sub-pixel mapping image so that the unmixing result is

not good. As the endmembers are not appropriately located and the neighboring categories intercross to each other, so the classification map from this method is more fragmentized. The classical interpolation method applies the interpolation algorithm on the degraded image, while a lot of information has been lost so that the interpolation image is blurry and the classification image is coarse. In comparison, the unmixing result from our proposed method is more clearly and the most analogous to the original image. Meanwhile, the classification result is also finer and more accurate than other two and close to the original classified image.

Table 3.1 Confusion matrix of classified image after improved agent-based sub-pixel mapping

	Lake	Shrub	Grassland	Road	Total	User's accuracy
Lake	3962	671	311	10	4954	0.7998
Shrub	411	3468	345	0	4224	0.8210
Grassland	21	374	4744	177	5316	0.8924
Road	3	33	668	678	1382	0.4831
Total	4397	4546	6068	865	15876	
Producer's accuracy	0.9011	0.7629	0.7818	0.7838		Overall accuracy = 0. 8095
Kappa statistics						Overall Kappa = 0. 7297

Table 3.2 Confusion matrix of classified image after reliability-based sub-pixel mapping

	Lake	Shrub	Grassland	Road	Total	User's accuracy
Lake	3951	508	46	1	4506	0. 8768
Shrub	425	3613	394	0	4432	0. 8152
Grassland	20	415	5137	175	5747	0. 8939
Road	1	10	511	669	1191	0. 5617
Total	4397	4546	6088	845	15876	
Producer's accuracy	0.8986	0. 7948	0. 8438	0.7917		Overall accuracy = 0.8422
Kappa statistics						Overall Kappa = 0.7741

Table 3.3 Confusion matrix of classified image after interpolation

	Lake	Shrub	Grassland	Road	Total	User's accuracy
Lake	3908	855	0	0	4763	0. 8205
Shrub	472	3309	375	0	4156	0. 7962
Grassland	17	380	5105	114	5616	0. 9090
Road	0	2	608	731	1341	0. 5451
Total	4397	4546	6088	845	15876	
Producer's accuracy	0.8888	0. 7279	0. 8385	0.8651		Overall accuracy = 0.8222
Kappa statistics						Overall Kappa = 0.7466

In this accuracy assessment, there were a total 15876 pixels of ground reference data, including 4397 pixels for lake, 4546 pixels for shrub, 6088 pixels for grassland and 845 pixels for road. The amount of samples fulfills the sample size requirement for significance test. In addition, on the basis of Table 3.1 to Table 3.3, we draw a histogram Figure 3.14 to compare the accuracy of three methods. We find the overall accuracy and kappa value of the improved agent-based sub-pixel mapping method, the interpolation method and our proposed reliability-based sub-pixel mapping method are 0.8095, 0.8222, 0.8422 and 0.7297, 0.7466, 0.7741 respectively. Obviously, the kappa value of the proposed reliability-based sub-pixel mapping method is absolutely higher than other two methods, which prove the significance of the proposed method.

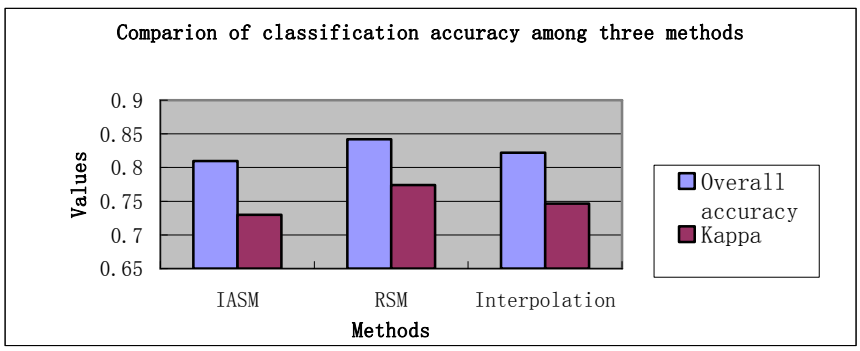

Figure 3.14 1st Comparison of Classification Accuracy among Three Methods

We can find the result drawn from our method improve 3% and 2% than interpolation method and improved agent-based sub-pixel mapping method for the overall accuracy; and almost improve 5% and 3% than the two methods for kappa value. So we can prove that the unmixing result of our method is better than the interpolation method and the improved agent-based sub-pixel mapping method.

3.4.2.2 2nd Experiment base on Data set 2

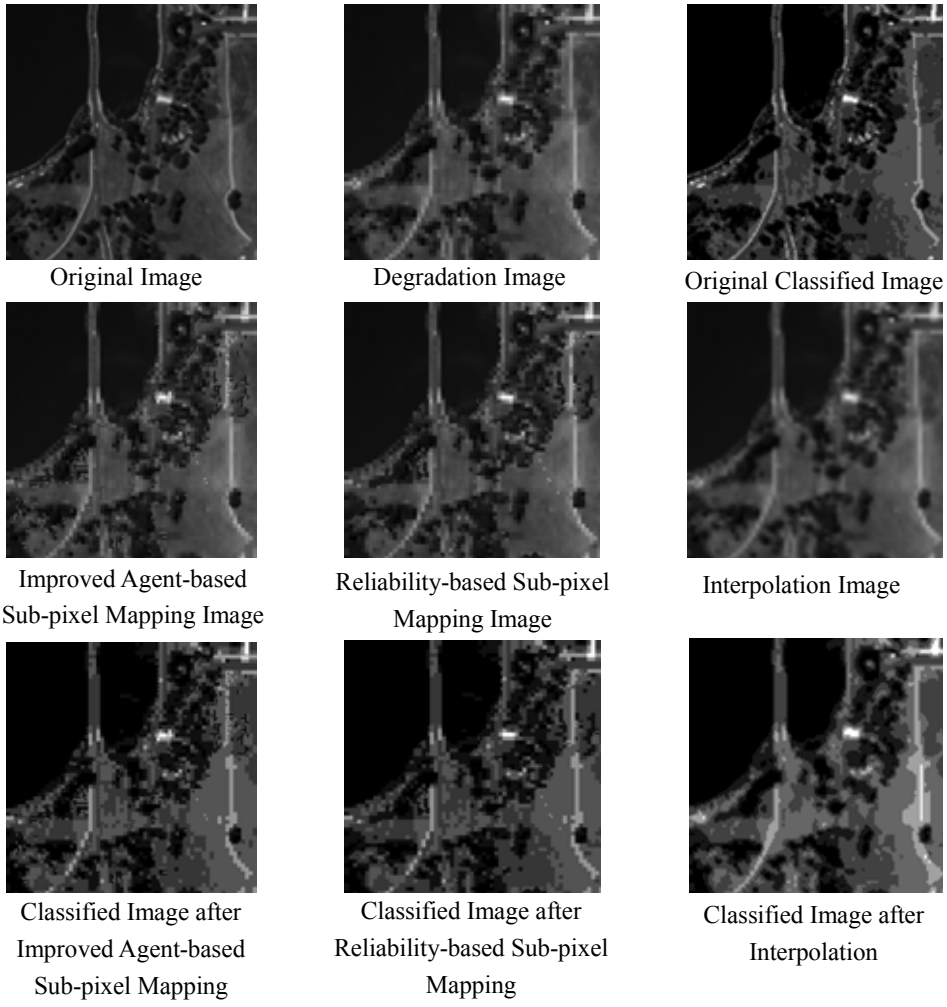

Figure 3.15 Unimproved Sub-pixel Mapping

From Figure 3.15, we can find that there are a lot of breaking points around

boundaries of land categories on the improved agent-based sub-pixel mapping image so that the unmixing result is not good. And the classification map from this method is more fragmentized. The classical interpolation method shows that a lot of information has been lost so that the interpolation image is blurry and the classification image is coarse. In comparison, the unmixing result from our proposed method is more analogous to the original image. Meanwhile, the classification result is also closer to the original classified image than other two.

Table 3.4 Confusion matrix of classified image after improved agent-based sub-pixel mapping

	Lake	Shrub	Mud Road	Concrete Road	Grassland	Building	Total	User's accuracy
Lake	5129	128	0	9	0	0	5266	0. 9740
Shrub	792	1405	8	466	79	1	2751	0. 5107
Mud Road	0	1	299	21	213	19	553	0. 5407
Concrete Road	106	453	14	2883	434	2	3892	0. 7408
Grassland	14	86	137	932	2722	1	3892	0. 6994
Building	0	0	8	0	4	18	30	0. 6000
Total	6041	2073	466	4311	3452	41	16384	
Producer's accuracy	0. 8490	0. 6778	0. 6416	0. 6688	0. 7885	0. 4390		Overall accuracy = 0.7603
Kappa statistics								Overall Kappa = 0.6789

Table 3.5 Confusion matrix of classified image after reliability-based sub-pixel mapping

	Lake	Shrub	Mud Road	Concrete Road	Grassland	Building	Total	User's accuracy
Lake	5126	125	0	6	1	0	5258	0.9749
Shrub	793	1447	5	551	100	0	2896	0.4997
Mud Road	0	1	307	21	219	16	564	0.5443
Concrete Road	118	458	30	3066	554	4	4230	0.7248
Grassland	4	42	114	667	2577	0	3404	0.7571
Building	0	0	10	0	1	21	32	0.6563
Total	6041	2073	466	4311	3452	41	16384	
Producer's accuracy	0.8485	0.6980	0.6588	0.7112	0.7465	0.5122		Overall accuracy = 0.7656
Kappa statistics								Overall Kappa = 0.6861

Table 3.6 Confusion matrix of classified image after interpolation

	Lake	Shrub	Mud Road	Concrete Road	Grassland	Building	Total	User's accuracy
Lake	5017	91	0	0	0	0	5108	0.9822
Shrub	956	1425	1	241	4	0	2627	0.5424
Mud Road	0	1	301	30	530	11	873	0.3448
Concrete Road	64	529	2	3035	473	0	4103	0.7397
Grassland	3	27	109	1004	2440	1	3584	0.6808
Building	1	0	53	1	5	29	89	0.3258
Total	6041	2073	466	4311	3452	41	16384	
Producer's accuracy	0.8305	0.6874	0.6459	0.7040	0.7068	0.7073		Overall accuracy = 0.7475
Kappa statistics								Overall Kappa = 0.6639

In this accuracy assessment, there were a total 16384 pixels of ground reference data, including 6041 pixels for lake, 2073 pixels for shrub, 466 pixels for mud

road, 4311 pixels for concrete road, 3452 pixels for grassland and 41 pixels for building. The amount of samples fulfills the sample size requirement for significance test. Furthermore, on the basis of Table 3.4 to Table 3.6, we draw a histogram in Figure 3.16 to compare the accuracy of three methods. We find the overall accuracy and kappa value of the IASM method, the interpolation method and our proposed method are 0.7603, 0.7475, 0.7656 and 0.6789, 0.6639, 0.6861 respectively. The kappa value of our proposed method is higher than other two methods, which prove the significance of the proposed method.

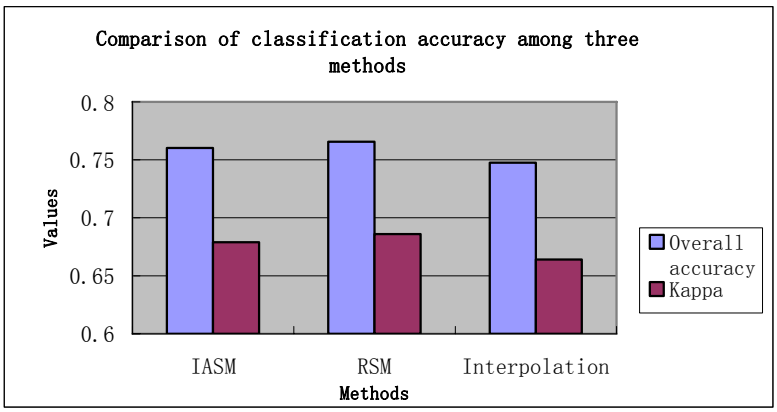

Figure 3.16 2nd Comparison of Classification Accuracy among Three Methods

The selection of classification method may be the reason why the classification accuracy is all low. However, the classification method has the same impact on three kinds of unmixing images, so the comparison is still valid in this situation. However, we can find the result drawn from our method is still better than other two methods. Therefore, we can prove that the unmixing result of our method is better than the interpolation method and the improved agent-based sub-pixel mapping method.

3.5 Summary

In this chapter, linear mixing model is applied in the proposed pixel unmixing for hyper-spectral remotely sensed images. Similar as most of the unmixing steps, we involve three steps for this work, including endmember extraction, abundance generation and sub-pixel mapping.

The first contribution of this research is the proof for the assumption of the AMEE algorithm and proposal of the improved AMEE algorithm, which improves the performance of endmember extraction. Based on the comparison experiment, we find the endmember has been accurately extracted than the original AMEE algorithm. The experimental results demonstrate that it has the capacity to produce an effective endmember sets.

The second contribution is, before applying the least squares method to compute the abundance of each endmember within mixed pixel, we propose pre-judgment to enhance the effect of least squares and reduce the computation cost. The experiments are carried out to prove the performance of the proposed idea and the improved efficiency than previous means.

Finally, we propose the reliability-based sub-pixel mapping for dealing with the unmixing problem at the level of sub-pixel. To address the validity, we conduct several experiments and collect enough amounts of samples to prove the significance of the proposal method. We introduce the classical interpolation method and improved agent-based sub-pixel mapping method, to compare with our method. The results show that our method has improved 3%-5% for the

classification accuracy, which means that our method has greatly improved the image quality. Therefore, it can be concluded that the newly proposed pixel unmixing method for hyper-spectral images is effective and significant.

4 Pixel Unmixing for Multi-spectral Images

In this chapter, we present a new idea different from the one used in hyper-spectral image unmixing. We unmix a multi-spectral image at single band level, and synthesize the unmixing results from each single band in order to obtain the final unmixing results. Firstly, we introduce the concept of mountain clustering to extract endmembers by finding the center of a category. Secondly, we use the existing gray correlation method to generate the abundance of each endmember. Thirdly, we improve the existing cellular automata model to carry out sub-pixel mapping defined by a specific evolution rule. Finally, we consider the spatial correlation among pixels to obtain the final unmixing result by multiband synthesis technology.

4.1 The Framework for Multi-spectral Image Unmixing

Similar with hyper-spectral image, there are mixed pixels in a multi-spectral image. The difference is that a multi-spectral image is short of spectral information, but with abundant spatial information. Consequently, with the same solution for unmixing a hyper-spectral image by building simultaneous equations to generate abundances for multi-spectral images is not pragmatic. Here, we propose a different strategy to unmix the mixed pixels for multi-spectral remotely sensed images.

We propose to first unmix a multi-spectral image at single band level, and then synthesize the separate results into the final unmixing results. There are four steps in our method as follows: 1) we build up mountain functions in an

iterative way and every time select the grid corresponding to the peak in the mountain function as the center of a category. We extract endmembers by finding these centers of categories; 2) based on above step, endmembers can be input automatically instead of manually at the beginning of abundance generation. Because there is the grey correlation among neighboring pixels, we compute the abundances of component endmembers at the central mixed pixel, according to the impact of the grey values of the pixels in central pixel's 8-neighboring region; 3) we improve the cellular automata model by modifying the evolution rules to carry out our sup-pixel mapping experiment in term of the spatial correlation among pixels; and 4) each single band of a multi-spectral image has been unmixed successfully and we synthesize the results through multiband synthesis technology to finish unmixing mixed pixels for multi-spectral images. The framework of unmixing multi-spectral images based on single band is describes in Figure 4.1:

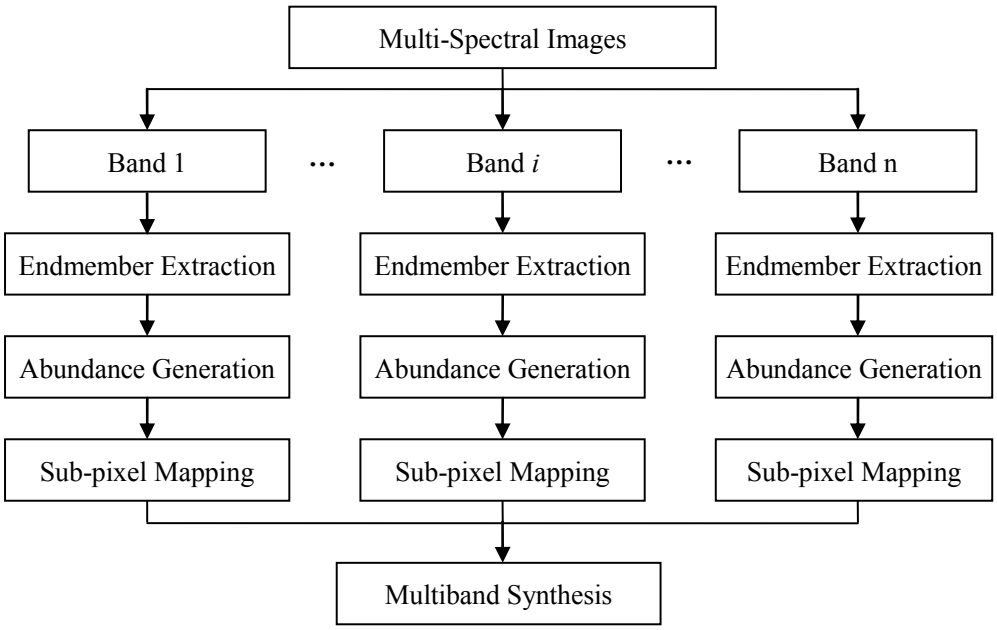

Figure 4.1 A framework for unmixing mixed pixel on single band images

4.2 Endmember Extraction

4.2.1 Mountain Clustering

Yager and Filev (1994) propose the mountain clustering, in which the corresponding grid at the peak value in the proposed mountain function is considered as the center of a category. After finding a center of a category, we rebuild the mountain function by removing the impact of the previous center of a category on the new center. We build up mountain functions in an iterative way until we find all the centers of the categories. In general, the more the data with closer grey values to the one at a category center are, the higher the peaks in a mountain function are. In other words, the ground objects that are mass and distinct in an image will be clustered easily, whereas the ground objects that are sporadic and blurry are not easy to be clustered.

In this section, we introduced the existing mountain clustering with 5 steps as follows. Step 1, we build up grids in the data space. The intersections of the grid lines are the candidate set of the category centers. In general, the more grained the grids are, the more members in the candidate set are and the more cost the computation is. Therefore, there is a trade-off between the grained level of a gird and the cost of computation.

Let Z^m be an m-dimension space. There are n data items in each dimension. Let $x_{i,j}$ be the i^{th} data item in the j^{th} dimension in Z^m, thus we have data set $X_j = \{x_{1,j}, x_{2,j}, ..., x_{n,j}\}$, where $i = 1,2,...,n$ and $j = 1,2,...,m$. Let I_j $(j = 1,2,...,m)$ be the range of grey values for the set X_j.

$$I_j = [\min_i(x_{i,j}), \max_i(x_{i,j})] \quad (i = 1,2,\cdots n; \quad j = 1,2,\cdots m) \tag{4.1}$$

Next, we divide the interval I_j into N_j individual intervals as Figure 4.2 shows.

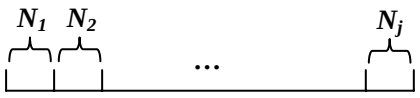

Figure 4.2 Sketch map for the grid of I_j

Let $f_j = (f_{j,1}, \cdots, f_{j,N_j})$ be the N_j individual intervals in I_j, where we have $f_{j,k} < f_{j,k+1}$ $(k = 1,2,\cdots N_j)$. We build up a hypercube $\mathrm{V} = \mathrm{I}_1 \times \mathrm{I}_2 \times \cdots \times \mathrm{I}_\mathrm{m}$ for all the elements in the data set X in n dimensions. Total number of such a hypercube is $N_V = N_1 \times \cdots \times N_j \times \cdots N_m$. The greater N_j is, the more grained the grid is and the more cost of computation is.

Step 2, we build up a mountain function according to the density of data items. The mountain function for the candidate center $v_i \in V$ can be presented by the following equation:

$$m_1(v_i) = \sum_{j=1}^{N_V} \exp(-\frac{||v_i - x_j||^2}{2\sigma^2}) \tag{4.2}$$

where V is the candidate set of the category centers, and x_j is an m-dimension vector to represent the j^{th} data item in the space V. The

quantity of contribution from x_j is monotony decreasing with the distance between x_j and the cluster center v_i. σ is a constant greater than 0, which varies with the applications and control the contribution of each data item to the peak $m_1(v_i)$. The smaller the parameter σ is, the more mountain peaks are.

Step 3, we need to find the peaks in a mountain function. We select the corresponding grid point at the peak as the center of a category. Let $m_1(v_1)$ be the mountain function with the highest peak, v_1 is the first center of a category. We have

$$m_1(v_1) = \max_i \{m_1(v_i)\} \tag{4.3}$$

Step 4, we remove the impact from the previous center of a category and rebuild the mountain function to select the next center of a category. The new mountain function is described as follows:

$$m_{1+k}(v_i) = m_k(v_i) - m_k(v_k) \times \exp\left(-\frac{||v_i - v_k||^2}{2\beta^2}\right) \tag{4.4}$$

where β is the parameter that is used to control the impact from the selected category center on the next category center. It should be selected carefully.

Step 5, we repeat the above steps until we find the centers of all the categories.

As an example, we do the experiment below in Figure 4.3 which explains the

procedure of peak pruning when the mountain function is configured in an iterative way.

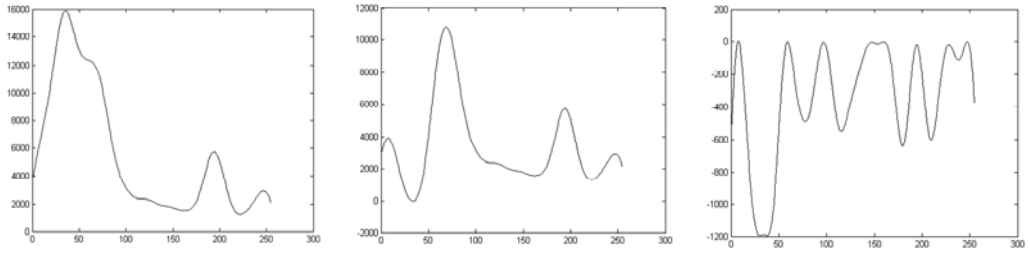

(a) Mountain function in the original image

(b)Mountain function after the first pruning

(c) Final mountain function after iterations

Figure 4.3 Mountain function with several clustering

4.2.2 Endmember Extraction based on Mountain Clustering

The mountain clustering is used to classify image based on the identified category centers. From the view of pixel unmixing, to find the category center is equal to find the pure pixel, which can be regarded as the representative endmember. From this point of view, the selection of category center is equal to endmember extraction. In addition, mountain clustering is a comparatively simple and effective way to cluster a category center, so we introduce the mountain clustering to extract endmember.

To remotely sensed image, the detail steps of endmember extraction based on mountain clustering is as follows:

Step 1. Build up a grid with 255 intervals, as the range of the gray values in a single band image is from 0 to 255, i.e., each gray level is considered as a grid point.

Step2. Define the mountain function at the grid points. After finding the first grid point corresponding to the highest peak in a mountain function as a center of the category, we rebuild a new mountain function to find the next center of a category by removing the impact from the previous center. Next we repeat the above operations until we find the centers of all the categories.

We note the fact that if we set a smaller σ, we can find more local maximums in the mountain function, which means more category centers can be found by clustering. Consequently, we can tune the value of σ according to the number of endmembers in an image. Moreover, we mentioned that if we set a smaller β, the impact from the previous category center is harder to be removed. Normally, we set the number of endmembers as the known number of category centers. If we do not set the number of endmembers, we can also obtain a satisfying number from the mountain function. For example, we obtain (1+k) category centers by the iterative clustering, the ending condition can be determined by $\frac{m_{1+k}(v_{1+k})}{m_1(v_1)} < \delta$, and $\delta < 1$. Where $m_1(v_1)$ is the peak value at the first category center and $m_{1+k}(v_{1+k})$ is the peak value at the $(1+k)^{th}$ category center.

Step 3. Output the category centers as endmembers.

However, note that we find the category centers by mountain clustering, so that most of the pixels with their grey values equal or closer to the one at these centers can be considered as pure pixels. Maybe there are still some mixed

pixels with their grey values closer to the one at the centers. To avoid such a case, we should select category centers located at the center of ground objects with the same characteristic, rather than the borders or margins of ground objects.

In general, the flowchart of endmember extraction by mountain clustering is described as follows:

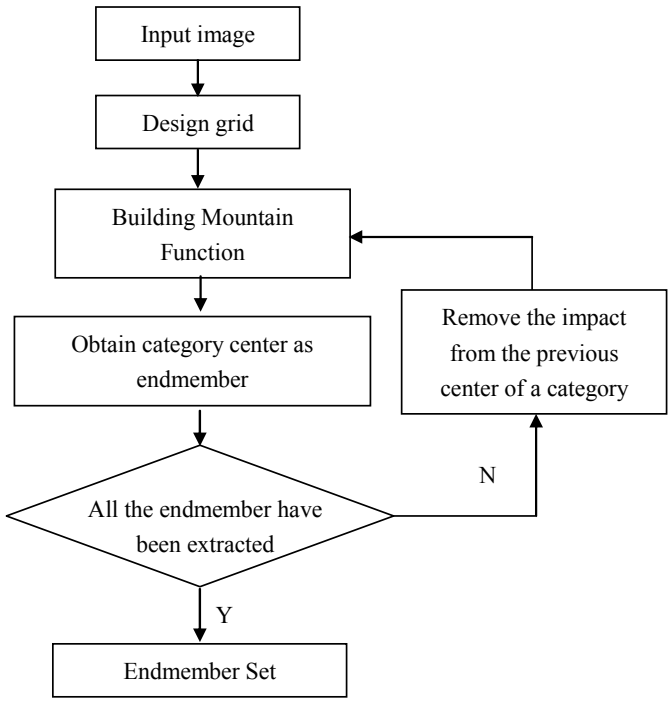

Figure 4.4 The flowchart of endmember extaction by Mountain Clustering

4.2.3 Experiment and Analysis

To validate the introduced mountain clustering algorithm, the experiment from Data set 3 are showed. The data are Landset TM image, including 7 spectrum bands and the spatial resolution is 30m. The size of the data in the experiments is 512*512. In Data set 3, there are land covers of water, farmland, woodland, building and road etc.

For each image, we first extract endmembers within each single band. Considering the effectiveness of every spectrum and their correlation, we select five spectrums to carry out the experiment on the basis of the mountain clustering algorithm.

4.2.3.1 Experiment with Data set 3

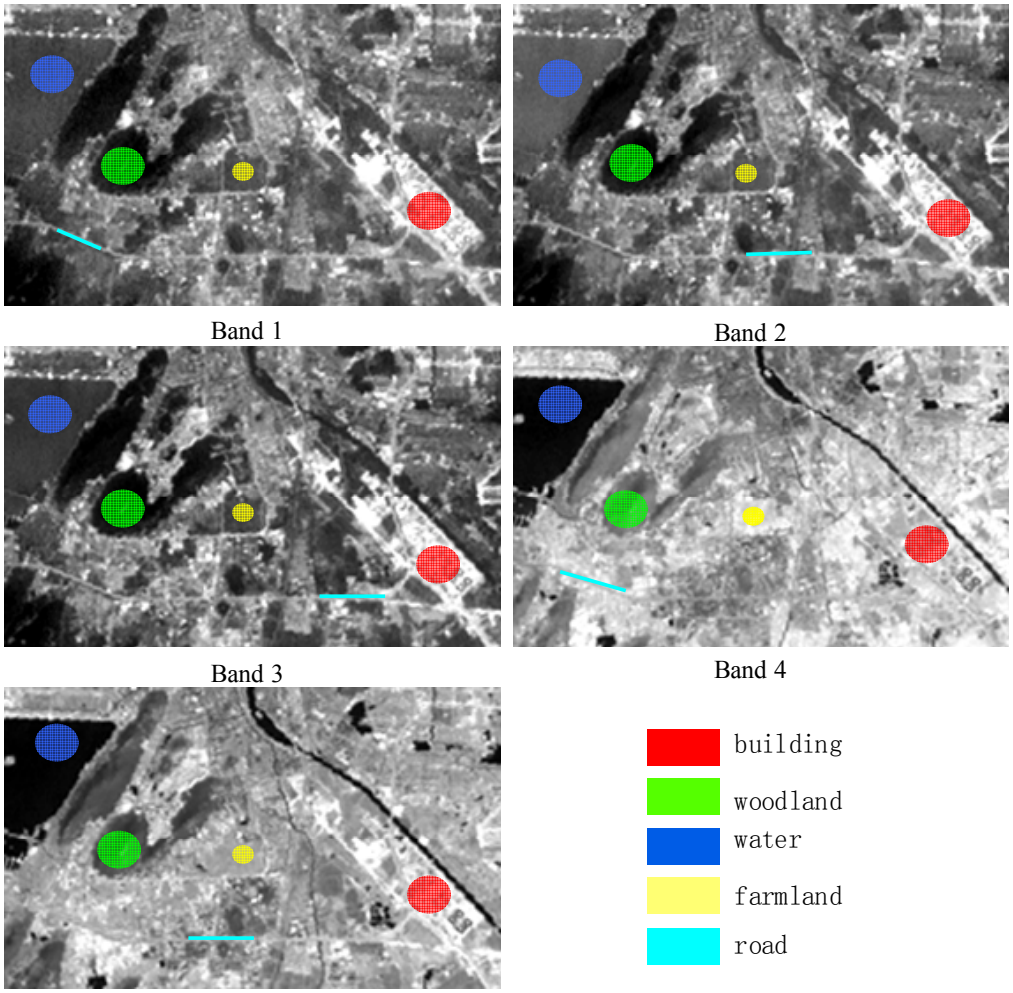

Figure 4.5 Experiment of Endmember Extraction by Mountain Clustering

We select five categories in the image to demonstrate the performance of mountain clustering. The experimental results are described on five bands respectively. We mark the five regions on the image to show the most possible

locations of the clustered category centers. The grey value of each category center is obtained from each grid point corresponding to the peaks in the mountain function. The result in each single band is a five-tuple $(G_1, G_2, G_3, G_4, G_5)$, where G_i means the grey value in the i^{th} region marked on the image.

Band 1: the grey values of endmembers are (18,74,111,143,172)

Band 2: the grey values of endmembers are (19,68,94,128,158)

Band 3: the grey values of endmembers are (10,57,101,140,172)

Band 4: the grey values of endmembers are (8,126,160,198,229)

Band 5: the grey values of endmembers are (5,82,135,167,197)

4.3 Abundance Generation

4.3.1 Grey Correlation Method

The grey correlation based method (Yang and Zhang, 2004) is proposed to generate abundances for unmixing mixed pixels by using the grey correlation in the grey system theory. This method is based on the fact that the grey of each mixed pixel is dependent on that of its neighboring pixels. This means that pixels are grey-correlated. This method considers not only the grayness of pixels, but also the spatial correlation between mixed pixels and its neighboring pixels.

The existing grey correlation based method can be describes as follows:

Step 1, we select pure pixels as endmembers (assume its grey is d) by the

visual interpretation. We consider the grayness of pixels and let T be a threshold. The pixels with its grey within $[d-T, d+T]$ are considered to be in the same category with the pure pixel. This grayness interval is denoted by $\otimes(d)$. If there are m kinds of typical ground objects (m kinds of endmembers), the grayness of each endmember is denoted by $\otimes(d(k)),\ (k=1,...,m)$.

Step 2, we find all the neighboring pixel pairs for a mixed pixel. For example, there are 4 neighboring pixel pairs in the 8-neighboring region of a mixed pixel, as Figure 4.6 shows.

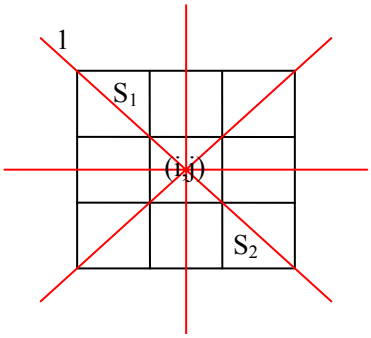

Figure 4.6 Sketch map of 4 neighboring pixel 2-tuple

Let $f(i,j)$ be the grey value of the mixed pixel (i,j). Let $S_1(i,j)$ and $S_2(i,j)$ be two grey values of one of the $(i,j)'s$ neighboring pixel pairs (such as the 1st direction in Figure 4.6). Thus the four neighboring pixel pairs can be represented by:

$$\{S_1(i,j), S_2(i,j)\} \in \{[f(i-1, j-1), f(i+1, j+1)], [f(i, j-1), f(i, j+1)],$$
$$[f(i+1, j-1), f(i-1, j+1)], [f(i+1, j), f(i-1, j)]\}$$

Step 3, we find the endmember category that a neighboring pixel pair in one direction is affiliated with, by using the conditions in Eq. (4.5).

$$\begin{aligned} &\min |S_1(i,j) - \otimes(d(t))| = |S_1(i,j) - \otimes(d(1))| \\ &\min |S_2(i,j) - \otimes(d(t))| = |S_2(i,j) - \otimes(d(2))| \end{aligned} \tag{4.5}$$

Thus we can find the most closer grayness of the endmembers $\otimes(d(1))$ and $\otimes(d(2))$ for $S_1(i,j)$ and $S_2(i,j)$.

Step 4, if the grey value $f(i,j)$ of mixed pixel (i,j) is greater or smaller than $\otimes(d(1))$ and $\otimes(d(2))$ in one direction, we consider the corresponding neighboring pixel pair will have no impact on the mixed pixel. Therefore, the pair will be excluded from abundance generation.

Step 5, if and only if the grey value $f(i,j)$ of mixed pixel (i,j) is greater than $\otimes(d(1))$ or $\otimes(d(2))$, the corresponding pair is a valid. We have Eq. (4.6) to generate the abundance from the contribution of this neighboring pixel pair.

$$\begin{cases} a_1^1 \times \otimes(d(1)) + a_2^1 \times \otimes(d(2)) = f(i,j) \\ a_1^1 + a_2^1 = 1 \end{cases} \tag{4.6}$$

Similar to the linear mixed model in Chapter 3, we have two constraints: the

sum-to-one constraint and the positive constraint, namely $\sum_{k=1}^{m} a_k{}^{i} = 1$ and $a_k{}^{i} > 0$, where $k = 1,...,m;\ i = 1,...,n$, m is the number of endmember categories and n is the number of valid neighboring pixel pairs. We generate the abundances of the endmembers served by the neighboring pixel pair in the 1st effective direction as follows.

$$\begin{cases} a_1{}^{1} = \dfrac{\otimes(d(2)) - f(i,j)}{\otimes(d(2)) - \otimes(d(1))} \\ a_2{}^{1} = \dfrac{f(i,j) - \otimes(d(1))}{\otimes(d(2)) - \otimes(d(1))} \end{cases} \tag{4.7}$$

Step 6, We repeat the step 4 and step 5 to evaluate the impact of each neighboring pixel pairs in each direction on the grayness of the mixed pixel, and generate the abundances of the two corresponding endmembers. Then we combine the abundances of the same endmember and use the arithmetic mean of the abundances as the general abundance of the endmember in the mixed pixel, denoted by a_k. Let n be the number of the valid neighboring pixel 2-tuples.

$$a_k = \frac{\sum_{i=1}^{n} a_k{}^{i}}{n}, \quad (k = 1,...,m;\ \ i = 1,...,n) \tag{4.8}$$

where k is the k^{th} endmember, i is the i^{th} valid neighboring pixel pair.

Step 7, we repeat from the step 2 to the step 6 for each mixed pixel on the image

and finish the abundance generation for all the mixed pixels.

4.3.2 Endmember Automatic Input

By using mountain clustering, we find the grey values of the center of each category, i.e., the grey value of each endmember. In order to find the grayness of each category endmember, we apply region growing to find the range of the grey values for each category endmember. The original grey correlation based method inputs the endmembers for abundance generation manually. In our study, we can input the grayness of endmembers automatically.

Moreover, we exclude some pure pixels from abundance generation to reduce the computation cost. Because there is a grayness region for each endmember, the grey value of the pixel locating in this region is pure pixel. Therefore, only mixed pixels are input to be generated their abundance and our method is much more accurate and efficient.

4.3.3 Experiment and Analysis

Based on the results of the endmember extraction in each single band for multi-spectral image, we generate the abundance for each endmember within the mixed pixel still in each single band level. Here, we carried out the experiment in Band 1 of the Data set 3.

The grey value of the endmembers extracted from band 1 is $(18,74,111,143,172)$, which is equal to mean that there are five typical land cover on the image, possibly be water, woodland, road, farmland and building. Set the threshold is five and we obtain grayness interval for each endmember

category.

Next, we select some representative pixels locating at (32,67), (33,102), (40,48), (70,77) highlighted with blue, red, yellow and green on the image. We call them pixel 1, 2, 3 and 4, then we will use grey correlation method to generate the abundances for them. Each abundance matrix is denoted by

$$A = \begin{bmatrix} ratio\ of\ water \\ ratio\ of\ woodland \\ ratio\ of\ road \\ ratio\ of\ farmland \\ ratio\ of\ building \end{bmatrix}.$$

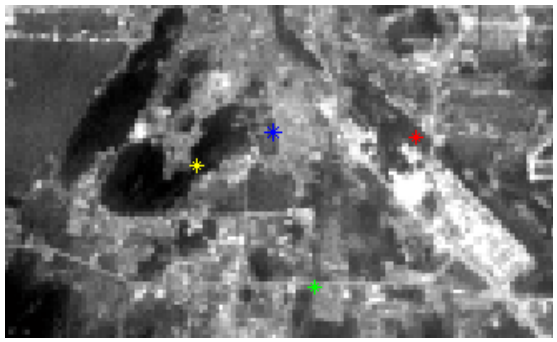

Figure 4.7 Abundance generation with grey correlation method

Before abundance generation, we try to exclude pure pixels. We find that pixel 2 and 3 is pure, and they belong to water and woodland respectively. Therefore, the abundance of water is 100% in pixel 2; and the abundance of woodland is also 100% in pixel 3.

Then we use grey correlation method to unmix pixel 1 and 4, we find pixel 1 is the combination of two materials, namely woodland and farmland, with the

abundance matrix $A_1 = \begin{bmatrix} 0.00\% \\ 81.48\% \\ 0.00\% \\ 18.52\% \\ 0.00\% \end{bmatrix}$; Pixel 4 is mixed by water and farmland and building, with the abundance matrix $A_4 = \begin{bmatrix} 0.00\% \\ 22.03\% \\ 43.90\% \\ 34.07\% \\ 0.00\% \end{bmatrix}$.

To explain the procedure of abundance generation in detail, we talked with pixel 1 as the example:

1. Noted endmember as 1, 2, 3, 4, 5, and obtain the grey value of five endmembers $(18,74,111,143,172)$, then their grayness interval is denoted by $\otimes(d(1))=[13,23]$, $\otimes(d(2))=[69,79]$, $\otimes(d(3))=[106,116]$, $\otimes(d(4))=[138,148]$, $\otimes(d(5))=[167,177]$

2. Get the grey value for the objective mixed pixel (32,67) is 89, and get the grey values of its 8-neighboring pixels, listed in the matrix as follow:

$$\begin{bmatrix} 85 & 91 & 157 \\ 73 & 89 & 144 \\ 77 & 82 & 141 \end{bmatrix}$$

So, we can get the grey value of the 4 neighboring pixel pairs, they are (85,141) (91,82) (157,77) (144,73) respectively.

3. Judge the endmember categories for each neighboring pixel pair, and replace their grey value with the grayness in its corresponding endmember category.

$$\begin{bmatrix} 79 & 79 & 148 \\ 73 & 89 & 144 \\ 77 & 79 & 141 \end{bmatrix}$$

4. Judge the validity of 4 neighboring pixel pair. Based on the matrix above, we find the pairs in 1st-, 3rd-, 4th-direction is valid, because the grey value of the mixed pixel is between the grey value of the pairs respectively. However, the grey values of neighboring pixel pairs in 2nd-direction are all lower than that of the mixed pixel, so they are invalid,

5. In each the effective directions, let the neighboring pixel pair as the component endmember and based on Eq. (4.6), the abundance can be calculated for the mixed pixel.

In 1st-direction

$$\begin{cases} a_2^{\,1} \times 79 + a_4^{\,1} \times 141 = 89 \\ a_2^{\,1} + a_4^{\,1} = 1 \end{cases}, \text{ then } \begin{cases} a_2^{\,1} = 0.8387 \\ a_4^{\,1} = 0.1613 \end{cases}$$

In 3rd-direction

$$\begin{cases} a_4^{\,2} \times 148 + a_2^{\,2} \times 77 = 89 \\ a_4^{\,2} + a_2^{\,2} = 1 \end{cases}, \text{ then } \begin{cases} a_2^{\,2} = 0.8310 \\ a_4^{\,2} = 0.1690 \end{cases}$$

In 4th-direction

$$\begin{cases} {a_4}^3 \times 144 + {a_2}^3 \times 73 = 89 \\ {a_4}^3 + {a_2}^3 = 1 \end{cases}, \text{ then } \begin{cases} {a_2}^3 = 0.7746 \\ {a_4}^3 = 0.2254 \end{cases}$$

6. Based on Eq. (4.8), combine all above partial abundance and get the final one for each endmember.

$$\begin{cases} a_2 = \dfrac{0.8387 + 0.8310 + 0.7746}{3} = 0.8148 \\ a_4 = \dfrac{0.1613 + 0.1690 + 0.2254}{3} = 0.1852 \end{cases}$$

So it can be concluded that this mixed pixel is combined by two component materials, namely woodland and farmland, and they occupy 81.48% and 18.52% respectively.

4.4 Sub-pixel Mapping

4.4.1 Cellular Automata

In the 1950s, Von Neumann proposed Cellular Automata (CA) system to simulate the self-reproductive behavior in biology. It is an evolutionary algorithm, in which the cellulars in a cellular space evolve with a specific evolution rule, so that their locations and states are changing until achieving the optimal result.

A CA system consists of cellular, cellular space, states, neighbors, and the evolution rules (see Figure 4.8). Each CA system can be represented by a 4-tuple $\{Z^n, S, N, f\}$. The detailed explanations are described as follows:

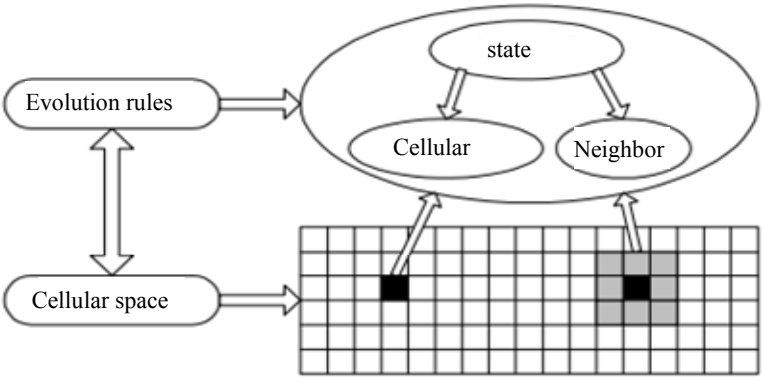

Figure 4.8 Cellular Automata System

(1) Cellular: cells, the basic elements in a CA system.

(2) Cellular space: defined as the set of grid intersections of all the cells, which can be a 1-dimension, 2-dimension, or n-dimension Euclidean space. Let Z^n be the n-dimension cellular space.

(3) State: a binary set $\{0,1\}$ or a discrete set $S = \{s_1,...,s_i,...,s_k\}$, where s_i is the i^{th} state of a cell.

(4) Neighbors: the neighbors of a central cell, denoted by $N = \{x_1, x_2, \cdots x_i, \cdots, x_n\}$, where x_i is the neighboring cell's location relative to the central cell. In a 2-dimension cellular automata system, there are two kinds of popular neighbors: the Von-Neumann neighbors and the Moore neighbors. Generally speaking, the next state of a central cell depends on its current state and its neighbors' states. Therefore, we must specify which cells are the neighbors of a central cell before we

establish the evolution rules.

Here, we introduce the Moore neighbor. As Figure 4.8 shows, the black cell is the central cell and the grey cells are its Moore neighbors. If the radius of neighboring is 1 and the dimension is n, total number of neighbors is $(3^n - 1)$. The definition of the Moore neighbors is described as follows:

$$N_{Moore} = \{v_i = (v_{ix}, v_{iy}) \,|\, |v_{ix} - v_{0x}| \le 1, |v_{iy} - v_{0y}| \le 1, (v_{ix}, v_{iy}) \in Z^n\}$$

(5) Evolution rules: f describes the rules for a cell evolving from the state s_i to s_{i+1}. These rules are represented by a dynamic function that determines the state of a cell at next step by considering its current state and neighbors' states. The dynamic function is also named as the state transition function.

In a CA system, the state of the system consists of the states of all the cells. The next state of a cell depends on its current state and its neighbors' states. A tiny change at a local cell results in macro dramatic changes in the system in terms of constitution, layout, and characteristics. The system can achieve the optimal state by the iterative evolution of all the cells.

In this chapter, we consider that sub-pixel mapping can be addressed by similar evolutions. As we all know, the objective of sub-pixel mapping is to fill the

optimal component endmember into sup-pixels in a mixed pixel so that the filled information makes the spatial correlation in an image optimal. This optimal solution should be found by iterative evolutions. Therefore, we improve the original CA model to achieve the optimal state of sub-pixel mapping in a multi-spectral image.

4.4.2 Improved Cellular Automata

To address sub-pixel mapping in a multi-spectral image, we should achieve the best state for the distribution of component endmembers in a mixed pixel. Thus we describe the five components in a CA system.

(1) Cell: Each sub-pixel in a mixed pixel is denoted by a cell.

(2) Cellular space: the set of sub-pixels in a mixed pixel is considered as a cellular space.

(3) State: The categories of component endmembers are considered as the set of cellular states. If there are m categories, there are m states of a cell.

(4) Neighbors: We take the cells in one cell's 8-neighboring region as the Moore neighbors.

(5) Evolution rules: The evolution in our improved cellular automata consists of a series of exchanging operations. We use the original exchange parameter E_1 and propose another exchange parameter E_2. With the two parameters, we estimate whether the state of a cell evolves or not. Let C be the cell to be exchanged. s_1 is the state of C before exchanging, while s_2 is the state after exchanging. The $C's$

neighbors are denoted by C^8. Thus the C^8's neighbors are denoted by C^{8^8} as Figure 4.9 shows.

(1) Cellular C and its neighbor C^8 (2) Neighbor C^8 and its neighbor C^{8^8}

Figure 4.9 Cellular's neighbors and neighbor's neighbors

To define the exchange parameter E_1, we denote the C^8's states by $C_{ij}^{\ 8}$, where $i \in \{-1, 0, 1\}$, $j \in \{-1, 0, 1\}$ and i, j cannot be 0 at the same time. We define the following function:

$$\frac{C_{ij}^{\ 8}}{C} = \begin{cases} 1, & \text{when } C_{ij}^{\ 8} \text{ and } C \text{ is in the same state} \\ 0, & \text{when } C_{ij}^{\ 8} \text{ and } C \text{ is not in the same state} \end{cases} \tag{4.9}$$

Let s_1 be the C's state before exchanging and let $\sum_{\text{pre-}} \frac{C_{ij}^{\ 8}}{C}$ as the sum of the function $\frac{C_{ij}^{\ 8}}{C}$. Let s_2 be the C's state after exchanging and let $\sum_{\text{post-}} \frac{C_{ij}^{\ 8}}{C}$ as the sum of the function $\frac{C_{ij}^{\ 8}}{C}$. Then from Eq. (4.9) we have

$$E_1 = \sum_{\text{post-}} \frac{C_{ij}^{\ 8}}{C} - \sum_{\text{pre-}} \frac{C_{ij}^{\ 8}}{C} \tag{4.10}$$

Moreover, we denote the $C^{8^8}{}'s$ states by $C_{mn}^{8^8}$, where $m \in \{-1, 0, 1\}$, $n \in \{-1, 0, 1\}$, and m, n cannot be 0 at the same time. We define the following function:

$$\frac{C_{mn}^{\ 8^8}}{C_{ij}^{\ 8}} = \begin{cases} 1, & \text{when } C_{mn}^{\ 8^8} \text{ and } C_{ij}^{\ 8} \text{ is in the same state} \\ 0, & \text{when } C_{mn}^{\ 8^8} \text{ and } C_{ij}^{\ 8} \text{ is not in the same state} \end{cases} \tag{4.11}$$

Similarly, from Eq. (4.11) we have

$$E_2 = \sum_{\text{post-}} \sum \frac{C_{mn}^{\ 8^8}}{C_{ij}^{\ 8}} - \sum_{\text{pre-}} \sum \frac{C_{mn}^{\ 8^8}}{C_{ij}^{\ 8}} \tag{4.12}$$

In two cases: 1) $E_1 > 0$, or 2) $E_1 < 0$ and $E_2 > 0$, the state of the cell evolves, otherwise the state is not changed. Compared with the original CA system, we introduce another parameter E_2 to improve the cases that the state of a cell should be exchanged but not. We consider the spatial correlation not only between the current sub-pixel and the sub-pixels in its 8-neighboring region, but also between the current sub-pixel and its $C^8{}'s$ neighboring sub-pixels. In this way, we improve the spatial correlation among sub-pixels in a global range, so that the performance of our CA system is better.

For example, we explain the evolution process in details.

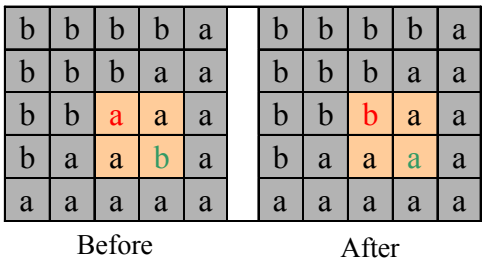

Figure 4.10 Before and after exchange the cellular state

As Figure 4.10 shows, the highlighted cellular space in apricot represents the mixed pixel. In this cellular space, we need to exchange the cellular highlighted in red and its neighbor in green. The state of the cell need to be evolved is a before exchanging, and the state of the neighbor cellular is b.

First, we need to count the number of the cell's neighbors with the same state a, which is 4. After exchanging, the state of the cell is b. Thus the number of the cell's neighbors with the same state b is 3. The exchange utility E_1 is equal to -1, smaller than 0. If we apply the evolution rules in the original CA system, the decision should be not to exchange. However, we know the effect after exchanging will be better, just by visual.

Therefore, we introduce another exchange parameter E_2. In the above example, we need count the number, which is satisfied the condition in Eq. (4.11), that the state of cell's neighbors'neighbors is same with the state of cell's neighbors is 39 before exchanging. And after exchanging, the number is 47. So the exchange parameter E_2 is 8, greater than 0. According to our new rule, the decision should be to exchange.

In general speaking, the original CA system can achieve well enough performance when dealing with sub-pixels mapping for smooth and regular-shaped ground objects. However, our improved CA system can deal with not only smooth and regular-shaped ground objects, but also unshaped and irregular ground objects.

The detail steps of the implementation of our CA system are described as follows:

Step 1. Set the state of the cellular, which can be obtained after knowing the component endmembers and their corresponding abundances based on the mountain clustering and the grey correlation method.

Step 2. Obtain the initial states of cellulars in each cellular space. We can know the number of sub-pixels of each component endmember based on its abundance in a mixed pixel. So we can assign the state to each cellular randomly as their initial states.

Step 3. Randomly select a cell to be evolved and then compare the states between selected cell and its neighbors. If the state of this cell's neighbor is the same as the state of itself, we do not change and select another neighbor. Otherwise, we calculate the exchange parameter E_1. If E_1 is greater than 0, the cell evolves, i.e. exchange their state.

Step 4. If E_1 is smaller than 0, we calculate another exchange parameter E_2.

If E_2 is greater than 0, the cell still evolves. If E_2 is smaller than 0, the cell does not evolve.

Step 5. The above evolution process can be looked as a sub-process, which is done in one of cellular spaces. We repeat the evolution for all the cellular spaces on an image. In practice, we can deal with all the mixed pixels simultaneously in order to improve the computation efficiency.

4.4.3 Multiband Synthesis

Up to now, we unmix a multi-spectral image on each band. The final objective requires us to synthesize all the images to achieve the final sub-pixel result. In general, the probability that the filling results from all the bands is the same is very low. Therefore, the filling results for many sub-pixels are not same. We consider that the best filling is that the spectral correlation between the filled sub-pixels and their neighbors is the best.

We take an example to show the process of band synthesis. We assume that a multi-spectral image is unmixed at each of the four bands. The filling results for sub-pixels at each band is denoted by A, B, C, and D, which are four endmembers.

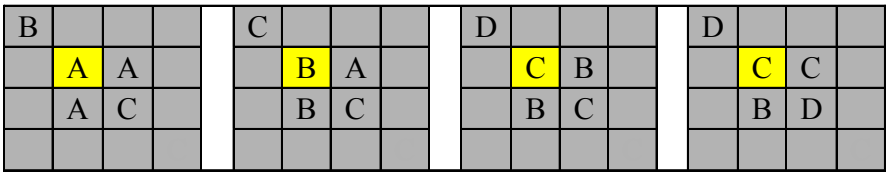

Figure 4.11 An example of Rule 2

Step 1, We count the number of categories at each sub-pixel on each band. We also count the number of the number of categories of typical ground objects at each sub-pixel on all the bands. For example, the marked sub-pixel in Figure 4.11 is with A on Band 1, B on Band 2, C on Band 3, and C on Band 4. The final category of the marked sub-pixel is one of three categories $\{A, B, C\}$.

Step 2, we firstly assign the marked sub-pixel with A on each band. Then we calculate the accumulated differences between the grey value of the marked sub-pixel and the grey values of all its 8-neighboring sub-pixels in Band 1. Next we calculate other three accumulated differences in Band 2, 3 and 4. We set the evaluation value for filling A in the marked sub-pixel with the sum of the four accumulated differences.

Step 3, we repeat the step 2 by assigning the marked sub-pixel with B on each band. We find the evaluation value for filling B in the marked sub-pixel.

Step 4, we repeat the step 2 by assigning the marked sub-pixel with C on each band. We find the evaluation value for filling C in the marked sub-pixel.

Step 5, we compare three evaluation values with each other. The smaller the evaluation value is, the better the correlation between the filled category and its neighboring categories is. Therefore, we select the category with

the minimum evaluation value as the final choice and complete band synthesis.

4.4.4 Experiment and Analysis

In this section, we design the experiments in three phases, including first, we carried out the full implementation of sub-pixel mapping based on improved CA system and multiband synthesis. Second, we compare the result from the sub-pixel mapping image and the synthesized image after sub-pixel mapping. Third, to verify the performance of our proposed method, we also introduce classical interpolation method as a comparison. As the sub-pixel mapping and interpolation will upgrade the resolution of the image to fourfold, before the experiments, we will degrade the original map and so that we can compare all the classification results from three methods with that of original image.

4.4.4.1 Experiment -- sub-pixel mapping in each single band

Sub-pixel mapping is done in each single band of the multi-spectral image, so we list all the pictures to explain and compare the results, including the original image, degradation image, sub-pixel mapping image and the image after multiband synthesis. Especially from the latter two, we can find that the image after multiband synthesis become clearer and no much zigzag border between different land covers. After comparing the result, we can obtain the conclusion that the image quality has been improved after multiband synthesizing on the sub-pixel mapping image.

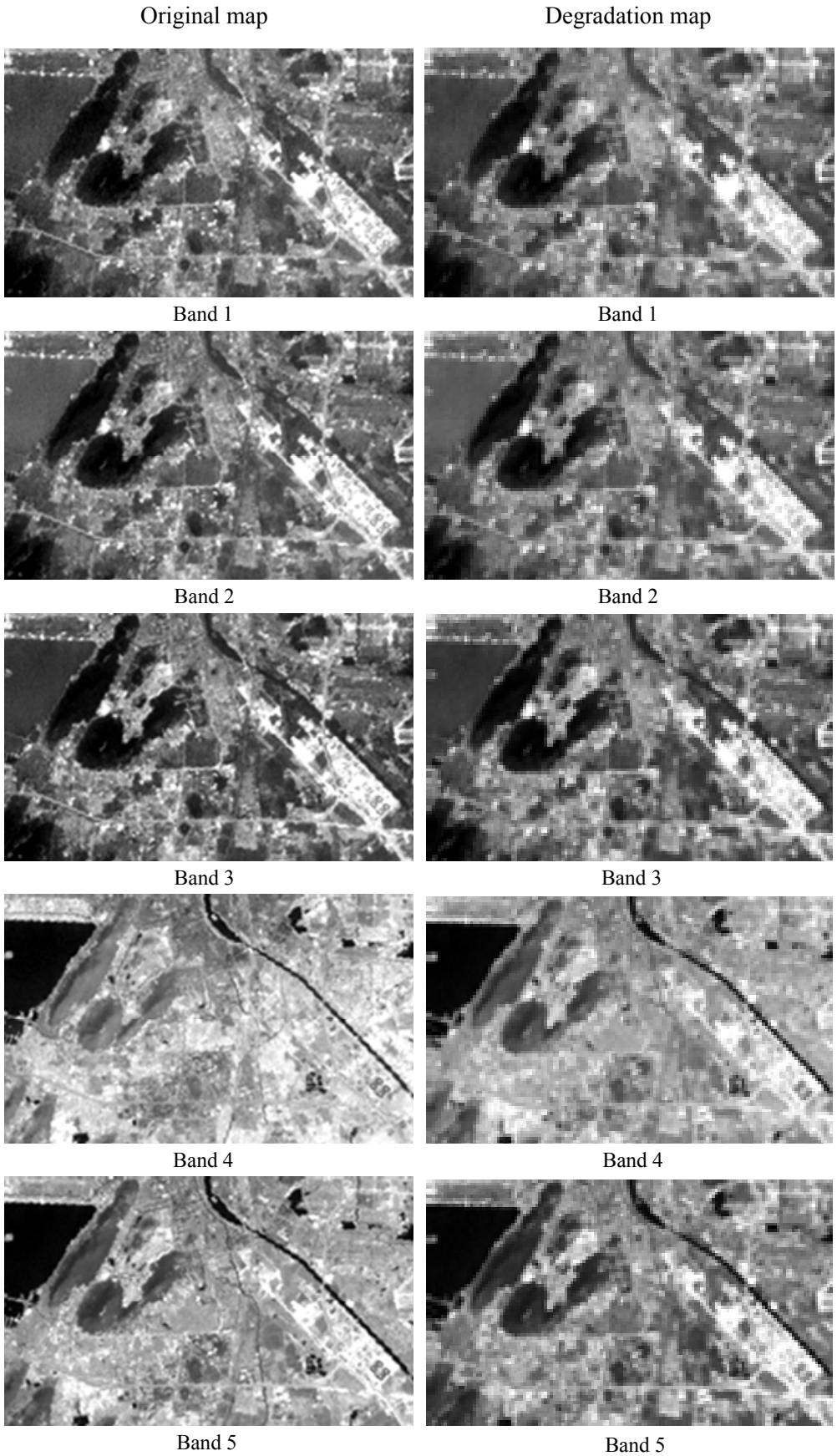

Figure 4.12 Original map and degradation map in each single band

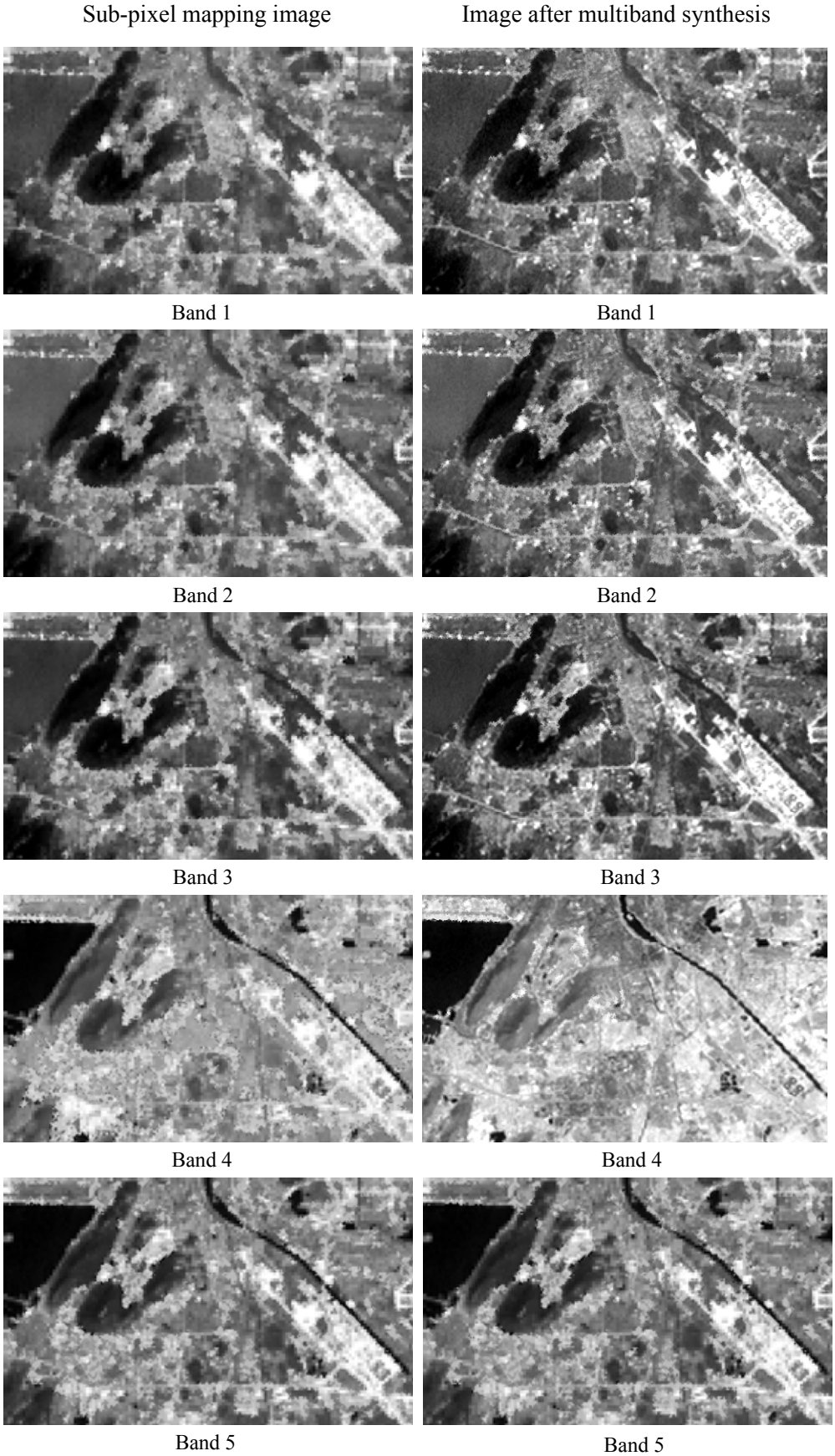

Figure 4.13 Sub-pixel mapping and after multiband synthesis images

4.4.4.2 Experiment -- comparison of the sub-pixel mapping result between single band images and the synthesized image

To compare the result of sub-pixel mapping image and the following synthesized image, we develop the classification on both images in Figure 4.14.

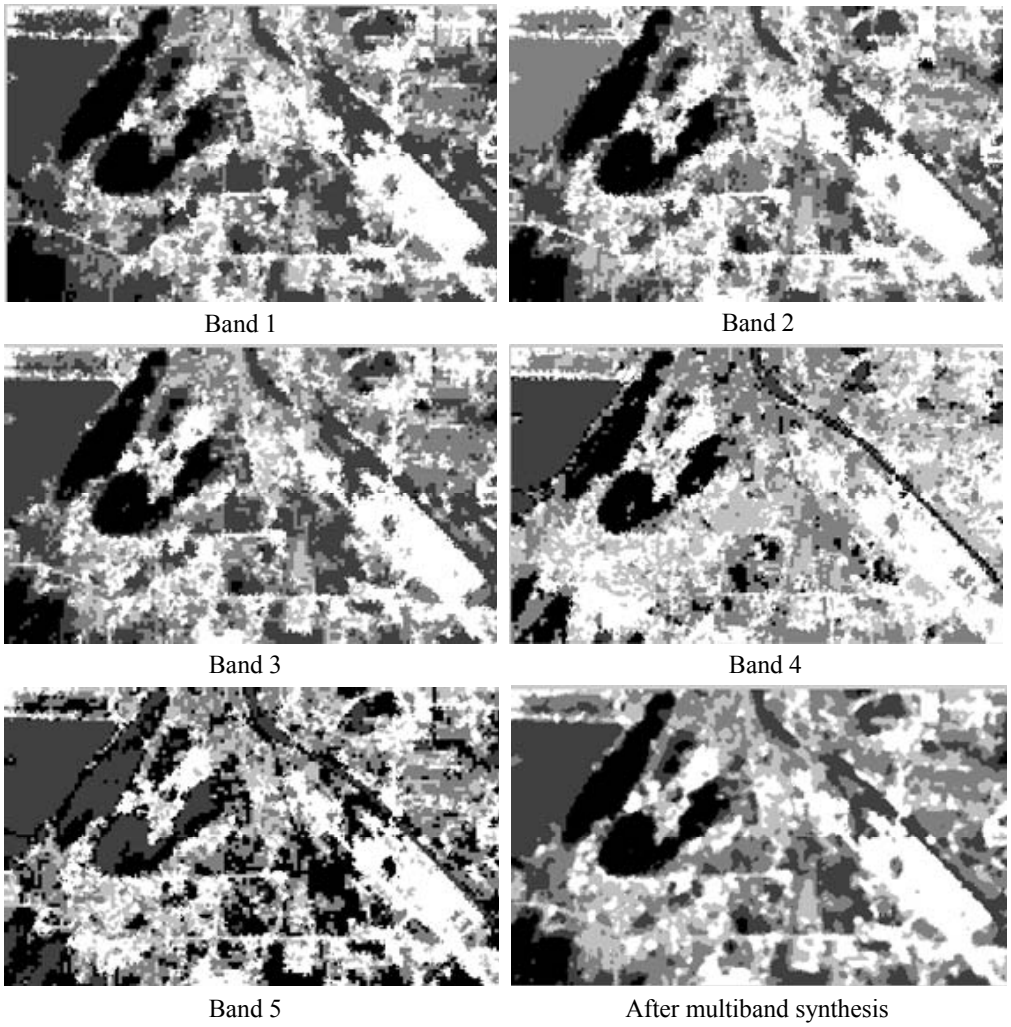

Figure 4.14 Classification results of single band images and synthesized image

We classify each single band image and the synthesized image, and configure the confusion matrixes as following tables. From the overall accuracy and Kappa statistic, we can judge the performance of sub-pixel mapping based on the classification result.

Table 4.1 Confusion matrix of classification on 1st band image

	Water	Woodland	Road	Farmland	Building	Total	User's accuracy
Water	3872	454	35	4	2	4367	0.8867
Woodland	278	8083	5154	1007	95	14617	0.5530
Road	3	279	4763	4689	514	10248	0.4648
Farmland	0	6	518	3716	1546	5786	0.6422
Building	0	9	181	2020	7380	9590	0.7696
Total	4153	8831	10651	11436	9537	44608	
Producer's accuracy	0.9323	0.9153	0.4472	0.3249	0.7738		Overall accuracy = 0.6235
Kappa statistics							Kappa = 0.5246

Table 4.2 Confusion matrix of classification on 2nd band image

	Water	Woodland	Road	Farmland	Building	Total	User's accuracy
Water	3882	292	40	11	0	4225	0.9188
Woodland	263	4840	1747	210	19	7079	0.6837
Road	6	3608	7159	2407	125	13305	0.5381
Farmland	2	52	1308	5208	626	7196	0.7237
Building	0	39	397	3600	8767	12803	0.6848
Total	4153	8831	10651	11436	9537	44608	
Producer's accuracy	0.9347	0.5481	0.6721	0.4554	0.9193		Overall accuracy = 0.6693
Kappa statistics							Kappa = 0.5792

Table 4.3 Confusion matrix of classification on 3rd band image

	Water	Woodland	Road	Farmland	Building	Total	User's accuracy
Water	3751	297	32	9	3	4092	0.9167
Woodland	393	8098	3100	339	36	11966	0.6768
Road	4	393	6848	4021	266	11532	0.5938
Farmland	3	21	444	4811	977	6256	0.7690
Building	2	22	227	2256	8255	10762	0.7671
Total	4153	8831	10651	11436	9537	44608	
Producer's accuracy	0.9032	0.9170	0.6429	0.4207	0.8656		Overall accuracy = 0.7120
Kappa statistics							Kappa = 0.6351

Table 4.4 Confusion matrix of classification on 4th band image

	Water	Woodland	Road	Farmland	Building	Total	User's accuracy
Water	3489	1329	599	112	18	5547	0.6290
Woodland	67	3128	75	16	6	3292	0.9502
Road	568	2990	4413	2860	338	11169	0.3951
Farmland	21	1168	3931	4766	1523	11409	0.4177
Building	8	216	1633	3682	7652	13191	0.5801
Total	4153	8831	10651	11436	9537	44608	
Producer's accuracy	0.8401	0.3542	0.4143	0.4168	0.8023		Overall accuracy = 0.5256
Kappa statistics							Kappa = 0.3959

Table 4.5 Confusion matrix of classification on 5th band image

	Water	Woodland	Road	Farmland	Building	Total	User's accuracy
Water	1638	4692	3371	597	69	10367	0.1580
Woodland	2497	3530	138	25	5	6195	0.5698
Road	11	538	5833	3462	338	10182	0.5729
Farmland	4	31	987	4473	1220	6715	0.6661
Building	3	40	322	2879	7905	11149	0.7090
Total	4153	8831	10651	11436	9537	44608	
Producer's accuracy	0.3944	0.3997	0.5476	0.3911	0.8289		Overall accuracy = 0.5241
Kappa statistics							Kappa = 0.4083

Table 4.6 Confusion matrix of classification on multiband synthesized image

	Water	Woodland	Road	Farmland	Building	Total	User's accuracy
Water	3985	182	11	0	0	4178	0.9538
Woodland	168	8164	1164	19	1	9516	0.8579
Road	0	473	9048	2505	18	12044	0.7512
Farmland	0	10	382	7941	1035	9368	0.8477
Building	0	2	46	971	8483	9502	0.8928
Total	4153	8831	10651	11436	9537	44608	
Producer's accuracy	0.9595	0.9245	0.8495	0.6944	0.8895		Overall accuracy = 0.8434
Kappa statistics							Kappa = 0.8005

In this accuracy assessment, there were a total 44608 pixels of ground reference data, including 4153 pixels for water, 8831 pixels for woodland, 10651 pixels for road, 11436 pixels for farmland and 9537 pixels for building. The amount of samples fulfills the sample size requirement for significance test. From Table 4.1 to Table 4.6, we draw the histogram in Figure 4.15, and the MSASM in the figure means multiband synthesized image after sup-pixel mapping. We find the overall accuracy and kappa is different in bands from 1 to 5, some are higher, some are lower. However, after multiband synthesis based on 5 single sub-pixel mapping images, we find the accuracy is improved greatly. Obviously, the improvement of kappa value proves the significance of the proposed method.

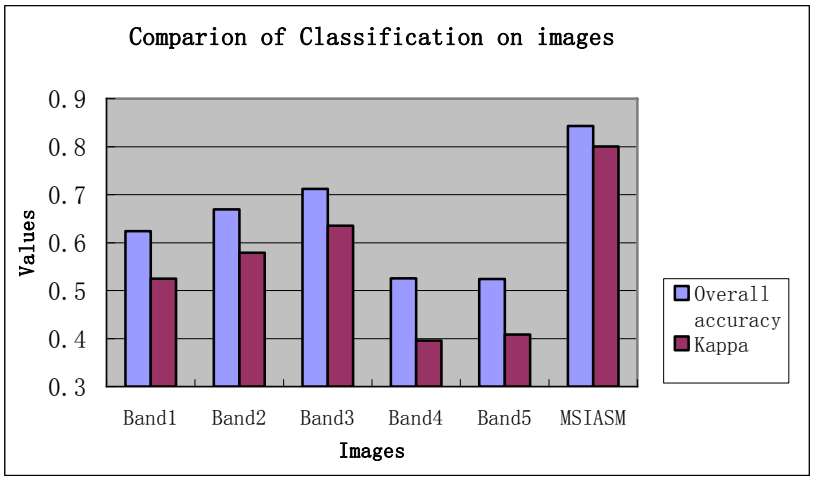

Figure 4.15 Accuracy comparison based on different images

4.4.4.3 Experiment -- comparison of the performance between the proposed sub-pixel mapping method and interpolation method

To prove the effectiveness of our proposed sub-pixel mapping method, we further compare its classified image with that from the classical interpolation

method. The classified images from our proposed method and interpolation method are showed in Figure 4.16.

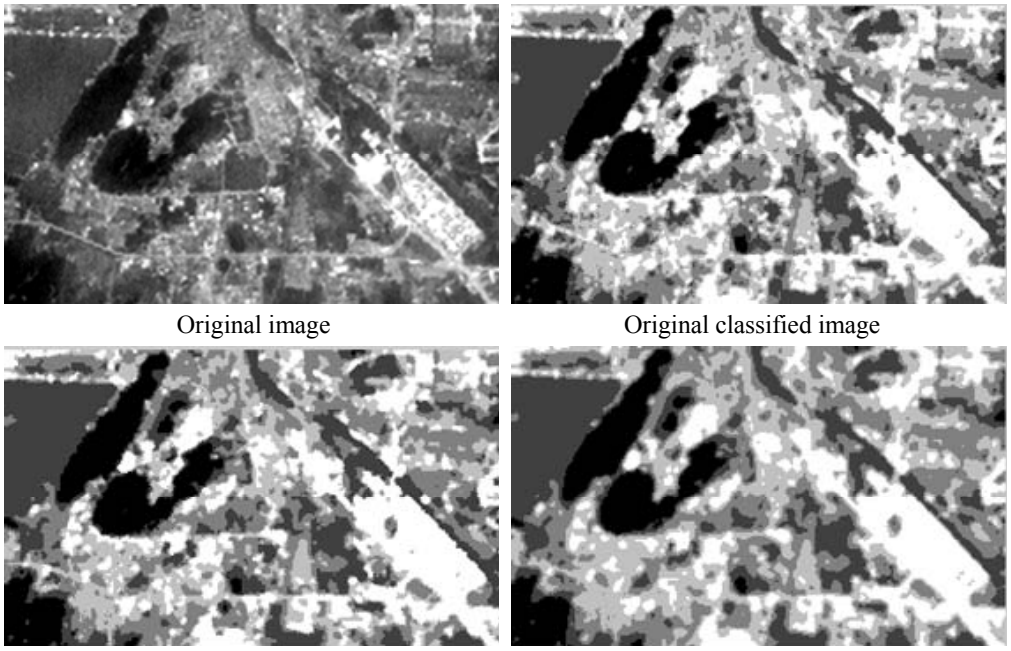

Figure 4.16 Classified images from proposed method and interpolation

Similarly, we obtain the confusion matrix for the classified image after interpolation, which is showed in Table 4.7.

Table 4.7 Confusion matrix of classified image after interpolation

	Water	Woodland	Road	Farmland	Building	Total	User's accuracy
Water	3913	122	1	0	0	4036	0.9695
Woodland	239	7804	811	4	0	8858	0.8810
Road	1	900	9024	1966	39	11930	0.7564
Farmland	0	5	813	9004	2008	11830	0.7611
Building	0	0	2	462	7490	7954	0.9417
Total	4153	8831	10651	11436	9537	44608	
Producer's accuracy	0.9422	0.8837	0.8472	0.7873	0.7854		Overall accuracy = 0.8347

Kappa statistics							Kappa = 0.7887

To compare the accuracy of classified images from our method and interpolation method, we sample a total 44608 pixels of ground reference data, including 4153 pixels for water, 8831 pixels for woodland, 10651 pixels for road, 11436 pixels for farmland and 9537 pixels for building. We draw the histogram based on Table 4.6 and Table 4.7, showing the overall accuracy and kappa in Figure 4.17. The overall accuracy and kappa of our method and interpolation method are 0.8434, 0.8005 and 0.8347, 0.7887 respectively. The amount of samples fulfills the sample size requirement for significance test. It is obvious that no matter from the overall accuracy or kappa, our method is better. Further, the improvement of kappa value proves the significance of the proposed method.

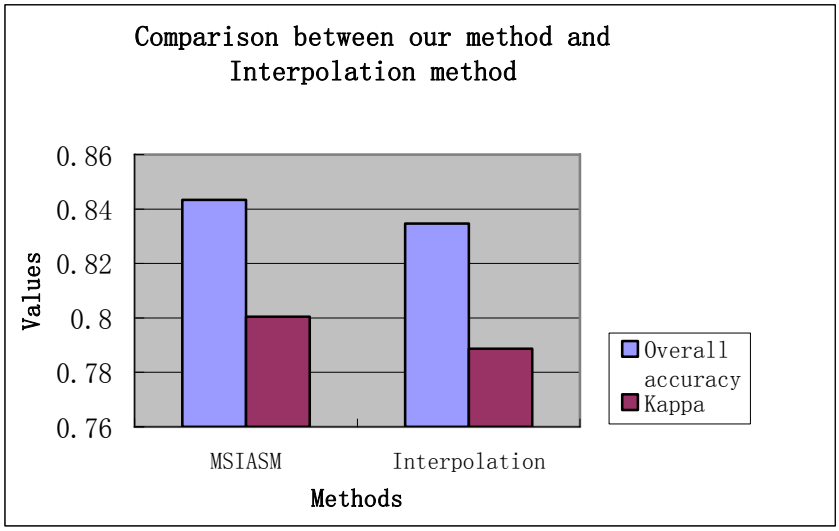

Figure 4.17 Performance comparison of two methods

Based on above three phases of experiments, we can learn that the classification results of unmixing on each spectrum are much worse. This is because the usage

of spatial information on each spectrum only is made and multiple spectrum information is neglected. While the result of our method, which is the multiband synthesis after sub-pixel mapping, shows dramatic improvement. As the spatial correlation information and spectrum information is made full use of, the mapping result is more accurate and effective in this regard.

Further, the results of the experiment, which compares the accuracy of classified images after our method and interpolation method, indicate that our method is better based on the overall accuracy and kappa. Thus, our proposed sub-pixel mapping strategy is better than interpolation, which means our method is effective.

4.5 Summary

In this section, a framework for unmixing mixed pixels in multi-spectral image based on single band has been proposed. The major contributions of the proposed work include: 1) the Mountain Clustering algorithm is introduced to improve the performance of pure endmember extraction; 2) based on step 1, we can input endmember automatically and apply grey correlation method to calculate the abundance of each endmember for mixed pixel; 3) the improved cellular automata system is proposed, which is designed to make improvements to evolve the state of cellular and 4) the result of sub-pixel mapping in each single band is integrated by multiband synthesis technology.

On the other hand, the experiments were carried out to evaluate the performance of each method included in the procedure of unmixing the mixed pixel. The

experiments were divided into three phases according to the proposed framework of the unmixing model. In the first phase, the performance of the mountain clustering in pure endmember extraction was evaluated; we can obtain the grey values of endmembers by through of capturing category centers. In the second phase, the performance of the grey correlation method for abundance generation was evaluated and computed with an instance step by step. Finally, the sub-pixel mapping was performed in each single band and the result is integrated by multiband synthesis. Meanwhile, we compare the classification results of images from sub-pixel mapping and the interpolation method respectively. Based on the collection of enough amounts of samples, we find the best result from sub-pixel mapping after multiband synthesis and prove the significance of the proposed method.

5 Multiple Classifier System for Remotely Sensed Images

In this chapter, maximum likelihood classifier, minimum distance classifier and Mahalanobis distance classifier are selected as the component of the proposed multiple classifier system. Furthermore, we propose to apply eigen-values-based sum rule to integrate them together. This meaningful weighting system is described in the sense of mathematics and demonstrated with several experimental results.

5.1 Structure of the Proposed Classification Method

5.1.1 Components of the Multiple Classifier System

In this section, several distances and relevant classifiers, which build the multiple classifier system, are briefly introduced. They include such as, the Maximum likelihood classifier, minimum distance classifier and Mahalanobis distance classifier are given below.

5.1.1.1 Maximum likelihood classifier

Maximum likelihood classification is a method for determining a known distribution as maximum probability in terms of statistics for given an image. This is a commonly used method in remotely sensed image classification in which a pixel with a maximum likelihood, is classified into the corresponding class. Suppose there are m predefined classes, the posterior probability is defined as

$$P(k \mid x) = \frac{P(k)P(x \mid k)}{\sum_{i=1}^{m} P(i)P(x \mid i)} \tag{5.1}$$

where $P(k)$ is the prior probability of class k, $P(x \mid k)$ is conditional probability to observe *x* from class k.

In the case of normal distributions, the likelihood function, $P(x \mid k)$, can be expressed as

$$L_k(x) = \frac{1}{(2\pi)^{\frac{n}{2}} |\Sigma_k|^{\frac{1}{2}}} \exp\left(-\frac{1}{2}(x - \mu_k)^T \Sigma_k^{-1} (x - \mu_k) \right) \tag{5.2}$$

5.1.1.2 Minimum distance classifier

The minimum distance classifier classifies unknown image pixels into that class where the normalized Euclidian distance between the pixel and the class mean is the minimum, with respect to the standard deviation. In the case of the minimum distance classifier, the posterior probability of pixel x classified as class *k* is defined as

$$P_k(x) = \frac{\exp\left(-\frac{1}{2}(x - \mu_k)^T \sigma_k^{-1} (x - \mu_k) \right)}{\sum_{j=i}^{m} \exp\left(-\frac{1}{2}(x - \mu_j)^T \sigma_j^{-1} (x - \mu_j) \right)} \tag{5.3}$$

5.1.1.3 Mahalanobis distance classifier

The Mahalanobis distance classifier is similar to the minimum distance

classifier, except that the covariance matrix is used to compute the distance between the pixel and the mean value of the classes. The use of the Mahalanobis distance overcomes several disadvantages of the Euclidean distance-based classifier. In the case of the Mahalanobis distance classifier, the posterior probability of pixel x classified as class k is defined as

$$P_k(x) = \frac{\exp\left(-\frac{1}{2}(x-\mu_k)^T \Sigma_k^{-1}(x-\mu_k)\right)}{\sum_{j=i}^{m} \exp\left(-\frac{1}{2}(x-\mu_j)^T \Sigma_j^{-1}(x-\mu_j)\right)} \tag{5.4}$$

Where $x = (x_1, x_2, ...x_n)^T$ is the vector of a point, in an n-dimensional space, such as a pixel in a multispectral space of n bands; $\mu_k = \begin{pmatrix} \mu_{k_1} & \mu_{k_2} & \dots & \mu_{k_n} \end{pmatrix}^T$ is the mean of the k^{th} class; $\sigma_k = \begin{pmatrix} \sigma_{11} & 0 & \dots & 0 \\ 0 & \sigma_{22} & & 0 \\ \vdots & & \ddots & \\ 0 & & \dots & \sigma_{nn} \end{pmatrix}$ is the variance matrix and $\Sigma_k = \begin{pmatrix} \sigma_{11} & \sigma_{12} & \dots & \sigma_{1n} \\ \sigma_{21} & \sigma_{22} & \dots & \sigma_{2n} \\ \vdots & \vdots & \ddots & \vdots \\ \sigma_{n1} & \sigma_{n1} & \dots & \sigma_{nn} \end{pmatrix}$ is the variance covariance matrix.

5.1.2 Sum Rule Based on Weightings

The classifiers utilized for this study provide the estimation of the posterior probabilities for each of the classes, information on posterior probabilities can be combined via either the sum rule (Benzeghiba and Bourlard, 2003; Mak et al.,

2003; Fumera and Roli, 2005), the product rule or other possible rules. The sum rule is based on a weighted sum of the posterior probabilities of a class from each classifier. The weightings can either be chosen to be equal for each component classifier, in which case just a simple average sum rule is performed, or they can be chosen to be different to represent, for instance, the reliability of the given classifiers.

Generally, if a mixed pixel contains several classes, when using different classifier on this pixel, the followings are several possible cases of a mixed pixel:

- If several classes distribute within a particular pixel evenly, the corresponding probability are nearly the same. Then the sum of square of these probabilities is "small".
- If a particular class within the pixel is dominated, and it must have larger probability than other classes. The sum of square of these probabilities is "large".

On the basis of above understanding, we can judge the performance of each classifier when they are used to classify the corresponding classes. Consequently, weightings are given to each classifier. In this study, we proposed a new sum rule for combining multi-classifiers – the sum rule based on the eigen-values of the matrix P^TP (P is the posterior probability matrix of component classifier). Based on the weighting system, the effect of the classifier should be enhanced because of their good performance and vice versa.

5.2 An Analysis of the Proposed Weighting System

5.2.1 Origin of Eigen value

The aim of the newly proposed eigen-values-based method is to provide a better estimation of the weightings for each of the classifier. Hence, the final classification by the sum for multi-classifiers can thus have a better quality. Here, the most critical issue is to determine the weightings of the classifiers effectively and correctly.

Suppose there are m classifiers, c_1, …, c_m with n predefined classes objects, O_1, …, O_n. At pixel y with position x_o, let the probability of y classified as O_i with classifier c_j is $P_{c_j}\left(y \in O_i \middle| x_o\right)$ or $P_i^j\left(x_o\right)$ for simplification. Let $P = P\left(x_o\right) = \left(P_i^j\left(x_o\right)\right)_{n\times m} = \begin{pmatrix} P_1^1 & P_1^2 & .. & .. & P_1^m \\ P_2^1 & P_2^2 & .. & .. & P_2^m \\ .. & .. & .. & .. & .. \\ .. & .. & .. & .. & .. \\ P_n^1 & P_n^2 & & P_n^{m-1} & P_n^m \end{pmatrix}$ with $n > m$, suppose P is full rank and WLOG. We may let $\left\|P^1\right\| \geq \left\|P^2\right\| \geq ... \geq \left\|P^m\right\|$, where $\left\|P^j\right\|$ is the Euclidian length of j^{th} column of the matrix $P\left(x_o\right) = \left(P_i^j\left(x_o\right)\right)_{n\times m}$, here the Euclidian length indicates the sum of square of P_i^j ($i=1,2...n$). Then we configure a matrix P^TP from the posterior probabilities matrix P, and compute the corresponding eigen-values arranged by $\lambda_1 \geq \lambda_2 \geq ... \geq \lambda_m$.

In the eigen-values-based classification method, it is assumed that each pixel

must belong to a particular class. Hence, if a particular classifier has a high probability result for a particular pixel, the sum of squares is “large”. In other words, the classifier is either sensitive to the particular class or is, in fact, an effective classifier. If either is the case, the classifier is termed “good” and the weighting of the classifier is high, and a larger eigen-value will be assigned. However, if a particular classifier has an even probability result regarding the pixel classification, the sum of square of the probabilities is “small”. This can be either because the classifier is not sensitive to the particular class, or the classifier, itself, is not effective. If either is the case, the classifier is termed “bad” and the weighting of the result should be low, and the corresponding weighting is small. Thus, a smaller eigen-value will be assigned to this classifier.

In order to provide the solution, we have proposed the eigen values as the weightings. Based on above considerations, *m* eigen values ranking from large to small are assigned as the weightings to *m* classifiers ranking from good to bad. In practice, we will select the root of eigen value as the weighting.

5.2.2 Probability of Eigen-values-based MCS

In this section, a description on the nature of this method in the sense of mathematics is given.

Suppose there are m classifiers, c_1, …, c_m with n predefined classes objects, O_1, …, O_n. At the pixel y with position x_o, let the probability of y classified as O_i with classifier c_j is $P_i^j(x_o)$. Let

$P = \left(P_i^j\left(x_o\right)\right)_{n\times m} = \begin{pmatrix} P_1^1 & P_1^2 & .. & .. & P_1^m \\ P_2^1 & P_2^2 & .. & .. & P_2^m \\ .. & .. & .. & .. & .. \\ .. & .. & .. & .. & .. \\ P_n^1 & P_n^2 & .. & .. & P_n^m \end{pmatrix}$ be the posterior probabilities matrix.

At the pixel y with position x_o, $P_h^j\left(x_o\right)$ means the probability of y is classified as O_h with classifier c_j.

λ_j is one of the eigen-value of P^TP, it has a significant meaning of the magnitude of j^{th} eigen-vector of the matrix P^TP. This value can thus be used to represent the corresponding weighting of the probability of y is classified as O_h with classifier c_j. Therefore, $s_h\left(x_o\right) = \sum_{j=1}^{m}\sqrt{\lambda_j}P_h^j\left(x_o\right)$ should be used to denote the overall probability of y is classified as O_h.

Based on the definition of sum rule, if $s_h\left(x_o\right) = \sum_{j=1}^{m}\sqrt{\lambda_j}P_h^j\left(x_o\right)$ is the largest among $s_1\left(x_o\right),...,s_n\left(x_o\right)$, then x_o is assigned as class O_h. In addition, the probability of y classified as O_h at position x_o is estimated as

$$P\left(y\in O_h \middle| x_o\right) = P_h\left(x_o\right) = \frac{s_h\left(x_o\right)}{\sum_{i=1}^{n}s_i\left(x_o\right)} = \frac{\sum_{j=1}^{m}\sqrt{\lambda_j}P_h^j\left(x_o\right)}{\sum_{j=1}^{m}\sqrt{\lambda_j}} \tag{5.5}$$

5.2.3 Instance

Let the probabilities of pixel y classified as the predefined classes are $P_{ML}\left(O_1\right) = 0.4$, $P_{ML}\left(O_2\right) = 0.3$ and $P_{ML}\left(O_3\right) = 0.3$ respectively by using

maximum likelihood classifier.

By using minimum distance classifier, let the probabilities of pixel y belonging to the predefined classes are $P_{MD}(O_1) = 0.6$, $P_{MD}(O_2) = 0.15$ and $P_{MD}(O_3) = 0.25$, respectively.

Then the posterior probability matrix is $\left(P_i^j\right) = \left(P_i^j\right)_{3\times 2} = \begin{pmatrix} 0.6 & 0.4 \\ 0.15 & 0.3 \\ 0.25 & 0.3 \end{pmatrix}$ and the square roots of eigen-values of $\left(P_i^j\right)^T \left(P_i^j\right)$ are 0.1694 and 0.8697. Since large square sum of column corresponds to weighting. Thus, 0.8697 and 0.1694 correspond $\begin{pmatrix} 0.6 \\ 0.15 \\ 0.25 \end{pmatrix}$ and $\begin{pmatrix} 0.4 \\ 0.3 \\ 0.3 \end{pmatrix}$, respectively. Therefore,

$$P(O_1) = \frac{0.6 \times 0.8697 + 0.4 \times 0.1694}{0.8697 + 0.1694} = 0.5674$$

$$P(O_2) = \frac{0.15 \times 0.8697 + 0.3 \times 0.1694}{0.8697 + 0.1694} = 0.1745$$

$$P(O_3) = \frac{0.25 \times 0.8697 + 0.3 \times 0.1694}{0.8697 + 0.1694} = 0.2582$$

Figure 5.1 shows an example of the proposed eigen-values-based method to assign weightings when combining maximum likelihood classifier and minimum distance classifier.

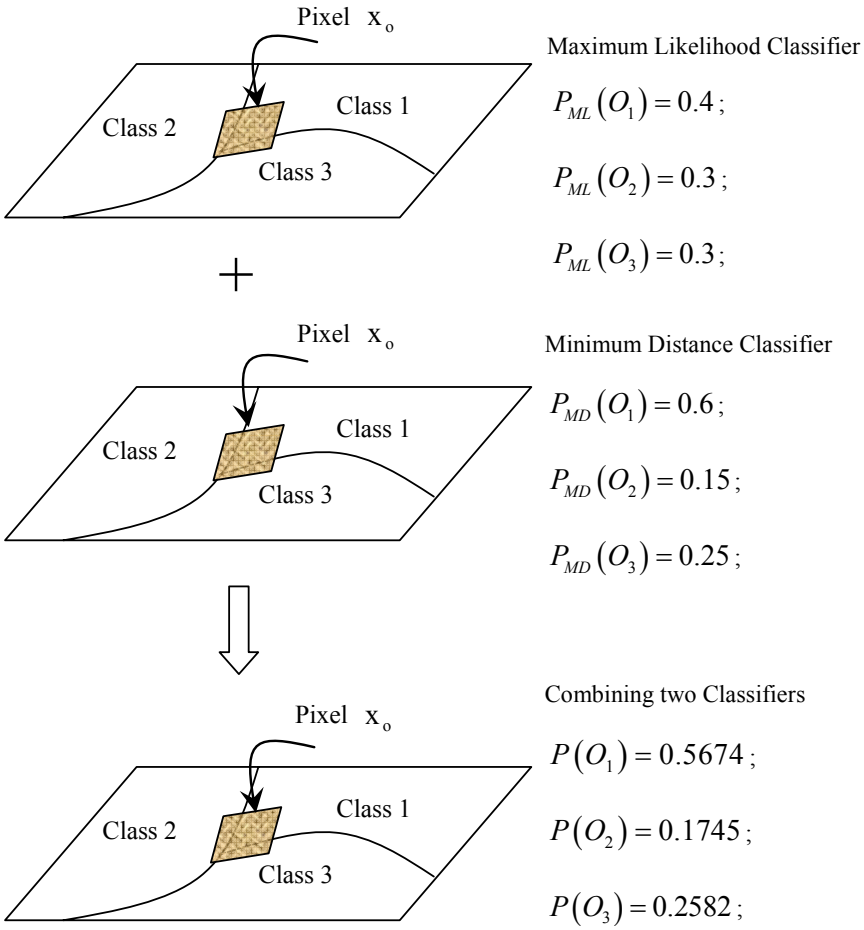

Figure 5.1 Combining two classifiers by the eigen-values-based sum rule

5.3 Implementation of the Proposed Multiple Classifier System

5.3.1 The Logic Flow of the Proposed Method

Figure 5.2 shows the logic flow of this the proposed classification method based on the eigen-values.

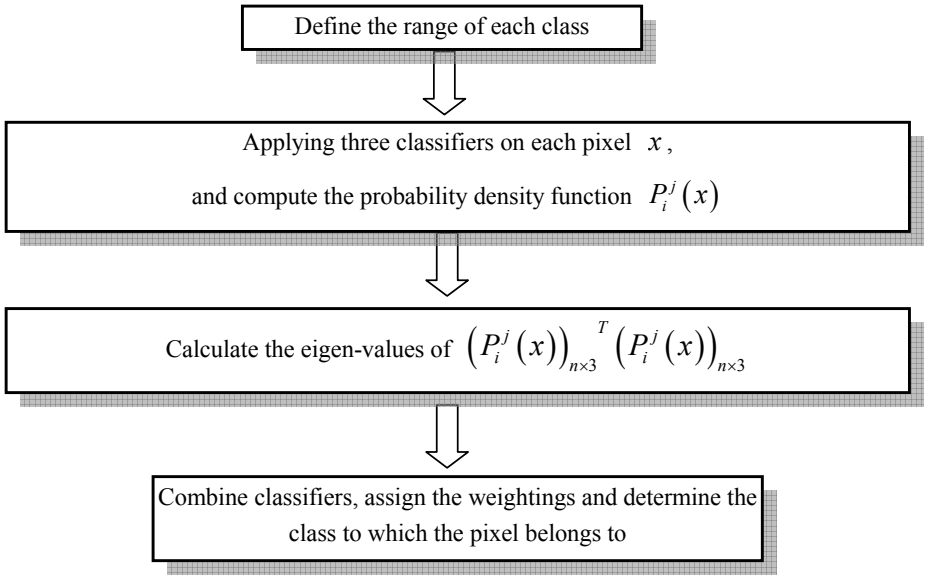

Figure 5.2 The logic flow of the proposed classification method

5.3.2 The Implementation Steps

The four steps of the logic flow of the proposed eigen-values-based classification method are detailed as the follows.

Step 1. Define the range of each class. For each predefined class O_k, compute the mean μ_{O_k} variance matrix σ_{O_k} and variance-covariance matrix Σ_{O_k}, where $k = 1, 2, ..., n$.

Step 2. Compute the probability distribution function (PDF) for each method and each pixel x

For maximum likelihood classifier

The likelihood can be expressed as formula (5.2) and the posterior probability of pixel x classified as k^{th} class is defined as formula (5.1).

For Normalized Euclidian Distance Classifier

The Normalized Euclidian distance is $d_k^{\,2} = (x - \mu_k)^T \sigma_k^{-1} (x - \mu_k)$, therefore, in the case of Normalized Euclidian distance classifier, the posterior probability of pixel x classified as k^{th} class is defined as formula (5.3).

For Mahalanobis distance classifier

The Mahalanobis distance is $d_k^{\,2} = (x - \mu_k)^T \Sigma_k^{-1} (x - \mu_k)$, therefore, in the case of Mahalanobis distance classifier, the posterior probability of pixel x classified as k^{th} class is defined as formula (5.4).

Finally, obtained, is the posterior probability matrix

$$\left(P_i^j(x)\right)_{n\times 3} = \begin{pmatrix} P_1^1 & P_1^2 & P_1^3 \\ P_2^1 & P_2^2 & P_2^3 \\ .. & .. & .. \\ .. & .. & .. \\ P_n^1 & P_n^2 & P_n^3 \end{pmatrix}$$

Step 3. Calculate the eigen-values of $\left(P_i^j(x)\right)_{n\times 3}^T \left(P_i^j(x)\right)_{n\times 3}$, $P^T P$ for simplification. The eigen-values of $P^T P$ are obtained by using $(P^T P)v = \lambda v$.

Step 4. Combine classifiers, assign weightings and determine the class of the pixel concerned. Let $\lambda_1 \geq \lambda_2 \geq \lambda_3$ be the eigen-values of $P^T P$. Based on the principle of weighting assignment, large λ_j should correspond

to large sum of square of $\begin{pmatrix} P_1^j \\ P_2^j \\ .. \\ .. \\ P_n^j \end{pmatrix}$. Then for the concerned pixel x_o, define $s_i(x_o) = \sum_{j=1}^{3} \sqrt{\lambda_j} P_i^j(x_o)$, where $i = 1,2,...,n$. If $s_h(x_o) = \sum_{j=1}^{3} \sqrt{\lambda_j} P_h^j(x_o)$ is the largest among $s_1(x_o)$, …, $s_n(x_o)$, then x_o is assigned as class O_h. In addition, the probability of y classified as O_h at position x_o is estimated as formula (5.5).

5.4 Case Study I

5.4.1 Dataset

The experimental site locates in south-west of Xuzhou city, China. Figure 5.3 is the original Landset TM image for the classification test taken in 2000. The data includes 7 spectrum bands and the spatial resolution is 30m. The size of the data in the experiments is 512*512. Four land cover classes building, woodland, water and farmland were identified for the classification.

Figure 5.3 Landsat satellite image of the Xuzhou city taken in 2000

5.4.2 Comparisons among Different Classifiers

In the experimental study, firstly the pixels of these four classes were trained for classification, that is, the pixels from the image were extracted to train the classifiers for the later classification process. Based on these training results, (in other words, the statistical distribution of each of the four classes), each classifier, then, creates a probability density function by which each pixel was assigned to a land cover class.

The newly proposed eigen-values-based method was then compared with existing classification methods namely, the maximum likelihood classifier, minimum distance classifier, Mahalanobis distance classifier and simple average MCS. The details of the experimental results are given below.

Figure 5.4, Figure 5.5 and Figure 5.6 show the classification results, using the maximum likelihood classifier, minimum distance classifier and Mahalanobis distance classifier, respectively. Figure 5.7 shows the classification results from combining the three individual classifiers by simply averaging the sum of probabilities, from the maximum likelihood classifier, minimum distance classifier and Mahalanobis distance classifier. Figure 5.8 shows the classification result, based on the proposed eigen-values-based method, which combines the maximum likelihood classifier, minimum distance classifier and Mahalanobis distance classifier.

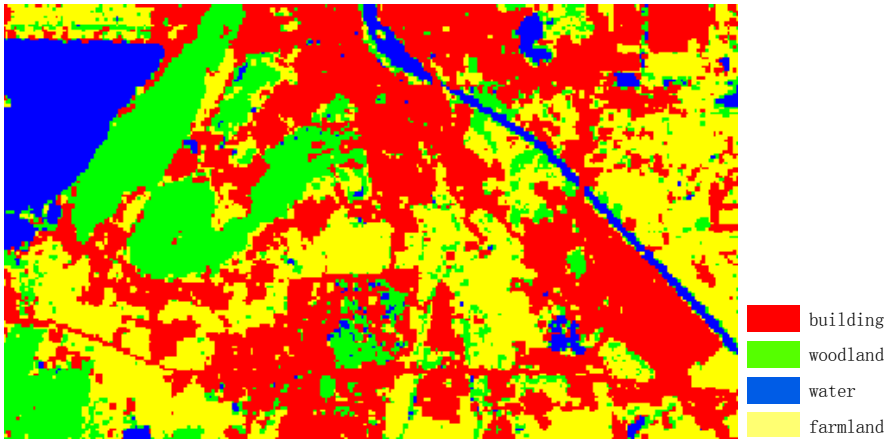

Figure 5.4 The result of maximum likelihood classification

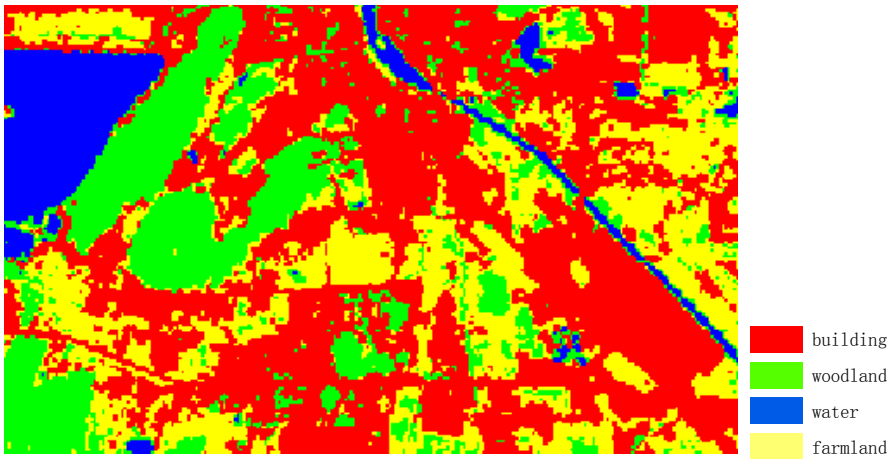

Figure 5.5 The result of minimum distance classification

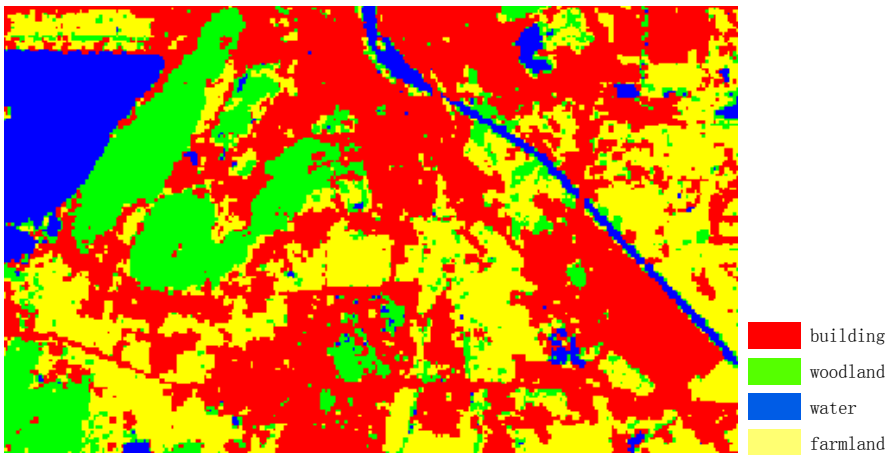

Figure 5.6 The result of Mahalanobis distance classification

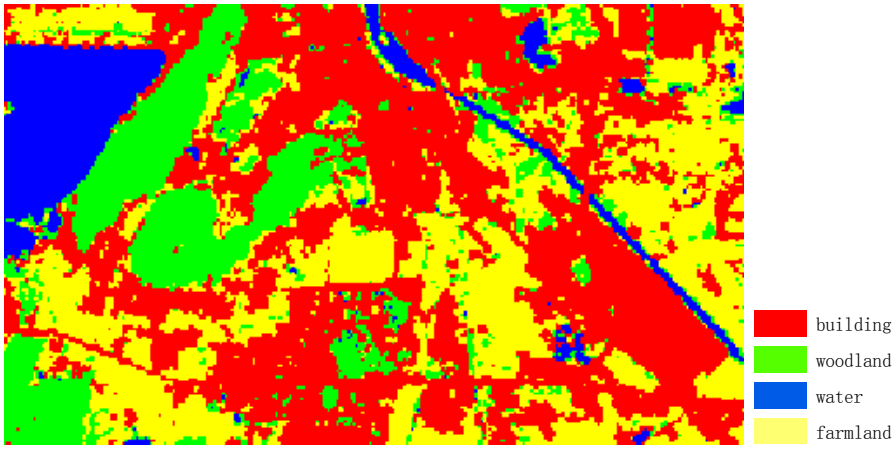

Figure 5.7 Combining three classifiers by simple average sum rule

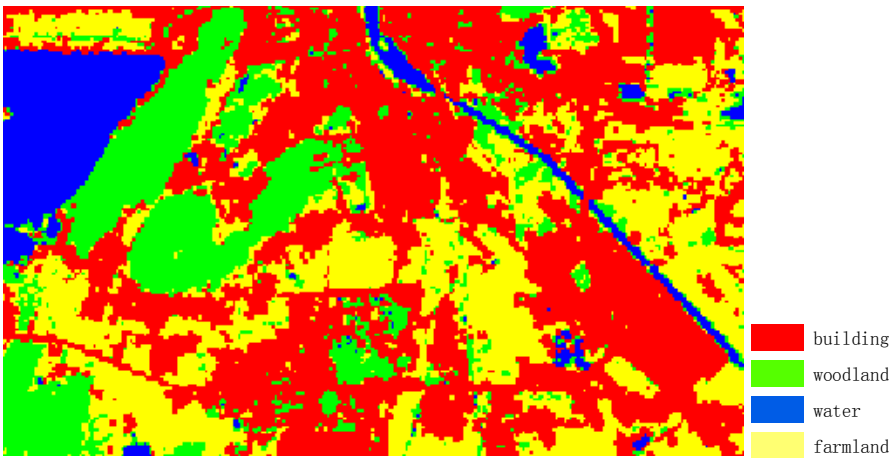

Figure 5.8 Combining three classifiers by the eigen-values-based sum rule

5.4.3 Accuracy Assessment

In assessing the accuracy of the classifications, the method of Efron and Tibshirani (1997) was applied which estimates classification accuracy and kappa by re-sampling the training data. In this accuracy assessment, there were a total 8721 pixels of ground reference data, including 5625 pixels for building, 1078 pixels for woodland, 742 pixels for water and 1276 pixels for farmland. The accuracy of the classification was computed based on a comparison of the classification results with the reference data sets.

The overall accuracy and the kappa of different classification methods, that is, the maximum likelihood classification (MLC) with 0.8344 and 0.7274 (see Table 5.1), the minimum distance classification (MIND) with 0.8376 and 0.7191 (see Table 5.2), the Mahalanobis distance classification (MAH) with 0.8593 and 0.7619 (see Table 5.3), the simple average method (SAVG) with 0.8563 and 0.7582 (see Table 5.4) and the eigen-values-based classification (EIGC) with 0.8622 and 0.7664 (see Table 5.5), were compared.

Table 5.1 The confusion matrix using MLC

	Building	Woodland	Water	Farmland	Total	User's accuracy
Building	4392	20	10	42	4464	0.9839
Woodland	333	1038	26	79	1476	0.7033
Water	34	3	694	2	733	0.9468
Farmland	866	17	12	1153	2048	0.5630
Total	5625	1078	742	1276	8721	
Producer's accuracy	0.7808	0.9629	0.9353	0.9036		Overall accuracy = 0.8344
Kappa statistics						Overall Kappa = 0.7274

Table 5.2 The confusion matrix using MIND

	Building	Woodland	Water	Farmland	Total	User's accuracy
Building	4733	15	26	201	4975	0.9513
Woodland	319	1035	59	189	1602	0.6460
Water	2	0	651	0	653	0.9969
Farmland	571	28	6	886	1491	0.5942
Total	5625	1078	742	1276	8721	
Producer's accuracy	0.8414	0.9601	0.8774	0.6944		Overall accuracy = 0.8376
Kappa statistics						Overall Kappa = 0.7191

Table 5.3 The confusion matrix using MAH

	Building	Woodland	Water	Farmland	Total	User's accuracy
Building	4626	32	19	69	4746	0.9747
Woodland	244	1028	21	55	1348	0.7626
Water	17	2	690	2	711	0.9705
Farmland	738	16	12	1150	1916	0.6002
Total	5625	1078	742	1276	8721	
Producer's accuracy	0.8224	0.9536	0.9299	0.9013		Overall accuracy = 0.8593
Kappa statistics						Overall Kappa = 0.7619

Table 5.4 The confusion matrix using SAVG

	Building	Woodland	Water	Farmland	Total	User's accuracy
Building	4592	19	15	60	4686	0.98004
Woodland	267	1036	28	62	1393	0.7437
Water	11	1	687	1	700	0.9814
Farmland	755	22	12	1153	1942	0.5937
Total	5625	1078	742	1276	8721	
Producer's accuracy	0.8164	0.9610	0.9259	0.9036		Overall accuracy = 0.8563
Kappa statistics						Overall Kappa = 0.7582

Table 5.5 The confusion matrix using EIGC

	Building	Woodland	Water	Farmland	Total	User's accuracy
Building	4661	15	14	72	4762	0.9788
Woodland	329	1038	31	69	1467	0.7076
Water	11	1	686	1	699	0.9814
Farmland	624	24	11	1134	1793	0.6325
Total	5625	1078	742	1276	8721	
Producer's accuracy	0.8286	0.9629	0.9245	0.8887		Overall accuracy = 0.8621
Kappa statistics						Overall Kappa = 0.7664

The distributions in Figure 5.9 show the overall accuracy and the kappa of different classification methods. The overall accuracy and the kappa value of the MLC, the MIND, the MAH, the SAVG and the EIGC are 0.8344, 0.8376,

0.8593, 0.8563, 0.8621 and 0.7274, 0.7191, 0.7619, 0.7582, 0.7664 respectively. The eigen-values-based classification reaches the highest overall classification accuracy and kappa value. Consequently, the performance of the eigen-values-based multiple classifier method is better than the simple average multiple classifier method and other single classifier. The main reason for this is that the eigen-values-based method can provide a set of effective weightings for each of the classifiers and hence can make a significant contribution to the improvement of the multiple classifier system.

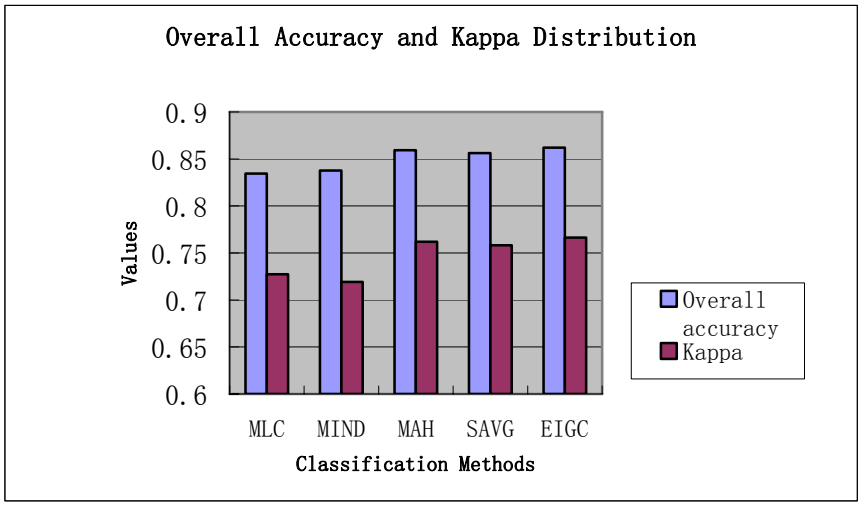

Figure 5.9 The distributions of the overall accuracy and the kappa of different classification methods

5.4.4 Discussion

As usual, the proposed multiple classifier is based on the assumption that all types of classifiers are complementary in terms of classification performance. Advantages of the newly designed multiple classifier method include the following: (a) the weightings of the classifiers are based on the eigen-values origin from the posterior probabilities matrix, thus, this weightings is based on

the spectrum of the image; (b) the principle that a large classifier value, assigned to a high weighting based on large eigen-value can enhance the effect of the classifier, naturally; (c) the principle that a small classifier value, assigned to a low weighting based on small eigen-value can reduce the effect of the classifier, naturally.

The disadvantages of the newly designed multiple classifier method is similar to those of the ordinary Multiple Classifier Systems (MCS). In the real case, not all classifiers are complementary, resulting in classifier fusion weakness. In an attempt to overcome this problem, classifiers are first selected to match the major classes, and classifier fusion is then conducted to process the classification scheme. As these mixed pixels must be assigned a particular class, the specific nature of each pixel class may cause incorrect classification. For example, if the mixed pixel contains 48% class *A*, 50% class *B* and 2% other classes, although the eigen-value-based method contributes to establishing certain classifiers, in that pixels are evenly classified, the classification result may have an error as to the nature of each pixel in the mixed pixel group. Thus, to find out the complementary set of classifiers is a major work in MCS.

Moreover, the difficulty for finding of the eigen-values of the characteristic polynomial increases rapidly with increasing the degree of the polynomial (Wikipedia). For the degree of the polynomial greater than or equal to 5, the exactly eigen-values cannot be found, values but only the approximation.

5.5 Case Study II

5.5.1 Dataset

In this study, pixel unmixing strategy for multi-spectral remotely sensed image is proposed in chapter 4. The objective of such unmixing strategy is to provide a much higher quality image for image classifications. In addition, in chapter 5, we proposed an effective classification method, which is called eigen-values based multiple classifier system and is proved to can improve the performance of the classification capability with Case study I in chapter 5.

Furthermore, in order to validate that our propose classification method cooperated with quality improved image by unmixing the mixed pixel can obtain much better effect in image classification area, we design the case study II.

The data is still the one used in chapter 4 and case study I in chapter 5. Here, we will not explain it again.

5.5.2 Classified unmixed images with Different Classifiers

The classified image is obtained from unmixing procedure which is interpreted in detail in chapter 4. After experiment, we would like to prove that the unmixing procedure can really improve the image quality, which is validated by different classification method applied on it.

Next, similarly like in case study I, firstly the pixels of these four classes were trained for classification, that is, the pixels from the image were extracted to train the classifiers for the later classification process. Based on these training

results, (in other words, the statistical distribution of each of the four classes), each classifier, then, creates a probability density function by which each pixel was assigned to a land cover class.

We apply the newly proposed eigen-values-based method, the maximum likelihood classifier, minimum distance classifier, Mahalanobis distance classifier and simple average MCS to classify the unmixed image. The details of the experimental results are given below.

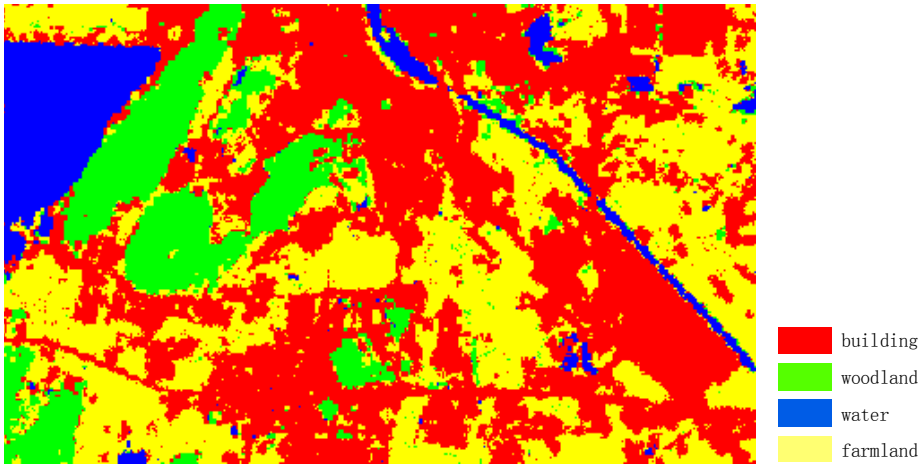

Figure 5.10 The result of maximum likelihood classification

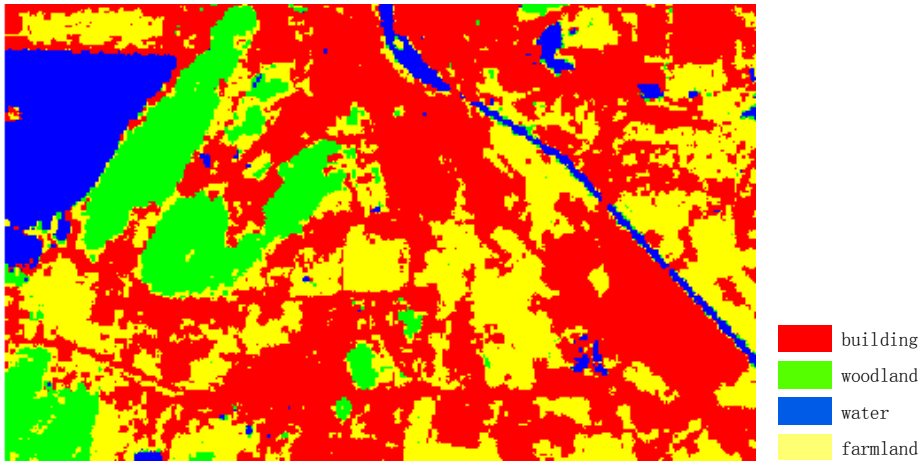

Figure 5.11 The result of minimum distance classification

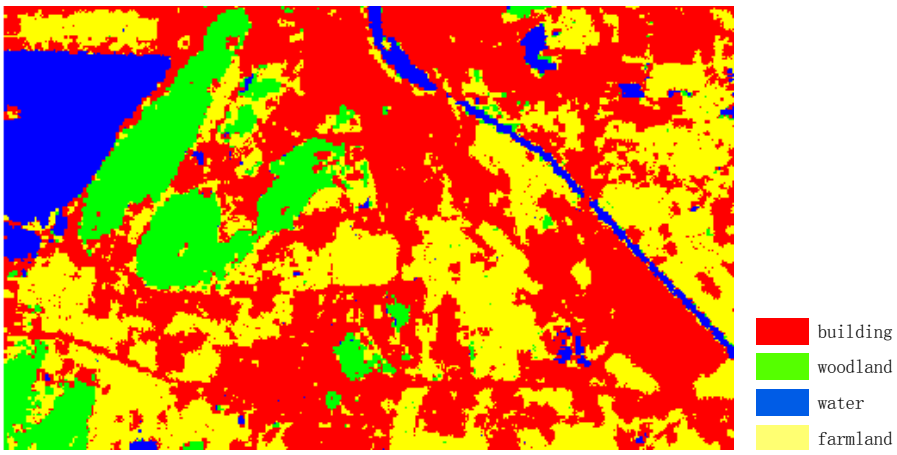

Figure 5.12 The result of Mahalanobis classification

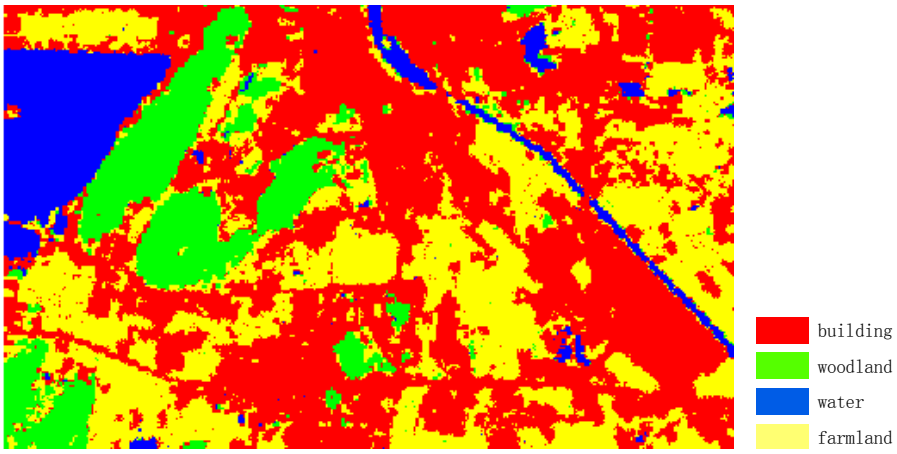

Figure 5.13 Combining three classifiers by simple average sum rule

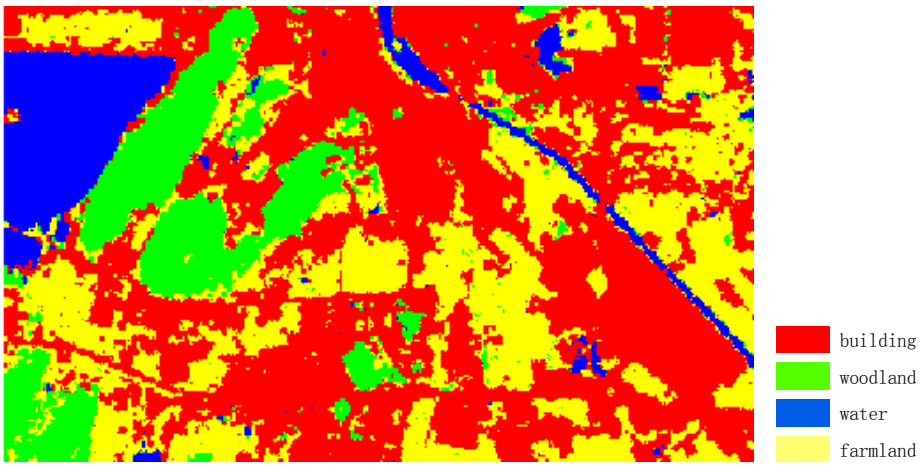

Figure 5.14 Combining three classifiers by eigen-values based sum rule

5.5.3 Accuracy Assessment

Corresponding to the classification results shown in Figure 5.10 to Figure 5.14, we can obtain the confusion matrixes for every classification method, and they are illustrated in Table 5.6 to Table 5.10. In this accuracy assessment, there were a total 21281 pixels of ground reference data, including 4000 pixels for building, 6281 pixels for woodland, 3000 pixels for water and 8000 pixels for farmland. The accuracy of the classification was computed based on a comparison of the classification results with the reference data sets.

Table 5.6 The confusion matrix using MLC

	Building	Woodland	Water	Farmland	Total	User's accuracy
Building	3720	387	67	358	4532	0.8208
Woodland	15	5142	46	112	5315	0.9675
Water	8	54	2837	31	2930	0.9683
Farmland	257	698	50	7499	8504	0.8818
Total	4000	6281	3000	8000	21281	
Producer's accuracy	0.9300	0.8187	0.9457	0.9374		Overall accuracy =0.9021
Kappa statistics						Kappa =0.8634

Table 5.7 The confusion matrix using MIND

	Building	Woodland	Water	Farmland	Total	User's accuracy
Building	3852	264	50	539	4705	0.8187
Woodland	13	4797	72	13	4895	0.9800
Water	3	23	2847	0	2873	0.9910
Farmland	132	1197	31	7448	8808	0.8456
Total	4000	6281	3000	8000	21281	
Producer's accuracy	0.9630	0.7637	0.9490	0.9310		Overall accuracy =0.8902
Kappa statistics						Kappa =0.8466

Table 5.8 The confusion matrix using MAH

	Building	Woodland	Water	Farmland	Total	User's accuracy
Building	3804	640	88	390	4922	0.7729
Woodland	3	4733	26	15	4777	0.9908
Water	4	45	2860	7	2916	0.9808
Farmland	189	863	26	7588	8666	0.8756
Total	4000	6281	3000	8000	21281	
Producer's accuracy	0.9510	0.7535	0.9533	0.9485		Overall accuracy =0.8921
Kappa statistics						Kappa =0.8497

Table 5.9 The confusion matrix using SAVG

	Building	Woodland	Water	Farmland	Total	User's accuracy
Building	3803	438	60	399	4700	0.8091
Woodland	9	4930	44	18	5001	0.9858
Water	4	37	2870	7	2918	0.9836
Farmland	184	876	26	7576	8662	0.8746
Total	4000	6281	3000	8000	21281	
Producer's accuracy	0.9508	0.7849	0.9567	0.9470		Overall accuracy =0.9012
Kappa statistics						Kappa =0.8622

Table 5.10 The confusion matrix using EIGC

	Building	Woodland	Water	Farmland	Total	User's accuracy
Building	3866	310	56	434	4666	0.8285
Woodland	15	5137	47	38	5237	0.9809
Water	4	40	2873	8	2925	0.9822
Farmland	115	794	24	7520	8453	0.8896
Total	4000	6281	3000	8000	21281	
Producer's accuracy	0.9665	0.8179	0.9577	0.9400		Overall accuracy =0.9114
Kappa statistics						Kappa =0.8765

The distributions in Figure 5.15 show the overall accuracy and the kappa of

different classification methods. The overall accuracy and the kappa value of the MLC, the MIND, the MAH, the SAVG and the EIGC are 0.9021, 0.8902, 0.8921, 0.9012, 0.9114 and 0.8634, 0.8466, 0.8497, 0.8622, 0.8765 respectively. The eigen-values-based classification reaches the highest overall classification accuracy and kappa value. Consequently, the performance of the eigen-values based multiple classifier method classified for unmixed images is still better than the simple average multiple classifier method and other single classifier.

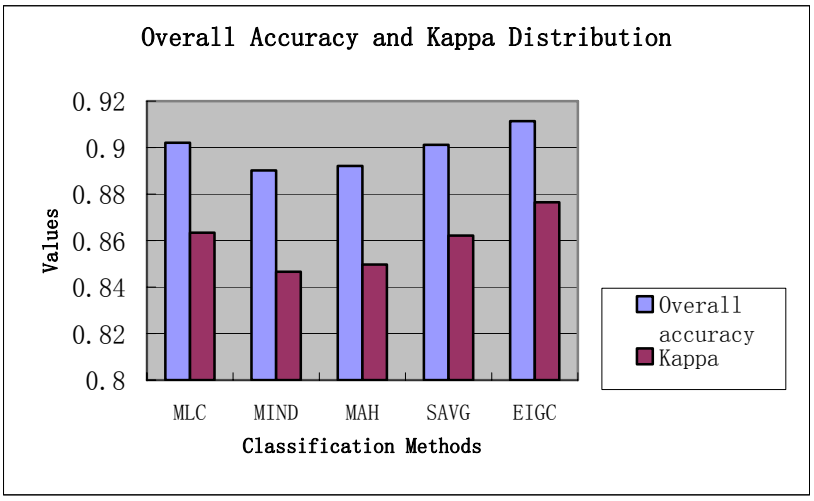

Figure 5.15 The distributions of the overall accuracy and the kappa of different classification methods

In addition, the distributions in Figure 5.16 and Figure 5.17 show the overall accuracy and the kappa of different classification methods on the same image before and after unmixing. Before the image being unmixed, the overall accuracy and the kappa value of the MLC, the MIND, the MAH, the SAVG and the EIGC are 0.8344, 0.8376, 0.8593, 0.8563, 0.8621 and 0.7274, 0.7191, 0.7619, 0.7582, 0.7664. After the image being unmixed, the overall accuracy and the kappa value of the MLC, the MIND, the MAH, the SAVG and the EIGC

are 0.9021, 0.8902, 0.8921, 0.9012, 0.9114 and 0.8634, 0.8466, 0.8497, 0.8622, 0.8765 respectively.

We find, no matter from the overall accuracy or kappa statistic, the classification accuracy of each classification method has been improved in vary degree. Consequently, the performance unmixing mixed pixels really play an important role in improving the quality of images.

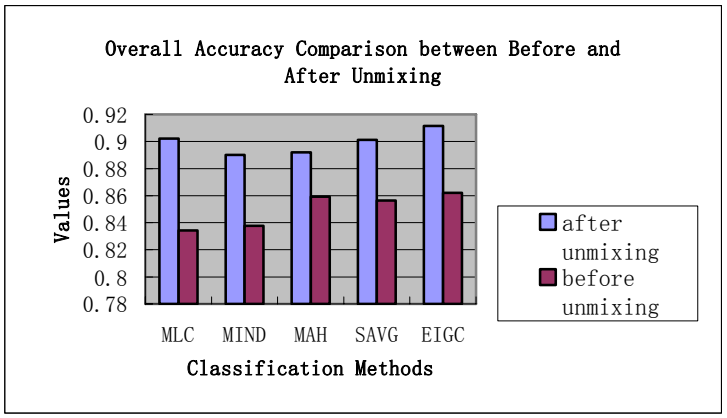

Figure 5.16 Distributions of overall accuracy of different classification methods on the same image before and after unmixing

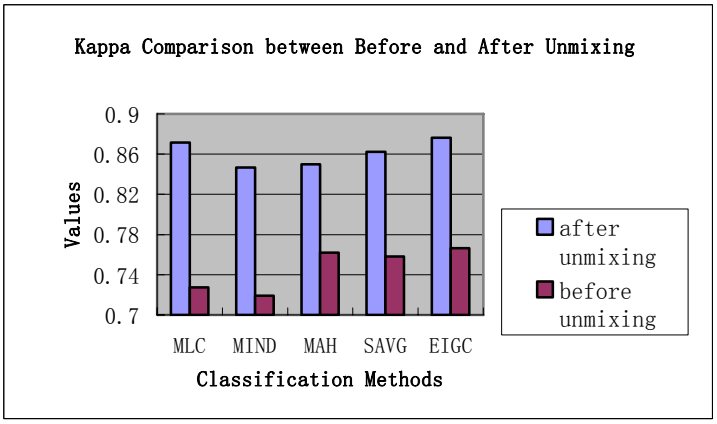

Figure 5.17 Distributions of Kappa of different classification methods on the same image before and after unmixing

5.6 Summary

In this chapter, a new weighting method based on eigen-values is brought forward when combing different classifier into a multiple classifier system. As indicated in section 5.2, this method has been based on the assumption that a larger sum of squares for a classifier should correspond to a higher weighting, i.e. larger eigen-value. A smaller sum of squares for a classifier should correspond to a lower weighting, i.e. smaller eigen-value.

Firstly, the range of each class was defined. The posterior probabilities matrix was then computed after applying each classifier on each pixel. This was followed by the computation of the eigen-values of the matrix $P^T P$ (P is the posterior probabilities matrix) and assignment of the square root of each eigen-value to different classifiers, in accordance with the classifier values. Finally, the pixel class was determined and the probability can be calculated based on the proposed weighting system.

The experimental results of case study I have demonstrated that the newly proposed eigen-values-based method have the highest overall accuracy and the highest kappa, compared to the maximum likelihood classification, minimum distance classification, Mahalanobis distance classification and simple average multiple classifiers method.

Although, the improvement is not too high, it provide a based for further classification process, topological method is an example. The significance of the proposed eigen-values-based method is the provision by the eigen-values of a

meaningful weighting to individual classifiers. The probability value of each pixel, classified by the eigen-values-based method, is between the smallest probability and the largest probability of the posterior probabilities matrix. Thus the eigen-value method resets the classifiers through a set of suitable weightings for each classifier.

The experimental results of case study II have demonstrated that the newly proposed eigen-values-based method and other common classifications, such as the maximum likelihood classification, minimum distance classification, Mahalanobis distance classification and simple average multiple classifiers method can improve the classification accuracy for the same image after unmixing.

Although the sample size has been increased and make the computation cost be higher, it is not a fatal disadvantage. In a sense, the more sample individuals are, the more sample close to population. Of course, this is not a good excuse for selecting so much sample point. This is partially because the spatial resolution of the unmixed image has been upgrade to fourfold. Anyway, the classification accuracy has obviously improvement. On the contrary, it leaved us a new research direction how to control and reduce the amount of sample points.

6 Validity of Error Distribution-based Spatial Sample

Evaluation of classification accuracy is also one of the important steps for image classification. The evaluation procedures include proposing accuracy measurements and sample strategy. In this chapter, we focus on the latter and proposed an error distribution-based spatial sample strategy. On the basis of error distribution, we configure the error surface subtracted from original data. Then we select the representative extreme points on the error surface and regard those points as the sample points. We finally simulate and demonstrate the validity of the proposed sample strategy.

6.1 Methodology of Proposed Sample Method

6.1.1 Statistical Distribution of Error

There are three kinds of error, namely random error, system error and gross error. A lot of methods and assessing rules have been researched to find the description of the error and its distribution, such as LP norm distribution (Meng et al., 1998; Zhou et al., 2003) etc. However, the error distribution of the classical measuring data obeys normal distribution. French mathematician De Moivere and Germanic mathematician Gauss have made landmark work for error theory and point out the normal distribution of the random error. Especially, Gauss contributed the basis for the distribution pattern of random error and brought forward the error processing method (Bolstad et al., 1990; Goodchild, 1991).

However, there are many other kinds of description for error distribution. In this study, I focus on the research how to perform the spatial sampling under this classical situation, and validate whether the sample result based on the error distribution can reflect the true situation of the whole error. In this study, suppose the error obeys the normal distribution. In addition, a set of surveyed data $(a_1, a_2, ...a_n)$ and suppose its corresponding error $(\varepsilon_1, \varepsilon_2, ...\varepsilon_n)$ obey the normal distribution. On the basis of such known information, I will try to assess the error based on its spatial distribution.

6.1.2 Similarity with Signal Processing

Before talking about the sample strategy, we would like to compare the error on the remotely sensed image and the noise in the signal (see Figure 6.1). They interweaved with the useful information, but are not the welcome information. We need remove the noise from the signal so that we can get clear signal; similarly, we also like to remove the error from the original data so that we can get effective information. So we can use the same methodology which is used for signal processing on spatial data. In this study, the idea of Gaussian distribution and multi-scale filter method is used for error removing.

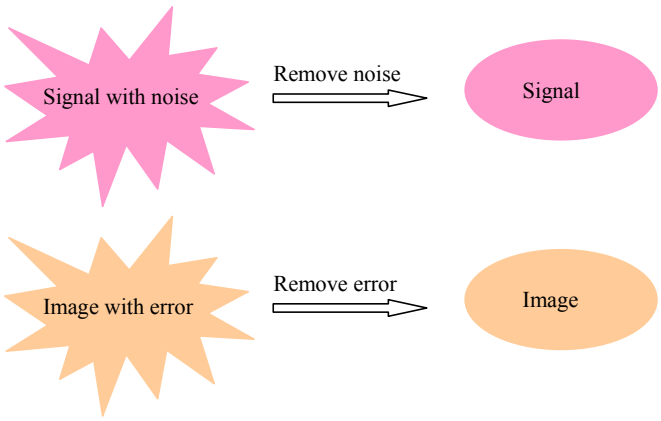

Figure 6.1 Similarity between noise remove and error remove

The positional accuracy is one important aspect to estimate the quality of the spatial data. Spatial sampling on the remote sensed data and GIS raster data has been discussed for a long time. There are already some mature technologies and methodologies based on the literature review. A systematic effort has been make to investigate various aspects of accuracy in spatial databases (Banjevic and Switzer, 2002; Bogaert and Russo, 1999; Muller and Zimmerman, 1999; Royle, 2002; Wiens, 2005; Zhu and Stein, 2005). As well there are many researches evolved in the GIS vector data, including many point, line and polygon error model. In addition, some good standards for description of spatial data quality are being adopted and are being supported by software (Devillers and Jeansoulin, 2006).

Besides the research on the error model, many spatial sampling schemes have been designed to select a finite set of locations where observations provide optimal information for parameter estimation and spatial inter/extrapolation on the basis of an appropriate statistical model (Angulo and Bueso, 2001; Angulo et al., 2005).

Error models for point, line and polygon have been developed on the theoretical and/or experimental basis. Meanwhile, error propagation model are researched widely to estimate the error induced by different GIS operations.

Current spatial sampling methods are almost combined with traditional sampling method. Simple random sampling and stratified sampling as well as systematic sampling scheme are widely used to design the spatial sampling in

GIS community. Using one scheme try to get sample points as a test and based on some statistics, spatial sampling scheme are used to solve some practical applications.

In this study, we hope to analyze the accuracy of the spatial data quantitatively by means of sample method, in a further step, we even hope to exactly know the distribution of the error. Under the direction of this idea, we try to find a novel method of spatial sampling for the spatial data.

6.1.3 The Logic Flow of the Proposed Method

The purpose is to give a reasonable sampling scheme which can perfect reflect the spatial distribution of surveyed error and need sample individuals as least as possible. To solve this problem, there are two principle steps to take, namely fitting the real estimation of the spatial data and seeking the description of error surface, the whole flowchart of this study is listed in Figure 6.2.

In the first part of this study, we try to obtain an approximate expression of the spatial data. First, a approximate partition is performed on the basis of the classification results. For example, we can divide the sample area into several sub-areas, such as water, building, grass etc.. Second, suppose the error obeying normal distribution, we use multi-scale filters (MSF), which is assigned with different parameters, to remove the different magnitude of error from the measuring data for each region. After removing the error, we anticipate the reserved data is only the representation of the error-free image. So if we can extract the extreme points on the filtered data, we can fit a function for the

error-free image. Finally, we put all the fitted functions from each region together as the true estimation of the error-free spatial data (Mao et al., 2007).

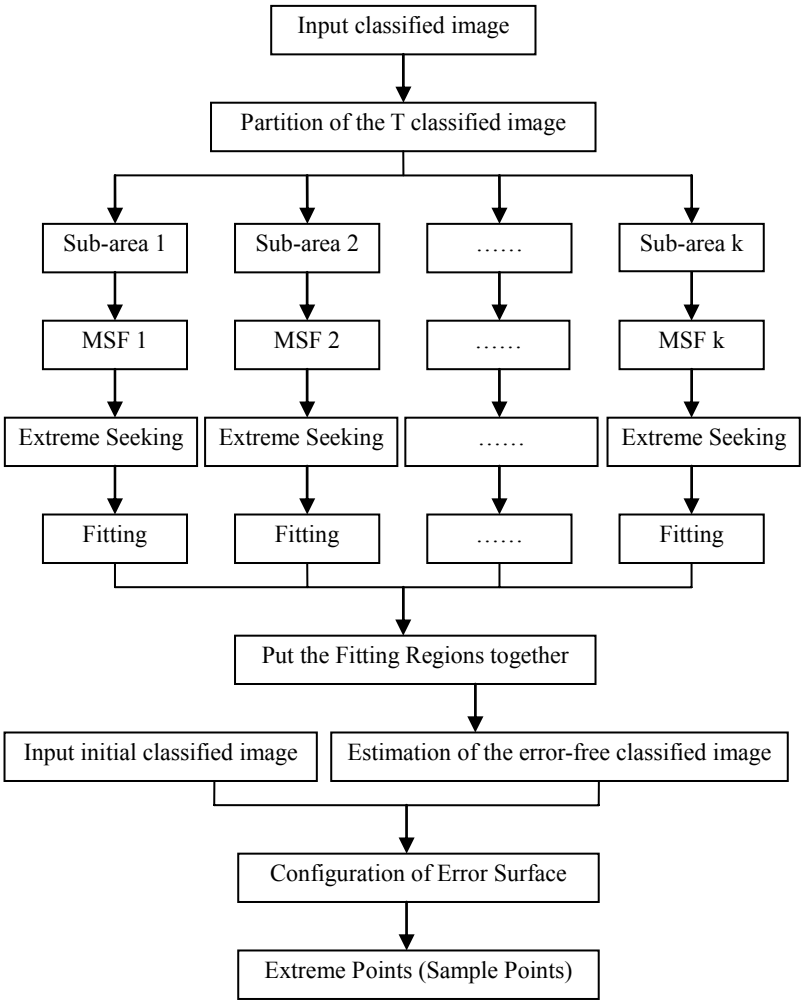

Figure 6.2 The logic flow of spatial sampling scheme

After obtaining the approximation of the error-free spatial data, together with the initial spatial data, obviously, the difference between the initial spatial data and the approximation of the initial spatial data should be represented as the error. Consequently, we can configure the error surface and further work out the extreme points. Finally, we can find the adapt amount of the sample points in optimum location for this spatial sample scheme.

6.2 Error Separation from the Initial Data

6.2.1 Prior Partition of the Sample Area

We can have some prior knowledge about the error in the classified remotely sensed image. Although we can not know the exact error distribution and error size, it's possible for us to roughly distinguish which part of a map is with high error, which part is with medium error and which part is with low error. For example, in aerial photogrammetry, the fringes of some features are easy to be distinguished and the accuracy of the stabbing points is comparative higher and vice versa. Another example, in field survey, the higher accuracy of traverse and the control survey, the lower error the features surveyed around the traverse are.

On basis of such prior knowledge, we can plan a approximate partition on the spatial data to be evaluated. In this study, experiment is executed on the spatial data obtained by maximum likelihood classification. As the accuracy of all features vary with the accuracy of a traverse and the degree of the difficulty of the feature points to be surveyed, we divide the map extent into two categories of areas with different level of error (Figure 6.3).

Figure 6.3 Prior partition for a sample extent

It’s the spatial data around Hong Kong Polytechnic University, divided by a red line with one side buildings inside the campus and other side roads outside campus. This spatial data is prior parted for sampling as there is a traverse in each partition respectively.

6.2.2 Multi-scale Filter

Based on the accuracy of measured data, we have divided the sample area into several sub-areas. Although we have no idea about the true value of the error, we can only distinguish the approximate distribution of error. It’s principle for us to take further multi-scale filter on such measured data. In this study, we will use the method of error removing based on Gauss filter. We think the measured data with error as the signal with noise.

Remember that what we want is to seek the extreme points which contained in the real classified remotely sensed images. The purpose for this is to fit a more accurate spatial data. However, in practice, the real extreme point is covered by the noise. So we want to use certain filtering method to reveal the extreme point. Unfortunately, the real extreme point may be deduced by the filter to certain extend if the scale of the filter is too large. If the scale of the filter is small, then the noise may be not removed completely. In fact, this is a classical problem for noise removing. In this section, we adopt a multi-scale filtering method to resolve this problem. Suppose we can describe the measuring data into a continuous curve in red and the error in blue line as shown in Figure 6.4.

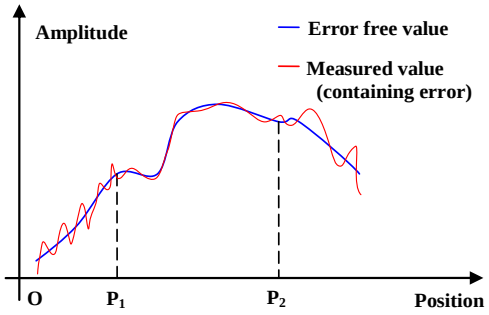

Figure 6.4 Error simulation on measured data

In Figure 6.4, we can obviously find the error between the interval [P_1, P_2] is less than that outside this interval. Actually, such condition is accordant with the case described in section 6.2.1. As the approximate error distribution is known, we can process the error apart. Here the Gaussian filter is used to remove the noise. In the spatial domain, the isotropic Gaussian can be expressed as follows:

$$G(x,y) = \frac{1}{\sqrt{2\pi\sigma^2}} e^{-\frac{x^2+y^2}{2\sigma^2}} \tag{6.1}$$

here, σ is used to control the filter degree based on the approximate error partition.

Considering that in different sub-regions, the noise is also different. Therefore, it is not reasonable that use the Gaussian filter with a fixed scale (that is the value of σ is given and fixed) to filter the whole regions. A nature idea is to use different scale filters to different sub-regions. The filter steps are designed as follows:

Step 1. the original spatial data is divided into K different sub-regions and denoted by $r_i^0\,(i = 1, \ldots, K)$. Their corresponding approximate errors are denoted by $E_i\ (i = 1, \ldots, K)$, and suppose $E_1 > E_2 > \ldots > E_K$ without lose of generality.

Step 2. Given the filter scales in equation (6.1) for above sub-regions $\sigma_i^0\ (i = 1, \ldots, K)$, and let $\sigma_1^0 > \sigma_2^0 > \ldots > \sigma_K^0$.

Step 3. The sub-regions are filtered by using the filters given in equation (6.1) with the scales given in step 2 and denoted the filtered by $r_i^1\,(i = 1, \ldots, K)$.

Step 4. set another groups of scales as $\sigma_i^1 = \frac{\sigma_i^0}{2}(i = 1, \ldots, K)$, the same procedure as step 3 is performed, the corresponding results are denoted by $r_i^2\,(i = 1, \ldots, K)$.

Step 5. repeat the procedure of step 4 and set the scales of Gaussian as $\sigma_i^n = \frac{\sigma_i^0}{n-1}(i = 1, 2, \ldots, K)$, the filtered result is then represented as $r_i^n\,(i = 1, \ldots, K)$.

Step 6. extracting the extreme points of $r_i^1, r_i^2, \ldots, r_i^n\,(i = 1, \ldots, K)$, and checking the extreme points which disappeared. Those across many layers are selected as robust extreme points. And then the corresponding locations are recorded.

Remark 1: the reason for the step 6 is based on the understanding that the robust extreme point is disappeared slowly. Those points disappeared quickly (that is

remained in few layers) are not the real extreme points. It geometric illustration in one dimensional case is given in Figure 6.4. From Figure 6.5, we see that the points labeled by green star symbols is weaken slowly, while the points labeled by yellow cross symbols are disappeared quickly, so we have reason to conclude that the green star points are really the extreme points while the yellow cross points are false extreme points or noise points.

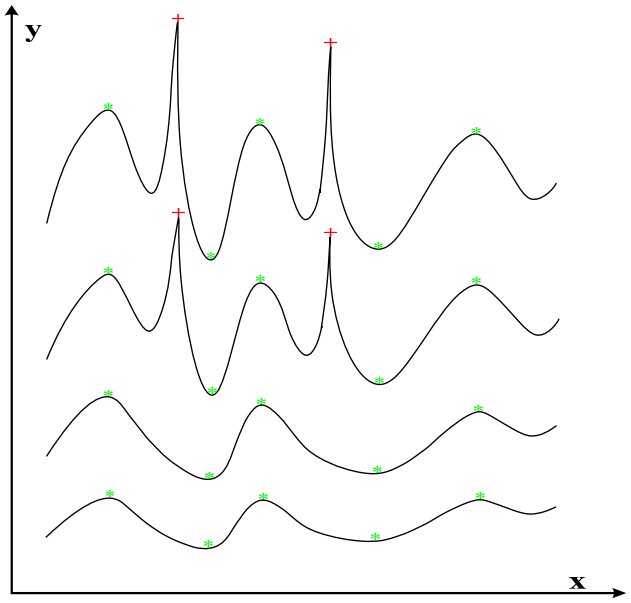

Figure 6.5 Extreme points across layers

Remark 2: in practice, the number of the filtered layers should be considered. That is the times of the filters used must be determined. There are two simple strategies for this problem. One is to give a filtered time in advance, and another is that the filtering time can be given by comparing two adjacent filtered results, if the difference of their extreme points is smaller than a given threshold, then the filtered procedure can be end. Certainly, the filtered times in each sub-region may be different.

6.2.3 Fitting Function

Different filters are proposed for different sub-areas and the function curve of the measuring data is obtained after filtering the error. After the Gauss filtering, several extreme points are obtained on the curve filtered, which represent the true location of the spatial data contrast to the measured data with error.

Although some extreme points on the measuring data will be weakened, and even be eliminated after the filtering. But the left extreme points are the real extreme of the spatial data in high confidence.

After we extract several extreme points from the measuring spatial data in each of the sub-regions, the next task is to fit these extreme points into a dense point set by certain method. In fact, there are many methods can be employed to this task such as interpolation techniques and other fitting methods. For sake of simplicity, the bi-cubic interpolation method which is used frequently in many applications is adopted. Its formula is expressed as

$$\begin{aligned} z = {} & a_1 + a_2 x + a_3 y + a_4 x^2 + a_5 xy + a_6 y^2 \\ & + a_7 x^3 + a_8 x^2 y + a_9 xy^2 + a_{10} y^3 \end{aligned} \tag{6.2}$$

By the steps introduced in section 6.2.1, the approximated sub spatial data partitions are obtained. As mentioned before, on the basis of the prior knowledge about the approximate error distribution on the spatial data, we have divided the image into several sub-areas. In order to assess the integrated accuracy of the spatial data, we have to put all the fitted function together to

represent the integrated representative expression of the whole spatial data.

Remember that above interpolation method is implemented on each of the sub-regions, then for each location on the boundary of each sub-region, there are two interpolated results, which interpolated result should be accepted? A simple method is to take the average value of these two results. An illustration for this point is given in Figure 6.6.

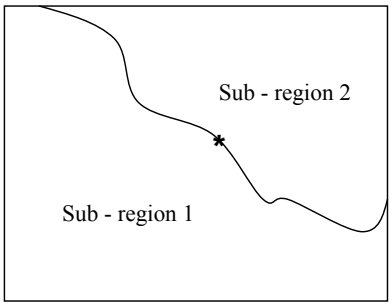

Figure 6.6 Illustration of boundary point

6.3 Selection of Sample Points

6.3.1 Construction of Error Surface

After fitting the true function for the real data, denoted as $F_1(x)$; and we already have the function of the measuring data, denoted as $F_0(x)$, and then we can obviously obtain the error surface for the research data, which can be denoted as $E = F_0(x) - F_1(x)$. By means of several filters with different scale, error surface is obtained as the difference between the original data and the fitting data after filtered. Then, error can be sampled from this error surface.

6.3.2 Sample Location on the Error Surface

During the spatial sample on the spatial data, we would like to select the points

which is representative of the population to the most extend. To satisfy this request, such points in the sample areas will be characteristic of the error value. We would not like to use only the maximum error or the minimum error to represent the whole error of the spatial data, because it will magnify or shorten the actual error and can not reflect the true situation. However, we can select all the maximum error and the minimum error together as a solution.

The function description of the error is obtained by the method introduced in section 6.2.3. The key problem of sample location on the error surface is equal to find the solution how to select the extreme points on the error surface (maybe a discrete and irregular surface).The method of extraction flow can be designed as follows:

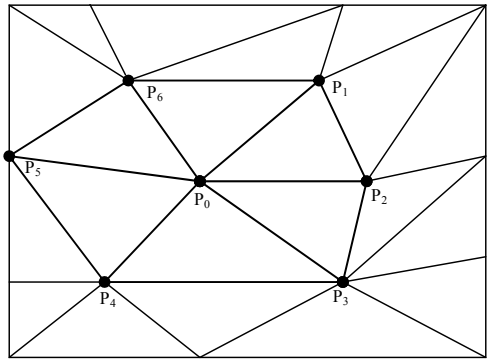

Figure 6.7 Extraction of extreme points on the error surface

Step 1. for the points located on the error surface, construct a Delauney triangle network (see Figure 6.7).

Step 2. for a point P , comparing it with the points linked with this point, if it is the smallest or the largest, then it is a extreme point, otherwise, it is not.

An example is given in Figure 6.7, if we want to determine whether the point P_0 is the extreme point, the points $P_i(i = 1,\ldots 6)$ should be compared with the point P_0, if the point P_0 is the smallest or the biggest among these six points, then the point P_0 is a extreme point. This procedure is implemented over each of the points, and then all the extreme points can be extracted.

The extreme points extracted are thought as the representative to describe the whole situation of the error surface, which is equal to be said as the accuracy reflection of measured data. As the error contribution from such points can be used to describe the integrated accuracy, they can be used to decide the selection of the sample points in this study. In other words, if we can find out these extreme points, the spatial sampling scheme can be decided.

6.4 Simulation

In this section, a simulation will be conformed to illustrate the effectiveness of the proposed method. A function used for testing is given as follows:

$$f(x) = \begin{cases} \sin 4x, & 0 \le x < 3\pi \\ \sin 8x, & 3\pi \le x \le 5\pi \end{cases} \tag{6.3}$$

Suppose it is polluted by a Gaussian error and changed as:

$$F(x) = f(x) + Gaussian \tag{6.4}$$

Here, $F(x)$ and $Gaussian$ are the observed data and Gaussian error respectively. Formula (6.3) and (6.4) are shown in Figure 6.8 and Figure 6.9

respectively.

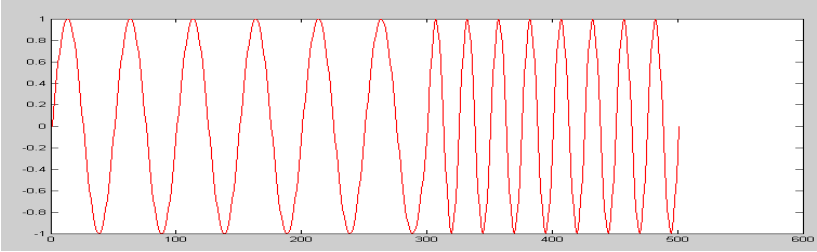

Figure 6.8 The function of f(x)

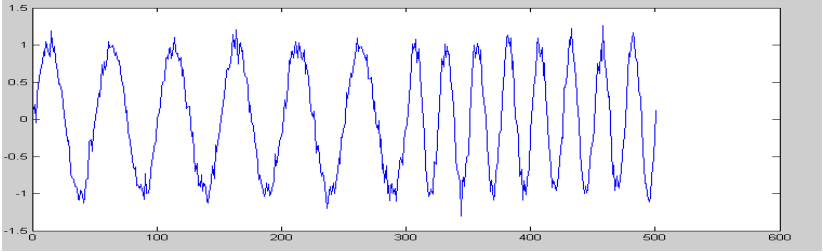

Figure 6.9 The function of F(x)

In this case, the whole region is divided into two parts, part 1 is $(0, 3\pi)$ and part 2 is $[3\pi, 5\pi]$. The initial scales of multi-scale Gaussian filters used for part 1 are set $\sigma_1^0 = 1.2$ and $\sigma_2^0 = 2.75$ respectively. And the times for multi-scale filtering are 3 and 5 respectively. After the multi-scale filtering procedure, the extreme points of the filtered data are determined and shown in Table 6.1.

Table 6.1 Positions of the extreme points on the filtered data

	1	2	3	4	5	6	7	8	9	10	11	12	13	14
Maximum	18	68	117	169	216	268	309	334	359	384	409	433	459	484
Minimum	42	92	142	193	243	293	321	346	371	397	422	447	471	497

By these extreme points, the fitting technique is implemented and the result is shown in Figure 6.10.

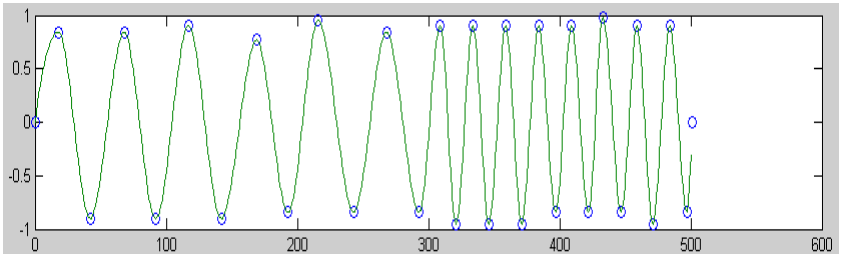

Figure 6.10 Fitting results of the two parts

After calculating the error surface and its extreme points are shown in Table 6.2.

Table 6.2 Positions of the extreme points on the error surface

	1	2	3	4	5	6	7	8	9	10	11	12	13	14
Maximum	13	63	113	163	213	264	307	332	357	382	407	432	457	482
Minimum	38	88	138	188	238	289	320	345	370	395	420	445	470	495

The points are listed in Table 6.2 is the sampling points. To illustrate the validity of the selecting of the sampling points, we can obtain a surface by fitting the sampling points and comparing with the original surface expressed by formula (6.3) (Figure 6.11). It can be found that these two surfaces are very close (the original surface is in red, the fitting surface is in blue).

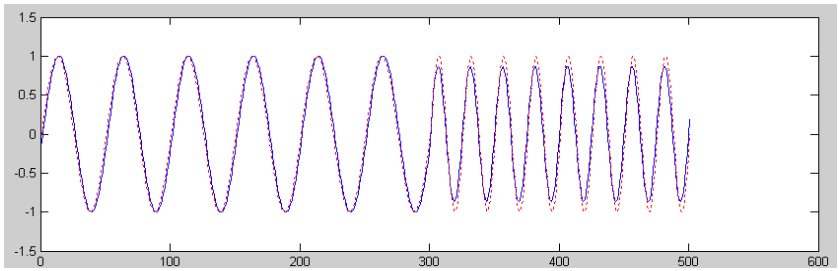

Figure 6.11 Fitting surface by the sample points and the original surface

6.5 Summary

In this paper, the proposed approach aims at sampling as least points as possible to reflect the whole error of the spatial data. Based on the proposed method, the

adapt sample points would hope to be selected not only reflect the true error situation of a whole spatial data, but also provide the description of the error distribution.

Compared with existing spatial sampling methods for spatial data in GIS, the approach presented in this paper provides a possibility to give a generic solution for error removing. We suppose the survey error obey Gaussian distribution. The most novel idea of this method is that considered and regarded as a noise in the viewpoint of signal. We try to remove the survey error as if removing the noise using different Gaussian filters in image processing. The error-free data can help us to obtain the error surface. The optimum sample points would hope to be selected based on the searching the extreme points on the error surface. What's more, error surface can rightly reflect the error distribution of the spatial data.

Error distribution-based consideration can help to detect the error situation and direct sample strategy selection. An important application of this method is to hope to assess the accuracy of the spatial data. On the condition when we only have measuring spatial data at hand and prior knowledge of the approximate error distribution about the spatial data, and we would design a good solution for spatial sampling to select the right sample points to reflect the whole accuracy and the error distribution of the spatial data.

7 Conclusions and Further Research

Land use inventory provides an important and useful means for world wide sustainable development, from which data can be collected to facilitate land resource management and decision making. However, uncertainties exist in each step of the data transmission processes. This in turn, significantly affects the quality of the inventory output and the subsequent spatial decisions making. This research has aimed to understand, model and control the quality of the land use inventory by studying a number of the key technologies developed during land use inventory. Image classification is one of the most important parts of land use inventory. We will focus on image classification to explore the inherent uncertainty sources, and evaluate and control those uncertainties.

To select an appropriate classification method and hence the improvement of the accuracy of the land use inventory, the following three research topics have been identified as the focuses of this study. (a) the production of a high quality remotely sensed images by means of a newly proposed unmixing method for hyper-spectral and multi-spectral remotely sensed images, (b) the provision of high accuracy land cover classification results by means of the development of new classification methods, and (c) a more reliable report method for classification accuracy by means of the proposition of a new spatial sampling strategy. The three research topics are cohesive issues in remotely sensed image classification-based land use inventory development.

7.1 Conclusions and Discussions

7.1.1 The Methods of Unmixing Mixed Pixel

The problem of mixed pixels is mainly due to the following two reasons: (a) the limited spatial resolution of the remotely sensed images, and (b) the combination of various constituent materials within a heterogeneous mixed pixel. This problem of mixed pixel weakens the legible boundary between different land cover classes, and accounts for one of the most serious problems affecting the accuracy of remotely sensed image classification. Normally, hyper-spectral images have lower spatial resolution than the panchromatic image for the same remote sensing satellite. Therefore, hyper-spectral images are affected by the problems of mixed pixels more seriously than panchromatic images are. If this shortcoming of hyper-spectral images can be overcome by the newly proposed unmixing methods, the advantages of the abundant spectral information of the hyper-spectral images can be used even more effectively. In this research, the methods of unmixing the mixed pixel for hyper-spectral and multi-spectral remotely sensed images have been developed and are reported in Chapters 3 and 4 respectively.

In this study, the methods for unmixing mixed pixels have been developed based on the linear mixing model. The logic flow of the existing procedure is: (a) extract pure endmember, (b) compute abundance coefficients based on the model, and (c) conduct sub-pixel mapping. A fundamental development of the existing methods of unmixing mixed pixels, has been achieved by the improvements to the existing methods of unmixing mixed pixels, described below.

The mixed pixels in hyper-spectral image have been unmixed using the following steps. Firstly, we give the theoretical proof for the assumption of the existing AMEE algorithm and propose the improved AMEE algorithm for extracting the endmember. Secondly, we pre-judge before applying the Least Square method compute the abundance coefficient so that the effect of the least square method has been improved and the computation cost has been reduced. Thirdly, solution for the sub-pixel mapping of the mixed pixel, based on the spatial distribution of each endmember within the mixed pixel has been studied. At this point, we propose reliability-based sub-pixel mapping methods based on the consideration of spectral correlation of neighboring sub-pixels. On the basis of significance test, we find the accuracy of image classification is improved with 2%-3% and 1%-5%, when using the unmixed images from the proposed method for image classification, comparing those from the interpolation method and other unmixing method respectively.

Methods for unmixing mixed pixels for multi-spectral remotely sensed images have also been developed in this study. Similarly with the assumption made for the method of unmixing the mixed pixel, for hyper-spectral images, the linear mixing model has also been adopted. The difference is we unmix the multi-spectral images based on each single band images. One fundamental difficulty in building the unmixing matrix for the single band image is the shortage of spectral information. Because characteristics of single band images are different from those of the hyper-spectral image, the solution for unmixing multi-spectral image mixed pixels is quite different from that for the hyper-spectral images; thus, the methods for unmixing single band image mixed

pixels have been developed separately.

Firstly, the Mountain Clustering has been introduced to extract endmembers in every single band image. Secondly, a grey correlation method has been used to the abundance computation. Finally, to improve the spatial resolution of the image, the mixed pixel based on the spatial distribution of each endmember has been separated, and further the endmembers are classified into corresponding feature classes. The improved cellular automata system has been used to conduct sub-pixel mapping, which is based on the evolutive exchange of cellulars. To improve and unify the results of sub-pixel mapping in each single band, we propose multiband synthesis technology based on the spectral correlation of neighboring sub-pixels. On the basis of significance test, we find the accuracy of image classification is improved with 1%, when using the unmixed images from the proposed method for image classification, comparing that from the interpolation method.

In summary, this study has proposed two solution series for unmixing mixed pixels: (a) hyper-spectral remotely sensed images and (b) multi-spectral remotely sensed images, both of which are a further improvement on the existing solutions. The experimental studies have proved that the proposed methods for unmixing mixed pixels can improve the quality of both hyper-spectral remotely sensed images and multi-spectral remotely sensed images. With the improved quality of remotely sensed images resulting from unmixing, a better basis of data sources could be provided for a higher quality image classification for a land use inventory.

7.1.2 Improved Classification Method for Remotely Sensed Image

The quality of a land use classification method is determined by (a) the quality of the remotely sensed images used for the classification and (b) the classification scheme. It can be said that the higher quality image has been obtained by unmixing the original images, which is the problem (a). We need set about solving the problem (b). In many cases, one classification method, which is applicable for one kind of satellite image, or for an image of a specific area, may not be applicable to another type of image or area. In this thesis, a new Multiple Classifier System (MCS) for image classification has been proposed. The proposed new MCS takes into account the complementary characteristics of different kinds of classification methods. Thus each MCS classification method can be integrated, and hence presents a classification method which betters the established individual methods.

In this study, the eigen-values-based multiple classifier system has been proposed to improve classification accuracy, based on the mathematical properties of the posterior probabilities matrix for combining classifiers. Firstly, the range of each class was defined. Secondly, the posterior probabilities matrix was computed. Here, the posterior probabilities matrix consisted of the probabilities vectors of each classifier. The third step was to compute the eigen-values of the matrix, which is obtained from posterior probabilities matrix, with each square root of the eigen-value assigned to different classifiers based on a certain rule. The eigen-values of the matrix are used to weight the classifiers. Here, we assign large sum of squares of a classifier's probabilities corresponds with the large square root of the eigen-values, and small sum of

squares of the classifier probabilities corresponds with the small square root of the eigen-values. Finally, the pixel class was determined by the contribution of all the combined classifiers.

The significance of the proposed eigen-values-based method is that the eigen-values give a meaningful weight to the individual classifier. The experimental results, demonstrates that the newly proposed eigen-values-based method, has the highest overall accuracy compared with the maximum likelihood classification, minimum distance classification, the Mahalanobis distance classification and simple average multiple classifiers method.

In addition, we carried out a case study to validate the performance of unmixing. We find unmixing can really improve the image quality, where the evidence is that the classification accuracy of all selected classification method on the unmixed image has been enhanced obviously. On the basis of significance test, we find the kappa statistics of image classification are improved with 8%-14%, when applying the same classification method on the unmixed images.

7.1.3 The Spatial Sample Strategy based on Uncertainty Distribution

Assessing accuracy is a necessary part of remotely sensed image classification, and the sampling method is an effective solution used to estimate the accuracy of a classification. As the third objective of this study, an effective spatial sampling strategy for estimating the accuracy of image classification has been proposed. In the proposed method, the sample selections were based on the spatial distribution of uncertainty.

The proposed sampling method has been designed based on error distribution. Here, error has been treated as the noise in signal processing field, and thus the theories of signal processing have been transferred to the sampling study. Specifically, the removal of error in image classification has been transferred to the problem of removing noise, by using different Gaussian filters in signal processing.

It was assumed that the errors in the image follow the normal distribution after pre-partitioning the original spatial data into different error levels, based on a approximate classification, hence different Gaussian filters can be used to remove the errors in each region. After several different scale filtering procedures, the error-free spatial data can then be obtained. The difference found between the original spatial data and the error-free data was then used to build an error surface. The extreme points on the error surface were regarded as the representative sample points. Hence, the optimum sample points have been selected based on the extreme points searched from the error surface. The characteristic of the proposed sample strategy is that it is based on the spatial distribution of error.

7.2 Future Research Work

Three areas of work have been developed in this study to improve and estimate the classification accuracy of remotely sensed images. However, a number of issues are still to be further researched, such as how to combine other classification methods, such as ANN, SVM, Decision Tree, etc., into a multiple classifier system? How to take the spatial autocorrelation into account when

designing spatial sample strategy? How to present the accuracy assessment measurements for image classification? How to unify all the above work systematically? Owing to time limitation, only three parts of the work, corresponding to the image classification, have been addressed in this thesis. The methodologies of unmixing mixed pixel for hyper-spectral and multi-spectral remotely sensed image have been reported in chapters 3 and 4; a new effective image classification system - MCS has been proposed in chapter 5; and spatial sample strategy to assess the accuracy of image classification is described in chapter 6. However, they are three consistent but detached parts about the image classification. Consequently, further research need to be conducted to treat all the above individual parts as a whole from system engineering point of view.

Combination of Multiple Classifier System with Other Classifiers

Maximum likelihood classifier, minimum distance classifier and Mahalanobis distance classifier are three of the most basic and popular classification methods. We propose the combination of these classifiers in order to provide a new idea on MCS, which develops the advantages of each method as many as possible. The classification results and distance measuring style of these component classifiers are different and not compatible with each other. This is the main reason why we select them. In future, we'd like to evaluate the possibility for proposing a new integration way in our work, such as ANN, SVM, Decision Tree. These classifiers are popular intelligent methods, and there will be a wide space to integrate them into a multiple classifier system and maybe obtain a good result.

Effect of Spatial Autocorrelation on Sample Strategy

The proposed spatial sample strategy, based on the spatial distribution of uncertainty, has been proved to be better than other traditional spatial sampling methods. However, spatial autocorrelation between errors in the design of the proposed sample method has been neglected. Congalton (1991) pointed out that because of the existence of spatial autocorrelation, the presence, absence, or degree of a certain characteristics will affect the presence, absence, or degree of the same characteristics in neighboring units. Such positive or negative effects will greatly affect the accuracy assessment of image classification. Therefore, as a necessary complement to spatial sampling, it is also suggested that the effect of the spatial autocorrelation of the proposed spatial sample strategy, be addressed in future research.

Accuracy Measurements

The image classification accuracy assessment result generally consists of (a) sample and (b) measurements. In this study, the applied measurements for accuracy assessment have been addressed in chapter 2. The existing descriptive measurements, such as the error matrix analysis, can not fully fulfill the requirement of total quality assessment which further covers the assessment of such as land cover composition, landscape pattern, and accuracy of quantitative map products (Mao and Shi, 2008b; Stehman, 2008). Therefore the development of a measurement for the total quality assessment of image classification results needs to be proposed for further research.

References

Angulo, J.M. and Bueso, M.C., 2001. Random perturbation methods applied to multivariate spatial sampling design. *Environmetrics*, 12, 631-646.

Angulo, J.M., Ruiz-Medina, M.D., Alonso, F.J. and Bueso, M.C., 2005. Generalized approaches to spatial sampling design. *Environmetrics*, 16, 523-534.

Andrew J. T., Hugh G. L., Peter M. A. and Mark S. N., 2001. Super-resolution target identification from remotely sensed images using a hopfield Neural Network. *IEEE Transactions On Geoscience and Remote Sensing,* 39(4), 781-796.

Arai, K. and Terayama, Y., 1992, Label relaxation using a linear mixture model. *International Journal of Remote Sensing*, 13(16), 3217-3227.

Aronoff, S., 1985. The minimum accuracy value as an index of classification accuracy. *Photogrammetric Engineering and Remote Sensing*, 51(1), 99-111.

Atkinson P.M., Cutler M.E.J. and Lewis, H., 1997. Mapping sub-pixel proportional land cover with AVHRR imagery. *International Journal of Remote Sensing*, 18(4), 917-935.

Banjevic, M. and Switzer, P., 2002. Bayesian network designs for fields with variance as a function of the location. *In*: *Proceedings of the 2002 JSM Conference*, New York.

Bellehumeur, C., and Legendre, P., 1997, Aggregation of sample units: an analytical solution to predict variance. *Geographical Analysis*, 29, 258–266.

Benzeghiba, M.F. and Bourlard, H., 2003. Hybrid HMM/ANN and GMM combination for user-customized password speaker verification. *In*: *IEEE International Conference on Acoustics, Speech and Signal Processing*, Hong Kong, China, 225-228.

Berberoglu, S., Curran, P.J., Lloyd, C.D. and Atkinson, P.M., 2007. Texture classification of Mediterranean land cover. *International Journal of Applied Earth Observation and Geoinformation*, 9, 322-334.

Bezdek, J.C., 1981, *Pattern recognition with fuzzy objective function algorithms*, New York: Plenum Press.

Bian, Z.Q. and Zhang, X.G. et al., 2003. *Pattern Recognition*. Beijing: Tsinghua Universinty Press.

Boardman, J.W., Kruse, F.A., and Green, R.O., 1995, Mapping target signatures via partial unmixing of AVIRIS data, in *Summaries of JPL Airborne Earth Science Workshop*, Pasadena, CA.

Bogaert, P. and Russo, D., 1999. Optimal spatial sampling design for the estimation of the variogram based on a least squares approach. *Water Resources Research*, 35, 1275-1289.

Bolstad, P.V., Gessler, P. and Lillestand, T.M., 1990. Positional uncertainty in manually digitized map data. *International Journal of Geographical Information System*, 5, 159-168.

Bosdogianni, P., Petrou, M., and Kittler, J., 1994, Mixed pixel classification in remote sensing, In Proceedings of *the 1st European Symposium on Satellite Remote Sensing, conference on Image and Signal Processing for Remote Sensing*, Rome, 494-505.

Bowles, J., Palmadesso, P.J., Antoniades, J.A., Baumback, M.M. and Rickard, L.J., 1995, Use of filter vectors in hyperspectral data analysis, in *Proc. SPIE Infrared Spaceborne Remote Sensing III*, 148-157.

Briem, G.J., Benediktsson, J.A. and Sveinsson, J.R., 2002. Multiple classifiers applied to multisource remote sensing data. *IEEE Transactions on Geoscience and Remote Sensing*, 40(10), 2291-2299.

Bruzzone, L. and Carlin, L., 2006. A multilevel context-based system for classification of very high spatial resolution images. *IEEE Transactions on Geoscience and Remote Sensing*, 44(9), 2587-2600.

Campbell J., 1987. *Introduction to remote sensing*. New York: Guilford Press.

Caselton, W.F., Kan, L. and Zidek, J.V., 1992, Quality data networks that minimize entropy. *Statistics in the Environmental and Earth Sciences*, Walden AT, Guttorp P (eds). Edward Arnold Publishers Ltd: London, Baltimore; 10-38.

Chang, C.I. and Heinz, D.C., 2000. Constrained subpixel target detection for remotely sensed imagery. *IEEE Transactions on Geoscience and Remote Sensing*, 38(3), 1144-1159.

Chen, B.J., Li, J.L. and Chen, G. et al., 2006, 16, A MR image enhancement algorithm based on segmentation and accumulating index transformation, *Computer Engineering and Applications*, 16, 29-31.

Cochran, W.G., 1977. *Sampling Techniques*. 3rd ed. New York: Wiley Press.

Comber, A.J., 2008. The separation of land cover from land use using data primitives. *Journal of Land Use Science*, 3(4), 215-229.

Congalton, R.G., 1991. A review of assessing the accuracy of classifications of remotely sensed data. *Remote Sensing of Environment*, 37, 35-46.

Congalton, R.G., 1988. Using spatial autocorrelation analysis to explore the errors in maps generated from remotely sensed data. *Photogrammetric engineering and Remote Sensing*, 54, 587-592.

Congalton, R.G., Oderwald, R.G. and Mead, R.A., 1983. Assessing Landsat classification accuracy using discrete multivariate statistical techniques. *Photogrammetric Engineering and Remote Sensing*, 49(12), 1671-1678.

Cross, A.M., Settle, J.J., Drake, N.A. and Paivinen, R.T.M, 1991, Subpixel measurement of tropical forest cover using AVHRR data, International Journal of Remote Sensing, 12(5), 1119-1129.

Devillers, R. and Jeansoulin, R., 2006, *Fundamentals of Spatial Data Quality*, ISET Ltd, Britain and United States.

Drake, N.A., and Settle, J.J., 1989, Linear mixture modeling of Thematic Mapper data of the Peruvian Andes. In Proceedings of *the EARSeL Symposium*, Helsinki, Finland, 490-495.

Dunn, J.C., 1974, A fuzzy relative of the ISODATA process and its use in detecting compact well separated clusters. *Journal of Cybernetics*, 3(3), 32-57.

Dunn, R., and Harrison, A.R., 1993, Two dimensional systematic sampling of land use, *Applied Statistics*, 42, 585-601.

Efron, B., and Tibshirani, R., 1997. Improvements on cross-validation: The .632+ bootstrap method. *Journal of the American Statistical Association*, 92(438), 548-560.

Feng, Y.Q., Chen, W.F., Liang, B. et al, 2004, A new algorithm for image segmentation based on gibbs random field and fuzzy C-Means clustering, *Acta Electronica Sinica*, 32(4), 645-647.

Fotheringham, A., Charlton, M., and Brunsdon, C., 1996, The geography of parameter space: an investigation of spatial non-stationary. *International Journal of Geographical Information Systems*, 10, 605-627.

Fumera, G., and Roli, F., 2005. A theoretical and experimental analysis of linear combiners for multiple classifier. *IEEE Transactions on Pattern Analysis and Machine Intelligence*, 27(6), 942-956.

Foody, G.M., 1994, Ordinal-level classification of sub-pixel tropical forest cover, *Photogrammetric Engineering and Remote Sensing*, 60(1), 61-65.

Foody, G.M., 1997, Fully fuzzy supervised classification of land cover from remotely sensed imagery with an artificial neural network, *Neural Computing & Applications*, 5, 238-247.

Foody, G.M., 2002. Status of land cover classification accuracy assessment. *Remote Sensing of Environment*, 80, 185-201.

Foody, G.M. and Cox, D.P., 1994, Sub-pixel land cover composition estimation using a linear mixture model and fuzzy membership functions, *International Journal of Remote Sensing*, 15(3),619-631.

Gamba, P., Dell'Acqua, F., Lisini, G., et al., 2007. Improved VHR urban area mapping exploiting object boundaries. *IEEE Transactions on Geoscience and Remote Sensing*, 45(8), 2676-2682.

Gebbinck, M.S., 1998. *Decomposition of mixed pixels in remote sensing images to improve the area estimation of agricultural fields*. Thesis (PhD). University of Nijmegen, The Netherlands.

Goodchild, M.F., 1991. Keynote address: Symposium on spatial database accuracy. *In* Hunter G.J. ed. *Proceedings of Symposium on Spatial Database Accuracy*, 1-16.

Gorokhovich, Y. and Voustianiouk, A., 2006. Accuracy assessment of the processed SRTM-based elevation data by CGIAR using field data from USA and Thailand and its relation to the terrain characteristics. *Remote Sensing of Environment*, 104, 409-415.

Griffith, D.A., 1988, *Advanced spatial statistics*, Dordrecht: Kluwer Academic Publishers, 94-99.

Haining, R., 1990, *Spatial data analysis in the social and environmental sciences*, Cambridge: Cambridge University Press.

Heinz, D.C. and Chang, C.I., 2001. Fully constrained least squares linear spectral mixture analysis method for material quantification in hyperspectral imagery. *IEEE Transactions on Geoscience and Remote Sensing*, 39(3), 529-545.

Ho, T.K., Hull, J.J. and Srihari, S.N., 1994. Decision combination in multiple classifier systems. *IEEE Transactions on Pattern Analysis and Machine Intelligence*, 16(1), 66-75.

Hu, Y.H., Lee, H.B. and Scarpace, F.L., 1999. Optimal linear spectral unmixing. *IEEE Transactions on Geoscience and Remote Sensing*, 37(1), 639-644.

Huenupan, F., Yoma, N.B., Molina, C. and Garreton, C., 2008. Confidence based multiple classifier fusion in speaker verification. *Pattern Recognition Letters*, 29, 957-966.

Jakomulska, A., and Stawiecka, M., 2002. Integrating spectral and textural information for land cover mapping. *In*: Begni, G. ed. *Observing Our Environment from Space-New Solutions for a New Millennium*. Balkema publishers, 347-355.

Journel, A., and Huijbregts, C.H., 1978, *Mining geostatistics*, London: Academic Press.

Kasetkasem, T., Arora, M.K. and Varshney, P.K., 2005, Super-resolution land cover mapping using a Markov random field based approach, *Remote Sensing of Environment*, 96, 302-314.

Keshava N., 2003. A survey of spectral unmixing algorithms. *Lincoln Laboratory Journal*, 14(1), 55-78.

Kittler, J., Hatef, M., Duin, R.P.W. and Matas, J., 1998. On combining classifiers. *IEEE Transactions on Pattern Analysis and Machine Intelligence*, 20, 226-239.

Ko, C., Lee, J. and Queyranne, M., 1995, An exact algorithm for maximum entropy sampling, *Operations Research*, 43, 684-691.

Lark, R., 2002, Optimized spatial sampling of soil for estimation of the variogram by maximum likelihood, *Geoderma*, 105, 49-80.

Lee, J.H. and Philpot, W.D., 1991. Spectral texture pattern matching: a classifier for digital imagery. *IEEE Transactions on Geoscience and Remote Sensing*, 29, 545-554.

Liu, J.Z. and Xie, W.X., 1993, An efficient pyramidal color image segmentation method with fuzzy clustering, *Journal of XiDian University*, 20(1), 40-46.

Mak, M.W., Cheung, M.C. and Kung, S.Y., 2003. Robust speaker verification from GSM-transcoded speech based on decision fusion and feature transformation. *In*: *Proceedings of IEEE International Conference on Acoustics, Speech and Signal Processing*, Hong Kong, China, 745-748.

Mao, H.X. and Shi, W.Z., 2008a. Uncertainty and its Propagation in Land Investigation. *In*: Zhang and Goodchild ed. *Spatial Uncertainty:*

Proceedings of the 8th International Symposium on Spatial Accuracy Assessment in Natural Resources and Environmental Sciences, Shanghai, China, 8-15.

Mao, H.X and Shi, W.Z., 2008b. New Methodology of Representing the Positional Error of Non-point Features in GIS. *In*: *Congress of 21st ISPRS*, Beijing, China.

Mao, H.X, Shi, W.Z. and Tian Y., 2007. A Preliminary Study on Spatial Sampling for Topographic Data. *In*: Stain et al. ed. *Quality Aspects in Spatial Data Mining: Proceedings of the 5th International Symposium on Spatial Data Quality*, 59-72.

Marsh, S.E., Switzer, P. and Kowalik, W.S., 1980, Resolving the percentage of component terrains within single resolution elements, *Photogrammetric Engineering and Remote Sensing,* 46(8), 1079-1086.

Melnik O., Vardi Y. and Zhang C.H., 2004, Mixed group ranks: preference and confidence in classifier combination. *IEEE Transactions on Pattern Analysis and Machine Intelligence*, 26(8), 973-981.

Meng, X. L., Shi, W.Z. and Liu, D.J., 1998. Statistical tests of the distribution of errors in manually digitized cartographic lines. *Geographic Information Sciences*, 4, 52-58.

Mertens, K.C., Verbeke, L.P.C and De Wulf, R.R., 2003a, Sub-pixel mapping with neural net works: Real-world spatial configurations learned from artificial shapes, in *Proceedings of 4th International Symposium on Remote Sensing of Urban Areas*. Regensburg, German.

Mertens, K.C., Verbeke, L.P.C., Ducheyne, E.I., 2003b, Using genetic algorithms in sub-pixel mapping. *International Journal of Remote Sensing*, 24(21), 4241-4247.

Mertens, K.C., De Baets, B., Verbeke, L.P.C., De Wulf, R.R., 2004, Direct sub-pixel maping exploiting spatial dependence, *Geoscience and Remote Sensing Symposium, IGARSS 04*, 3046-3049.

Mesev, V., Gorte, B. and Longley, P., 2001. Modified maximum-likelihood classifications algorithms and their application to urban remote sensing, *In*: Donnay J.P. et al ed. *Remote Sensing and Urban Analysis*. London: Taylor & Francis, 71-94.

Muller, W.G. and Zimmerman, D.L., 1999. Optimal designs for variogram estimation. *Environmetrics*, 10, 23-37.

Neville, R.A., Staenz, K., Szeredi, T., Lefebvre, J. and Hauff, P., 1999. Automatic endmember extraction from hyperspectral data for mineral exploration. *In*: *Proceedings of 21st Canadian Symposium of Remote Sensing*. Ontario, Canada, 21-24.

Otsu N., 1979. Threshold selection method from gray-level histograms. *IEEE Transactions on Systems Man and Cybernetics*, 9(1), 62-66.

Pech, R.P., Davies, A.W., Lamcroft, R.R., and Graetz, R.D., 1986, Calibration of LANDSAT data for sparsely vegetated semi-arid rangelands, *International Journal of Remote Sensing*, 7(12), 1729-1750.

Pettitt, A.N., McBratney, A.B., 1993, Sampling designs for estimating spatial variance components, Journal of Applied Statistics, 42, 185-209.

Plaza A., Valencia, D. And Plaza, J., et al., 2006. Parallel implementation of endmember extraction algorithms from hyperspectral data. *IEEE Geoscience and Remote Sensing Letters*, 3(3), 334-338.

Plaza, A., Martínez, P., Perez, R. et al., 2002. Spatial/spectral endmember extraction by multidimensional morphological operations. *IEEE Transactions on Geoscience and Remote Sensing*, 40(9), 2025-2041.

Rashed, T., Weeks, J.R., Gadalla, M.S., et al, 2001. Revealing the anatomy of cities through spectral mixture analysis of multi-spectral satellite imagery: A case study of the Greater Cairo Region, Egypt. *Geocarto International*, 16(4), 5-13.

Rashed, T., Weeks, J.R., Roberts, D., et al., 2003. Measuring the physical composition of urban morphology using multiple endmember spectral mixture models. *Photogrammetric Engineering and Remote Sensing*, 69(9) 1011-1020.

Ronald, D., 2006, Probability and statistics, Burlington, Mass: Academic Press.

Rosenfield, G.H., 1981. Analysis of variance of thematic mapping experiment data. *Photogrammetric Engineering and Remote Sensing*, 47(12), 1685-1692.

Rosenfield, G.H. and Fitzpatricklins, K., 1986. A coefficient of agreement as a measure of thematic classiviation accuracy. *Photogrammetric Engineering and Remote Sensing*, 52(2), 223-227.

Royle, J.A., 2002. Exchange algorithms for construction large spatial designs. *Journal of Statistical Planning and Inference*, 100(2), 121-134.

Schouten, T. and Gebbinck, M.S.K., 1997a, Fuzzy classification of spectra, In *Neural networks: Best practice in Europe*, Amsterdam, 198-201.

Schouten, T. and Gebbinck, M.S.K., 1997b, A neural network approach to spectral mixture analysis. In *Neurocomputation in Remote Sensing Data Analysis: Proceedings of Concerted Action COMPARES*, 79-85.

Settle, J.J. and Drake, N.A., 1993, Linear mixing and the estimation of ground cover proportions, *International Journal of Remote Sensing*, 14(6), 1159-1177.

Skidmore, A. and Turner, B., 1989. Assessing the accuracy of resource inventory maps. *In*: *Proceedings of Global Natural Resource Monitoring and Assessments: Preparing for the 21st Century*, 2, 524-535.

Shih, E.H.H. and Schowengerdt, R.A., 1983. Classification of arid geomorphic surfaces using Landsat spectral and textural features. *Photogrammetric Engineering and Remote Sensing*, 49, 337-347.

Steele, B.M., 2000. Combining multiple classifiers: am application using spatial and remotely sensed information for land cover type mapping. *Remote Sensing of Environment*, 74, 545-556.

Stehman, S.V., 1999. Basic probability sampling designs for thematic map accuracy assessment. *International Journal of Remote Sensing*, 20(12), 2423-2441.

Stehman, S.V., 2000, Practical implications of design-based sampling inference for Thematic Map accuracy assessment, *Remote Sensing of Environment*, 72, 35-45.

Stehman, S.V., 2008. Sampling Designs for assessing map accuracy. *In*: Li, et al., ed. *Accuracy in Geomatics*: *Proceedings of the 8th International Symposium on Spatial Accuracy Assessment in Natural Resources and Environmental Sciences*, Shanghai, China, 8-15.

Sun, H.Y., Sun, X.P. and Li, H., 2006, 3D point cloud model segmentation based on K-means cluster analysis, *Computer Engineering and Applications*, 10, 42-45.

Tang, X.M., Kainz W. and Fang Y., 2005. Reasoning about changes of land covers with fuzzy settings. *International Journal of Remote Sensing,* 26 (14), 3025-3046.

Tatem, A.J., Lewis, H.G., Atkinson, P.M., 2000, Land cover mapping at the sub-pixel scale using a hopfield neural network, *International Symposium on Remote Sensing of Environment*. Cape Town, S. Africa.

Tseng, M.H., Chen S.J., Hwang G.H. and Shen M.Y., 2008. A genetic algorithm rule-based approach for land-cover classification. *ISPRS Journal of Photogrammetry & Remote Sensing*, 63(2), 202-212.

Van Groenigen, J.W. and Stein, A., 1998. Constrained optimization of spatial sampling using continuous simulated annealing. *Journal of Environmental Quality*, 27(5), 1078-1086.

Verhoeye J. and De Wulf R., 2002. Land cover mapping at sub-pixel scales using linear optimization techniques. *Remote Sensing of Environment*, 79, 96-104.

Wang, F., 1990, Fuzzy supervised classification of remote sensing images, *IEEE Transactions on Geoscience and Remote Sensing*, 28(2), 194-201.

Wang, J., Liu, J., Zhuan, D., Li, L. and Ge, Y., 2002, spatial sampling design for monitoring the area of cultivated land, International Journal of Remote Sensing, 23(2), 263-284.

Wiens, D.P., 2005. Robustness in spatial studies I: minimax prediction. *Environmetrics*, 16(2), 191-203.

Wilkinson, G. G., 2005, Results and Implications of a study of fifteen years of satellite image classification experiments, *IEEE Transactions on Geoscience and Remote Sensing*, 43(3), 433-440.

Winter, M.E., 1999, N-FINDR: an algorithm for fast autonomous spectral endmember determination in hyperspectral data, in *Proceeding of SPIE Conference on Imaging Spectrometry V*, 753, 266–277.

Wu, K., Li, P.X. and Zhang, L.P., 2009. Sub-pixel mapping of remote sensed images based on evolutionary agent algorithm. *Journal of Remote Sensing*, 1, 60-66.

Woods, K., Kegelmeyer, W.P. and Bowyer, K., 1997. Combination of multiple classifiers using local accuracy estimates. *IEEE Transactions on Pattern Analysis and Machine Intelligence*, 19(4), 405-410.

Xu L., Krzyzak, A. and Suen, C.Y., 1992. Methods of combining multiple classifiers and their applications to handwriting recognition. *IEEE Transactions on Pattern Analysis and Machine Intelligence*, 22(3), 418-435.

Yager, R.R. and Filev, D.P., 1994, Approximate clustering via the mountain method. *IEEE Transactions on System, Man, and Cybernetics*, 24, 1279-1284.

Yang, G.J. and Zhang, J.X., 2004, Research on method of decomposing remote sensing mixed pixel based on grey correlation theory, *Bulletin of Surveying and Mapping*, 10:1-3.

Zhang, A.H. and Tan, J., 2005, A semi-fuzzy clustered image segmentation method under edge detection, *Journal of Huazhong University of Science and Technology*, 33(6):8-11.

Zhang, D.Q.,Chen, S.C., Pan, Z.S. et al., 2003, Kernel-based fuzzy clustering incorporating spatial constraints for image segmentation. Proc. International Conference on Machine Learning and Cybernetics,4, 2189-2192.

Zhang, X., Sun R., Zhang, B. and Tong, Q.X., 2008. Land cover classification of the North China Plain using MODIS EVI time series. *ISPRS Journal of Photogrammetry & Remote Sensing*, 63, 476-484.

Zhang, Y.J., 2001. *Image Segmentation*. Beijing: Science Press.

Zhou, S.J., Lu, T.D., Guan, Y.L. and Zang, D.Y., 2003. The analytical collocation of the measurement errors distribution. *Acta Metrologica Sinica*, 24(3), 250-253.

Zhu, S.L., 1995. The classification of Remotely-sensed images with mixels. *Journal of the Plainstitute of Surveying and Mapping*, 12(4), 276-278.

Zhu, Z. and Stein, M., 2005. Spatial sampling design for parameter estimation of the covariance function. *Journal of Statistical Planning and Inference*, 134(2), 583-603.

Zhu, Z.Y., Stein, M.L., 2006, Spatial sample design for predictiton with estimated parameters, Journal of Agricultural Biological and Environmental Statistics, 11(1), 24-44.

Zhu, Z.Y. and Zhang H., 2006, Spatial sampling design under the infill asymptotic framework, *Environmetrics*, 17, 323-337.

Zimmerman, D.L., 2006, Optimal network design for spatial prediction, covariance parameter estimation, and empirical prediction, *Environmetrics* , 17(6), 635-652.